DEVELOPMENT OF CELL PERMEANT INHIBITORS OF TYPE 1 HUMAN ISOPENTENYL DIPHOSPHATE ISOMERASE

A Thesis Presented for the

Master of Science

Degree

The University of Tennessee, Knoxville

Vijani Wijayasekera

December 2024

ACKNOWLEDGEMENTS

I would first like to express my sincere gratitude to Professor Joshua Baccile for his mentorship, support and patience throughout my graduate studies. His guidance and encouragement have been instrumental in shaping my growth as a chemist. I am also profoundly grateful to my committee members, Professor Ampofo Darko and Professor Thanh Do, for their invaluable feedback and advice, which have greatly contributed to my academic and professional development.

I would like to extend my sincere appreciation to all the members of the Baccile Lab for their assistance throughout my research journey. In particular, I would like to thank Dillon McBee for his dedicated work in conducting the in vivo experiments related to my research, Nick Trybala for his support with conducting HPLC-MS experiments, and Anna-Kay West for her constant moral support and insightful feedback on my thesis.

I am also thankful to Professor Frank Rossi and his lab at SUNY Cortland for providing the photocleavable IPP analogue, which was integral to my research.

Lastly, but most importantly, I am eternally grateful to my family—my mother, father, sister, and brother—for their unconditional love, unwavering support, and the many sacrifices they have made for my education. Their belief in me, even in moments of doubt, has been my greatest source of strength.

ABSTRACT

Isopentenyl pyrophosphate (IPP) and dimethylallyl pyrophosphate (DMAPP) are the 5C precursors to all isoprenoids. Isoprenoid biosynthesis occurs via a head-to-tail condensation of the initiator, DMAPP, and extender unit, IPP which demonstrates high metabolic demand. However, the reversible isomerization catalyzed by type 1 isopentenyl diphosphate isomerase indicates a preference towards DMAPP synthesis, which combined with the limited evidence available of the independent functions of the 5C precursors in humans, underscores the requirement for interrogation of their distinct biological roles that occur to maintain homeostasis. We sought to modulate the metabolic flux of IPP and DMAPP by the inhibition of hIDI-1 which allows their isolation for independent investigations. Inhibitors of IDI-1 reported in the literature are pyrophosphates and the resulting cell impermeability limits the application in human systems. Herein, we demonstrate the application of self-immolative esters (SIE) as a prodrug approach to selectively mask the negative charges on the beta-phosphate of substrate analogs for the synthesis of a series of cell-permeant inhibitors of hIDI-1. The inhibitory potential of inhibitors 1-3 have been evaluated in vitro and inhibitors 1 and 2 have been subjected to further analysis on MDA-MB-231 breast cancer cells. The inhibitory efficiency of the reported analogs follows the trend 1>2>3. In the present study, we also investigated the photo uncaging efficiency of a mixed photocaged IPP compound, that employs a SIE to induce lipophilicity for exogenous delivery of IPP into the cell, and an ortho-nitrobenzyl (oNB) photocage, that utilizes light as an external stimulus for the non-invasive spatiotemporal control over the release of IPP.

TABLE OF CONTENTS

LIST OF TABLES

LIST OF FIGURES

LIST OF SCHEMES

CHAPTER ONE

INTRODUCTION

1.1 Isoprenoids

Isoprenoids represent a vast and structurally diverse class of biomolecules, with over 80,000 biomolecules that play crucial roles in various biological processes across all life forms, ranging from single-celled organisms to multicellular systems. [1-3] They are pivotal in processes such as cell recognition, signal transduction, protein prenylation, electron transport, and photosynthesis. Additionally, they serve as key components of cellular membranes, vitamins, pheromones, and hormones.[1]

All isoprenoids are derived from two key 5-carbon (5C) precursors, isopentenyl pyrophosphate (IPP) and dimethylallyl pyrophosphate (DMAPP).[4] These precursors are structural isomers biosynthesized via two distinct pathways; The mevalonic acid (MVA) pathway and methylerythritol phosphate (MEP) pathway, both of which are essential for the synthesis of sterol and non-sterol isoprenoids. The mevalonic acid (MVA) pathway, which was discovered in the 1960s by Bloch and Lynen while studying the biosynthesis of cholesterol, is predominantly found in mammals, whereas the methylerythritol phosphate (MEP) pathway, first described by Rohmer and Arigoni, is the dominant route for isoprenoid biosynthesis in plants and most eubacteria.[3,5-8] Sterol isoprenoids (**Figure 1**) such as cholesterol and hopanoids are critical for maintaining cell membrane integrity in mammalian and bacterial cells, respectively, whereas steroid hormones such as estrogen and progesterone are involved in the development of the human reproductive system.[8- 12] Non-sterol isoprenoids such as Coenzyme Q10 (CoQ10) participate in the electron transport chain, dolichols facilitate protein glycosylation for cell recognition and signaling, gibberellins function as plant growth hormones and, phytol and

carotenoids serve as essential pigments in photosynthesis.[2,13-15] Moreover, isoprene, limonene, farnesene, and phytene have been explored as biofuels and fuel additives, whereas long chain isoprenoids such as farnesyl pyrophosphate (FPP) and geranylgeranyl pyrophosphate (GGPP) have been recognized as the primary substrates for post-translational prenylation of proteins, which is vital for the regulation of protein localization, intracellular signaling and transport of growth factors.[2,15-18] This broad array of functions underscores the essential role of isoprenoids in cellular physiology and highlights their significance in both fundamental biology and potential industrial applications.

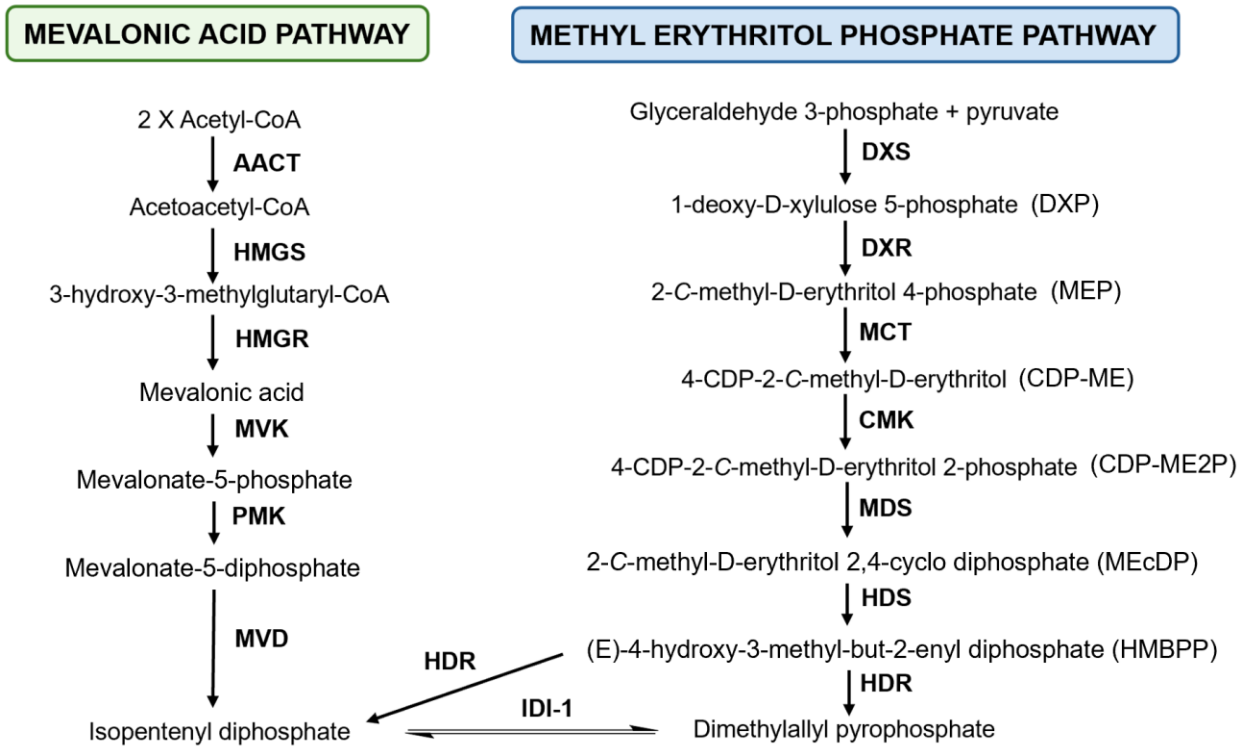

Figure 1 Biosynthesis of IPP and DMAPP via the mevalonic acid pathway and the methyl erythritol phosphate pathway.

1.2 Biosynthesis of Isoprenoids

Mevalonic Acid Pathway

The MVA pathway is initiated by the Claisen condensation of three acetyl CoA molecules to generate 3-hydroxy-3-methylglutaryl Co A (HMG CoA) catalyzed by the enzymes acetoacetyl thiolase (AACT) and HMG CoA synthase (HMGS).[4,5,15,19,20] The carboxyl moiety of HMG CoA undergoes reduction in the presence of NADPH, catalyzed by HMG CoA reductase (HMGR) - the rate limiting enzyme of the MVA pathway, to generate mevalonic acid.[1,21,22] MVA undergoes two ATP mediated phosphorylation steps at the terminal hydroxy group catalyzed by mevalonate kinase (MVK) and phosphomevalonate kinase (PMK).[1,8,15,23,24] In eukaryotes, mevalonate kinase is regulated by high affinity feedback inhibition by downstream isoprenoids such as farnesyl pyrophosphate (FPP) and geranylgeranyl pyrophosphate (GGPP), and to a lesser extent in prokaryotic bacteria such as *Staphylococcus aureus*.[4,15,25,26] The phosphorylated product, mevalonate-5-diphosphate, finally undergoes an ATP mediated dehydration followed by decarboxylation, catalyzed by mevalonate diphosphate decarboxylase (MVD) to generate the terminal alkene of IPP.[4,8,15,27] IPP is subjected to isomerization in the presence of isopentenyl diphosphate isomerase, to produce DMAPP.[5]

Methylerythritol Phosphate Pathway

The methylerythritol phosphate pathway is initiated by the condensation reaction between pyruvate and glyceraldehyde-3-phosphate to generate 1-deoxy-D-xylulose-5-phosphate (DXP) catalyzed by the DXP synthase (DXS) enzyme. [1,28-30] DXP undergoes a NADPH mediated reduction catalyzed by the DXP reductosiomerase (DXR) enzyme to biosynthesize 2-C-methyl-D-erythritol 4-phosphate (MEP). The activation and phosphorylation of MEP at the 2-hydroxy

group is mediated by CTP followed by ATP and is catalyzed by CDP-ME synthase (MCT) and CDP-Me2P kinase (CMK) respectively to produce 4-diphosphocytidyl-2-C-methyl-D-erythritol 2-phosphate (CDP-ME2P). CDP-ME2P undergoes a cyclization reaction facilitated by MEcDP synthase (MDS) followed by reduction catalyzed by HMBPP synthase (HDS) to form (E)-4-hydroxy-3-methylbut-2-enyl diphosphate (HMBPP), which is ultimately reduced by HMBPP reductase (HDR) to generate the isoprenoid precursors IPP and DMAPP in an 85:15 ratio.[1,3,31-33]

Following the biosynthesis of IPP and DMAPP, the two isomers react via a head-to-tail condensation reaction where DMAPP acts as the initiator molecule and IPP as the extender unit for chain elongation (**Figure 2**). Condensation of DMAPP and IPP in a 1:1 ratio results in the formation of 10C Geranyl pyrophosphate (GPP), a 1:2 ratio leads to 15C Farnesyl pyrophosphate (FPP) and a 1:3 ratio generates the 20C Geranylgeranyl pyrophosphate (GGPP).[1,3,34] FPP serves as the substrate for the biosynthesis of sterol isoprenoids and GGPP for nonsterol isoprenoids such as retinol and carotenoids, whereas continued polymerization forms higher-order isoprenoids such as natural rubber.[1,3,35] Some vital enzymes of the isoprenoid biosynthetic pathways have been extensively studied via enzyme regulation upstream and downstream of the 5C precursors. The most prominent examples are the clinical use of statins for the inhibition of the rate limiting enzyme of the MVA pathway – HMGR. Statins are a commonly prescribed class of drugs for the treatment of hypercholesterolemia and include compounds of natural and synthetic origin such as lovastatin and pitavastatin respectively.[1,36] The MEP pathway is regulated by the antibiotic fosmidomycin, which is a derivative of phosphonic acid that inhibits the rate limiting DXR enzyme, preventing the biosynthesis of MEP. The clinically used aminobisphosphonate compounds such as zoledronic acid and pamidronic acid have beenemployed to ameliorate metabolic bone diseases by inhibiting FPP synthase.[1,15,37] Inhibition

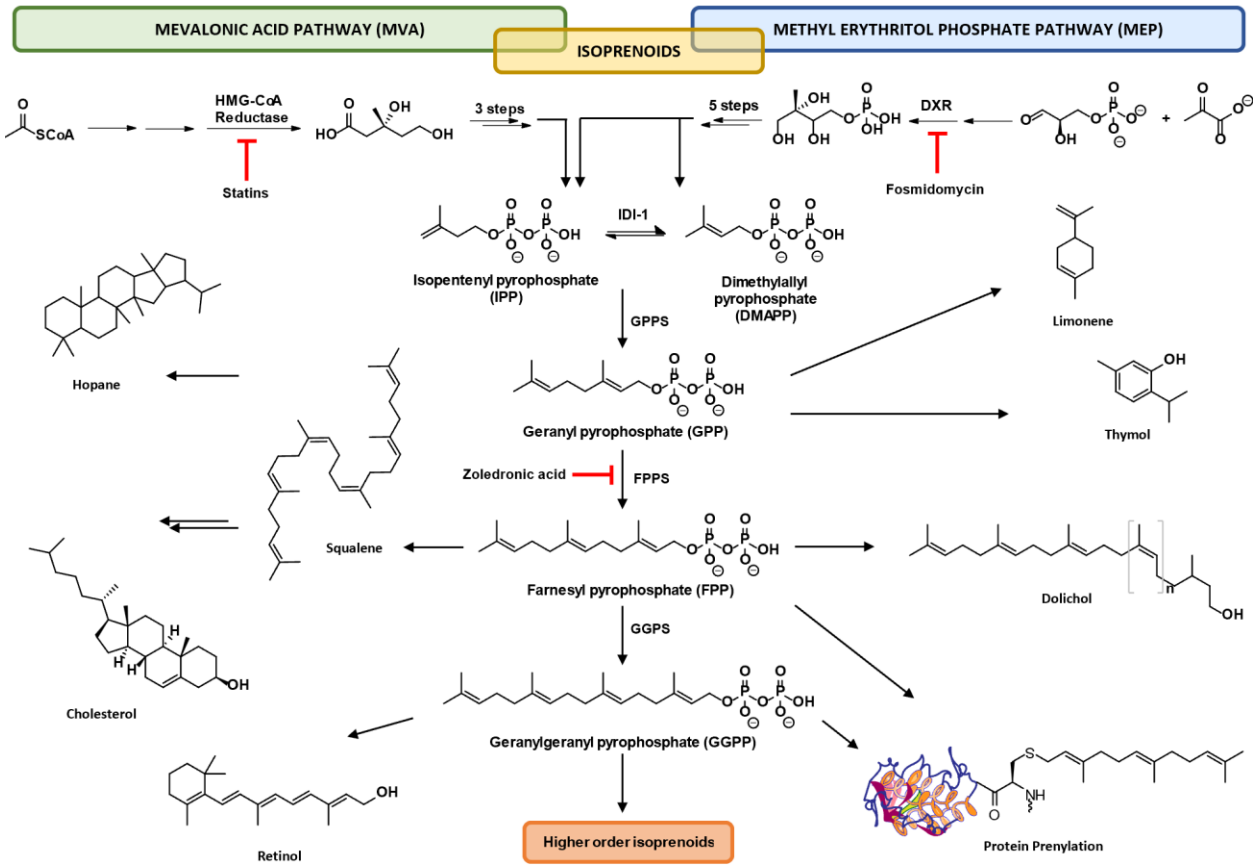

Figure 2 Isoprenoid biosynthetic pathways. Mevalonic acid pathway (left) and Methyl erythritol phosphate pathway (right).

of FPP synthase prevents the prenylation of small GTPases in osteoclasts and in turn alleviates bone resorption in bone tumours and osteoporosis.[1,38-40] However, in contrast to the intense research conducted on the MVA and MEP pathways and the functions of downstream isoprenoids, limited knowledge is available on the independent functions of IPP and DMAPP and their direct modifications. In prokaryotes, DMAPP functions as the precursor for the formation of isoprene gas and cytokinins, and is the 5C prenylating unit for normal and reverse prenylation of indole alkaloids.[1,41] However, the only reported modification in humans is the isopentenylation of adenosine 37 on the anticodon loop of tRNA to N6-isopentenyladenosine (i6A) which encodes for the expression of selenoproteins.[1,42] IPP is responsible for the isopentenylation of carbohydrates and the gamma phosphorous of adenosine triphosphate (ATP) which results in the formation of ApppI, a toxic metabolite that blocks the synthesis of ATP.[15,43] The formation of ApppI is also facilitated by using amino bisphosphonates which leads to the accumulation of IPP via the inhibition of FPP synthase.

Owing to the essential nature of the 5C precursors in isoprenoid biosynthesis and the limited knowledge of their independent biological activities and direct modifications in humans, it is important to investigate the possible biosynthetic routes that allow for the regulation of the pool of IPP and DMAPP beyond the metabolic incorporation into sterol and non-sterol isoprenoids. This emphasizes the necessity for developing chemical tools to probe human isopentenyl diphosphate isomerase (hIDI), the key enzyme responsible for maintaining the homeostasis of the pool of IPP and DMAPP.

1.3 Human Isopentenyl Diphosphate Isomerase

The type 1 human isopentenyl diphosphate isomerase (hIDI-1) enzyme functions as a checkpoint for isoprenoid metabolism in humans since the MVA pathway only generates IPP. The hIDI-1 enzyme is therefore essential for the biosynthesis of DMAPP and thereby regulates the pool of the 5C isoprenoid precursors in humans. Furthermore, hIDI-1 has been implicated in various neurodegenerative diseases and cancers. In sporadic amyotrophic lateral sclerosis (ALS) patients, a downregulated expression of hIDI-1 has been revealed in their motor cortex and a copy number gain in the gene region encompassing hIDI-1 has resulted in the reduction of enzyme expression.[44-46] Furthermore, a significant decrease in the activity of hIDI has been reported in peroxisomal deficiency diseases such as Zellweger syndrome and neonatal adrenoleukodystrophy.[47] In contrast, a study conducted on Alzheimer's disease in transgenic mouse brain tissue has revealed statistically significant overexpression of the hIDI enzyme resulting in an excessive production of prenylated proteins, which has been reported to be found in abundance in Alzheimer's disease patients.[48] An upregulation of IDI-1 has often been reported in studies conducted on cancer cell lines cultured in tumor-promoting environments such as a reported 4.5-fold increase in the expression of the gene encoding for hIDI in H358 (human non-small cell lung cancer) cells exposed to cigarette smoke and the implication of a direct relationship between the prenylation of RAS GTPases and Bhas42 cell line (mouse fibroblast cell line transfected with v-Ha-Ras gene) treated with a non-genotoxic carcinogen.[49,50] The prenylation of RAS GTPases and the prelamin A protein resulting from an increased expression of hIDI has thus been related to cancer and Hutchinson-Gilford progeria syndrome, respectively.[51] These implications further emphasize the importance and necessity to regulate the expression of the hIDI-1 enzyme.

The hIDI-1 catalyzes the reversible isomerization of homoallylic IPP into its electrophilic allylic isomer DMAPP via a stereoselective antarafacial [1.3] transposition of a proton, where the equilibrium favors the formation of DMAPP.[52] hIDI-1 was isolated for the first time in history, in 1994 by the Xuan lab, reporting a molecular mass of 26,450 Da. In 2007, the crystal structure analysis conducted by Zheng et al. (**Figure 3b**) revealed a compact globular monomeric structure constructed of seven α-helices and eight β-sheets with a deeply embedded active site that has been conserved across a range of species and is associated with the NUDIX enzyme superfamily. NUDIX enzymes are responsible for catalyzing the hydrolysis of nucleoside diphosphate linked to a group 'X' via nucleophilic substitution in the presence of a divalent cation.

The active site consists of precisely located catalytic residues Cys87 and Glu149 on opposite faces of the terminal alkene of IPP which facilitates isomerization via the protonation of the alkene by electrophilic attack on the Cys87 residue, generating a tertiary carbocation intermediate.[52-55] The intermediate is further stabilized by Trp197 via quadrupole charge interactions between the π electrons of the indole ring and the carbocation. Following the generation of the carbocation intermediate, the Glu149 residue carries out a nucleophilic attack for proton abstraction, generating an internal alkene bond. The diphosphate moiety of the substrate remains rigid during the isomerization by maintaining its stability via the hydrogen bonding interactions with active site residues Arg71 (proximal phosphate), Lys75 and Lys35 (bridging oxygen), and Ser88, Glu116, Arg112, and Cys87 (distal phosphate).[52]

Substrate analogs of IPP and DMAPP have been designed and developed by the Poulter group as small molecule inhibitors that target the active site of IDI-1. Some of the highly potent inhibitors reported are the epoxidized, acetylenic, allenic and diene substrate analogs eIPP, 1-OPP, 2-OPP, vIPP, (Z)-vDMAPP, (E)-vDMAPP respectively and the derivative of the

a)

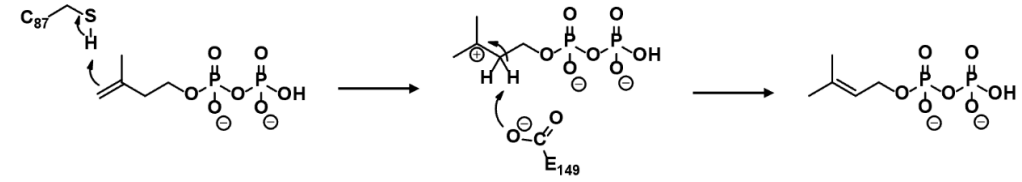

b)

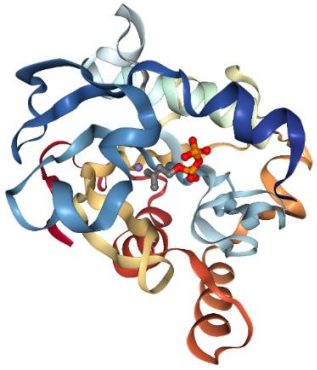

Figure 3 a) Isomerization reaction of IPP to DMAPP by active site residues of hIDI-1. b) Crystal structure of hIDI-1 with DMAPP at the active site, extracted from RSC PDB.

carbocation intermediate, nIPP (**Figure 4**). eIPP was demonstrated to be a highly effective inhibitor of IDI-1 isolated from *Claviceps* sp. with activity over a wide pH range.[56] Both eIPP and vIPP are active site-directed irreversible inhibitors of IDI, interacting via covalent bonding. They follow an inhibitory mechanism that allows the protonation of the inhibitor followed by electrophilic isomers that have originally been investigated as potential substrates of IDI, however, were later confirmed to be competitive inhibitors which rules out the possibility of isomerization at the active site.[58] However, the mechanism of inhibition has not been reported. In contrast to the substrate derivatized inhibitors, nIPP represents a transition state analogue for the putative tertiary carbocationic intermediate generated during the isomerization of the substrates and is reported to bind to the active site via a slow, yet tight ionic interaction.[59]

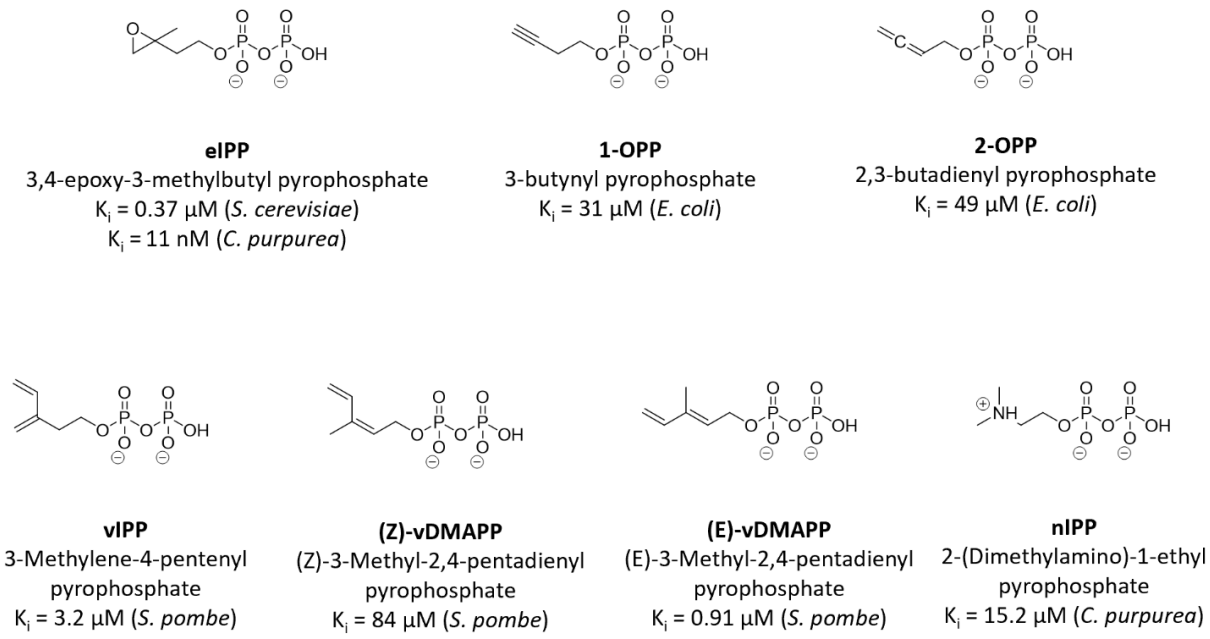

Figure 4 Type 1 Isopentenyl diphosphate isomerase inhibitors reported in the literature.

Despite the effective inhibitory activities exhibited by these inhibitors against type 1 IDI isolated from bacterial, fungal, and yeast species, their application for the inhibition of hIDI-1 has been discouraged due to the negative charges present on the pyrophosphate moiety and the short hydrocarbon chain lengths which render the molecules polar and prevents their permeation through the phospholipid bilayer of the cell membrane.[60] This poses a challenge for the exogenous incorporation of inhibitors into the cells for the modulation of hIDI-1 and emphasizes the requirement for the development of cell permeant inhibitors.

1.4 Design of Cell Permeant Inhibitors of hIDI-1

Passive targeting strategies can be employed to facilitate the exogenous delivery of hydrophilic molecules across the lipid membrane to increase their bioavailability with minimal cytotoxicity within the cell.[61] Such attempts would require establishing a balance between

lipophilicity and polarity of the compound, to enable passive permeation across the lipid membrane and sufficient solubility in the aqueous cellular environment.

The present work employs a prodrug strategy for the design of cell permeant inhibitors of hIDI-1. This strategy is commonly referred to as the 'double prodrug approach' which employs a 'trigger – linker – inhibitor' model, specific to the use of self-immolative linkers (**Figure 5**).[61,62] Masking the negative charges on the β-phosphate group of the pyrophosphate inhibitors with a self immolative linker and trigger unit contributes to the enhancement of lipophilicity and cell permeation. The 'trigger-linker' bond is susceptible to enzymatic cleavage within the cytosol of the cell which generates a highly unstable 'linker-inhibitor' intermediate that undergoes spontaneous disintegration to liberate the active, unmodified inhibitor molecule inside the cell. Self immolative linkers involving elimination reactions (p-hydroxybenzyl, p-hydroxy benzyloxy carbonyl, p-amino benzyloxy carbonyl) and cyclization reactions have been vastly exploited over the years. For the design of cell permeant inhibitors in this work, the p-hydroxy benzylic group has been employed as the linker, which in combination with an acyl moiety functioning as the trigger, form the acyloxybenzyl ester masking group.[63-65] The strategic masking of the β-phosphate group of pyrophosphates was originally studied by Baccile et al. with regards to the design, synthesis and evaluation of cell permeant IPP and DMAPP.[66] The study has revealed the successful application of acyloxybenzylic esters (acyl, hexyl, pivolyl and benzyl) to facilitate cell permeability of charged molecules with high polarity. The masked analog is susceptible to hydrolysis by esterases native to the cell which cleaves the acyl moiety (trigger) leading to the 1,6 benzylic elimination of the self immolative linker generating two molecules of carboxylic acid and quinone methide respectively. The study revealed that a variation in the alkyl chain length and steric effects of the acyl moiety posed a significant impact on lipophilicity and

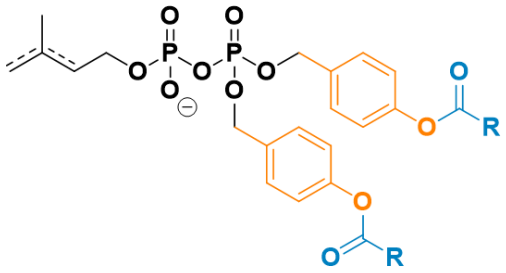

Figure 5 Masking approach adapted for the synthesis of cell-permeant inhibitors, as reported in Baccile et. al. The linker - p-hydroxy benzylic group is denoted in orange and the trigger - acyl moiety (R = alkyl group) is denoted in blue.

aqueous stability of the masked substrate analogs. In vitro studies on the masked DMAPP analogs revealed the hexyl, benzyl and pivolyl esters to be relatively stable in an aqueous environment in contrast to the acyl ester which has been prone to substantial degradation. Evaluation of the effect of masked analogs on the morphology and cell viability of the statin inhibited MVA pathway of U-87 MG cells has demonstrated a recovery of cell morphology by pivaloyl and benzyl esters and a rescue of cell viability by all ester masking groups used in the study.[66] Therefore, the study establishes the successful application of the acyl-, hexyl-, pivolyl- and benzyl- masked benzylic esters for inducing lipophilicity and sufficient aqueous stability of IPP and DMAPP within human cells. The masking strategy developed by Baccile et al. has been applied herein for the synthesis of a series of next generation cell-permeant inhibitors (**Figure 6**).

1.5 Mixed photocaged IPP

Over the last five decades, photolabile masking groups have been employed for the design of photocleavable probes which utilize light as a stimulus for the exogenous delivery of synthetic compounds with spatiotemporal precision for the regulation of cellular processes without perturbing the cellular system.[67-71] When designing photocleavable probes for cellular energy, especially in the NIR region (650 – 900 nm) are preferred since high energy photons

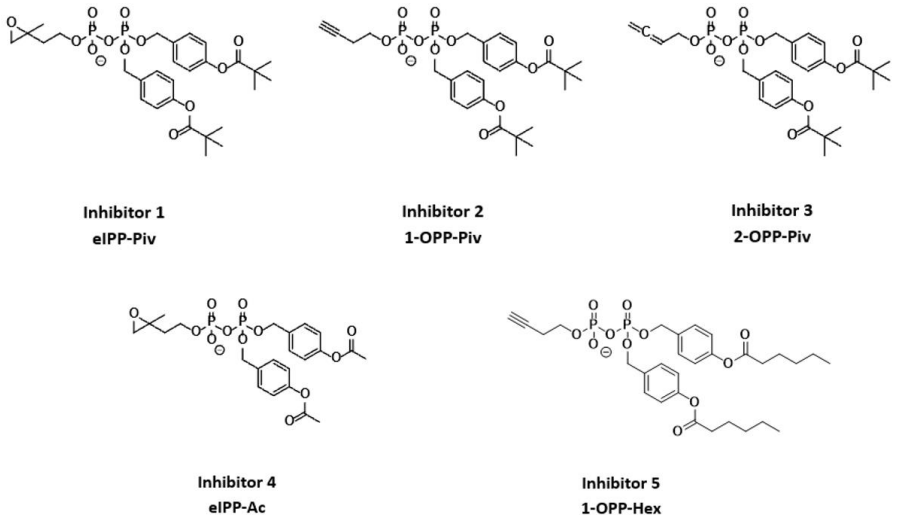

Figure 6 Series of next generation cell permeant inhibitors of type 1 human isopentenyl diphosphate isomerase, synthesized in the present work.

absorbing at lower wavelengths (< 650 nm) pose weak tissue penetration due to highly reactive interactions with intracellular biological matter such as hemoglobin and water.[72,73] Exposure to light in the UV range (< 400 nm) can cause phototoxicity via UV-induced formation of reactive oxygen species and reactive nitrogen species that damage membrane lipids and induce DNA and protein crosslinking, which result in mutations in cell signaling pathways.[73-75] Furthermore, it is of importance that photolabile groups maintain sufficient solubility and stability in aqueous media since > 70% of the cell environment is water. A large rate constant of cleavage ($k \propto$ molar absorptivity (ε) x quantum yield (ϕ)) and negligible toxicity from photocleaved byproducts are properties to be considered in the selection of the ideal photolabile group.[76,77]A wide range of photolabile groups and their derivatives absorbing in the wavelength range of UV – IR of the electromagnetic spectrum have been studied and their applications have been exhausted in biological systems. A few such important groups are bimane, p-hydroxy phenacyl, o-nitrobenzyl, (coumarin-4-yl)-methyl and boron dipyrromethene (BODIPY), and their properties have been discussed in **Table 1**.

Table 1 Properties of commonly encountered photocages.

Photocage	Maximum absorption wavelength / nm	Aqueous solubility	Byproduct toxicity	Efficiency
Bimane [78-81]	< 380	Good solubility	Hydroxyl bimane – nontoxic to living cells	Moderate quantum yields
p-hydroxy phenacyl [78,79,82]	< 380	Good solubility, stability, and compatibility in aq. Media and physiological conditions	p-hydroxyphenyl acetic acid – non-biocompatible and toxic.	High quantum yields (0.2-1.0), large rate constant (107 – 108 s^{-1}), high yields of leaving group released (60 – 90%).
o-nitrobenzyl 71,78,79	< 443	Good solubility	2-nitrosobenzaldehyde – highly reactive and toxic.	Moderately high quantum yields and rates of cleavage.
(Coumarin-4-yl)- methyl [78,79]	< 515	Poor solubility	Competitive fluorescent byproducts generated.	Moderately high quantum yields (0.05-0.39), high molar absorption coefficients, and rates of uncaging. The quantum yield of poorer leaving groups such as carboxylic acids, carbonic acids, and carbamic acids exhibits poor efficiency (0.004-0.03).
BODIPY [73,78,79]	< 700	Moderate solubility and stability in physiological conditions	BODIPY core is nontoxic. Styryl substitution for increased conjugation generates aldehyde upon cleavage. Heavy atom substitution/ halogenation favors photosensitizer behavior, generates singlet oxygen and poses toxicity.	High quantum yields with intense fluorescence and molar extinction coefficients. Alkylation of Boron and 2,6-diiodination drastically increase efficiency of photocleavage (9500 M^{-1} cm^{-1})

O-nitrobenzyl (oNB) is an efficient, yet simple photocage originated from the nitroaryl motif, which absorbs in the UV range at a λ_{max} of 365 nm.[83] The leaving group is often directly attached to the benzylic position and is the commonly employed method for the masking of phosphates, carboxylic acids and thiols, whereas alcohols and amines are attached as their carbonic acid derivatives.84-89 The photolytic cleavage of oNB is initiated by the excitation of molecules at the ground state (**Figure 7**), proceeding through the generation of an aci-nitro intermediate via intramolecular hydrogen abstraction by the nitro moiety.[83,84] The irreversible cyclization of the intermediate into a 1,3-dihdryobenzo[c]isoxazole-1-ol, and its subsequent ring opening and hydrolysis generates a hemiacetal intermediate, which releases a leaving group to form an o-nitroso benzaldehyde molecule as a byproduct.[90]

In the present study, a modification to the masking strategy discussed in **1.4** has been approached to introduce a photolabile group to mask a negative charge on the β-phosphate of IPP. A next-generation lipophilic and photocleavable derivative of IPP (Mixed photocaged IPP) has been synthesized by the Rossi lab at the Department of Chemistry, State University of New York at Cortland. The mixed photocaged IPP enhances the lipophilicity and facilitates the exogenous delivery of IPP into the cell via the pivaloyl masked benzyl ester group and facilitates the spatiotemporal controlled release of IPP via the noninvasive light induced cleavage (365 nm) of an unsubstituted oNB group (**Figure 8**). This approach results in a 'lock-in' effect as described by Meier et al., where the pivaloyl ester of the masked IPP would be subjected to hydrolysis by esterases native to the cell, generating the monoprotected oNB-IPP intermediate which is ideally non bioactive and avoids cellular efflux, thus 'locking in' the substrate within the cell.[71]

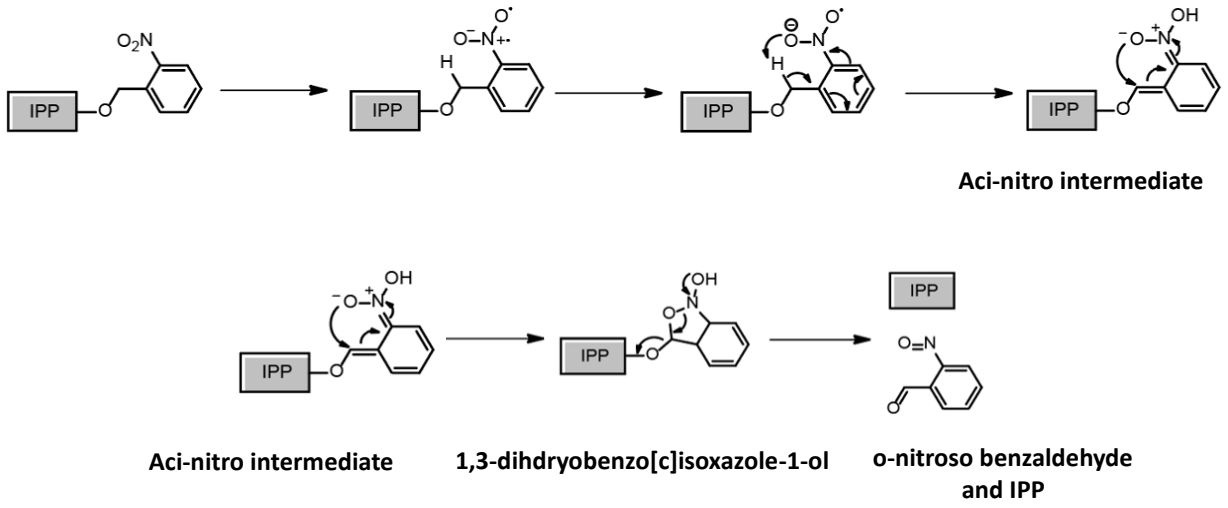

Figure 7 Photo-uncaging mechanism of ortho-nitrobenzyl photocage.

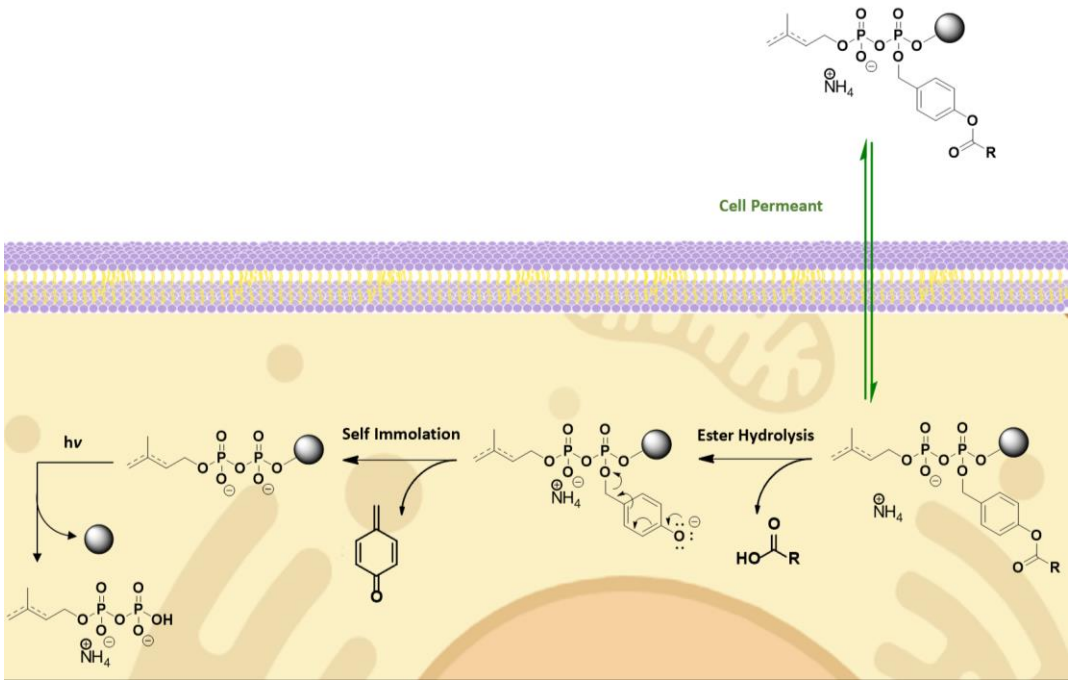

Figure 8 Masking approach employed for the synthesis of mixed photocaged IPP and the intracellular 'lock-in' mechanism of controlled substrate release.

CHAPTER TWO

MATERIALS AND METHODS

2.1 Synthesis of cell permeant inhibitors of human Isopentenyl Diphosphate Isomerase

The present study embarks primarily on synthesizing cell-permeant inhibitors of the hIDI-1 enzyme by inducing lipophilicity via masking negative charges on the β-phosphate of the pyrophosphate moiety by utilizing self-immolative esters.

A modular synthetic strategy was employed for the synthesis of the cell permeant inhibitors where **inhibitors 1-5** were synthesized via a one-pot reaction using their respective alcohols as the precursor compound. The initial step was the synthesis of the monophosphate, which occurred via the activation of the phosphate group by trichloro acetonitrile, followed by reacting with the precursor alcohol. The reaction of monophosphate with either the masked phosphonamidites (**inhibitors 1-4**) or masked H-phosphonate (**inhibitor 5**) results in the strategic incorporation of masking groups at the β-phosphate of the pyrophosphate compounds. The synthesized inhibitors were purified by gradient automated reverse phase chromatography, followed by ion exchange chromatography to exchange the cytotoxic tetrabutyl ammonium ion for ammonium ions, which have indicated little to no toxicity in human cells.

The synthesis of the cell-permeant epoxidized derivative of IPP was initiated by the epoxidation of the terminal alkene of isoprenol using meta-chloroperoxybenzoic acid (m-CPBA) as the oxidizing agent in a 1:1 ratio. Although the employed route for oxidation is direct and widely utilized for the epoxidation of alkenes, only low yields, approximating to 15% was afforded. These results can be attributed to the presence of excess unreacted acid in the reaction mixture which was not eliminated to its entirety via aqueous extraction. However, such low

yields did not disrupt the effective synthesis of pyrophosphates in sufficient yield. An alternate approach, such as dimethyl dioxirane-mediated epoxidation of alkenes can be employed to counteract the limitation of m-CPBA and improve the efficiency of IPP epoxidation. The reaction would generate oxygen gas and acetone as by-products, which can be eliminated rapidly and conveniently from the reaction system due to the high volatility of acetone, in contrast to the unreacted solid m-CPBA. The synthesis of the alkyne (inhibitors 1 and 5) and allene (inhibitor 3) based inhibitors proceeded via the direct phosphorylation of the respective alcohols 3-butyn-1-ol and 2,3-butadien-1-ol to form the monophosphates, which resulted in improved yields and synthetic efficiency. The successful synthesis of non-isolated monophosphates were primarily confirmed by the decoupled ^{31}P NMR. A singlet peak between 0 and 1 ppm in the spectra confirms the formation of monophosphate. Due the presence of unreacted starting material in the one-pot reaction mixture, the ^{1}H NMR exhibited repetitive peaks for the monophosphate and alcohol and therefore, have not been reported in this document.

The phosphorylation of monophosphates can proceed via the phosphoramidite pathway or alternatively, the H-phosphonate pathway. The incorporation of SIE onto phosphoramidites and H-phosphonates are initiated with the synthesis of acyloxy benzyl alcohol derivatives utilizing pivaloyl chloride, acyl chloride, and hexanoyl chloride for nucleophilic acyl substitution at the phenolic hydroxy group of p-hydroxy benzyl alcohol. In addition to proceeding via the reaction of interest, several byproducts are yielded such as mono-substitution at the benzylic hydroxy group, disubstituted derivative, and the unreacted p-hydroxy benzyl alcohol. However, the acyloxybenzyl alcohol was observed to be the major fraction and was isolated by purification in high yields. Although the phosphoramidite pathway and H-phosphonate pathway have been used alternatively for a common goal, they possess noteworthy advantages as opposed to the

other. Following the reaction of monophosphate with phosphoramidite, the oxidation of β-phosphorous to the phosphoryl group presents a requirement for an oxidizing agent such as tertbutyl hydrogen peroxide. In contrast, the need for an additional oxidation step is eliminated in the H-phosphonate route. However, proceeding the reaction of H-phosphonate with the one-pot reaction mixture containing monophosphate and unreacted alcohol requires the alcohol content to be less than 10% to allow for improved reaction efficiency and ease of purification.

The facile synthesis of the cell permeant pyrophosphate inhibitors of hIDI-1 result in low yields of < 30%. The poor efficiency of synthesis can be attributed to the extensive purification steps required for compound isolation. Pyrophosphates synthesized via the one-pot synthesis approach are subjected to two attempts of chromatographic purification and ion exchange. The initial purification via reverse phase column chromatography serves the purpose of isolating the pyrophosphate from the mixture phosphorylated compounds and unreacted monophosphate. The isolated pyrophosphate bears the tetrabutyl ammonium counterion which is bulky and reportedly cytotoxic. Ion exchange chromatography enables the exchange of the counter ion for nontoxic ammonium ions. However, the pyrophosphates are prone to degradation during ion exchange, generating monophosphate. A final reverse phase purification is essential for the isolation of the pyrophosphate inhibitors from the mixture of degradation products. Previous attempts at improving the yields and synthetic efficiency by eliminating the need for the first reverse phase purification was unsuccessful.

The successful synthesis of inhibitors was confirmed by ^{1}H NMR and ^{31}P NMR. The characteristic pair of doublets in the decoupled ^{31}P NMR appearing in the range of 11-14 ppm with similar coupling constants confirm the presence of two phosphorous atoms coupled to each other, indicative of a pyrophosphate moiety.

2.2 Synthetic Methodology

2.2.1 Materials

All reagents were purchased from either Fisher Scientific or Sigma-Aldrich and were used directly without additional purification. Dry solvents were prepared by distillation and stored over molecular sieves. All reactions were carried out in flame-dried glassware under an Argon atmosphere unless stated otherwise. Normal phase and reverse phase chromatography were conducted using prepacked silica gel and C18 columns respectively. Dowex50WX8 200-400 (H) cation exchange resin was used for the preparation of ion exchange columns. Gradient automated flash chromatography was performed on a Buchi Pure C-850 FlashPrep chromatography system. ^{1}H NMR and proton decoupled ^{31}P NMR spectra were recorded on a Bruker Ascend 500 at a field strength of 500 MHz with solvents indicated in the Appendix as the internal deuterium lock. Multiplicities have been recorded as s (singlet), d (doublet), dd (doublet of doublets), t (triplet), q (quartet) and m (multiplet). NMR analysis has been conducted using Mestrenova software (version 14.2.3) for the determination of coupling constants.

2.2.2 Synthesis of Bis(4-(hydroxymethyl)phenyl pivalate)-N,N-diisopropyl phosphoramidite (Compound 2)

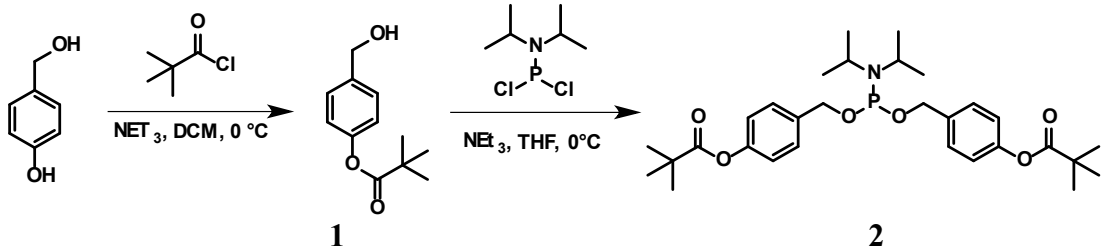

Scheme 1 Synthesis of Bis(4-(hydroxymethyl)phenyl pivalate)-N,N-diisopropyl phosphoramidite.

The synthesis of masked phospharamidites proceeds via the synthesis of the masked benzyl alcohol compounds. 4-hydroxybenzyl alcohol (7.45 g, 60 mmol, 1 eq) in 250 mL DCM was reacted with triethylamine (8.4 mL, 60 mmol, 1 eq) and the mixture was stirred under an Argon atmosphere over an ice bath. Trimethyl acetyl chloride (7.35 mL, 60 mmol, 1 eq) was added dropwise into the reaction mixture over 40 minutes, at a rate of 185 µL/min, and the reaction was allowed to stir for 24 hours. The resulting solution was extracted with water (2 x 100 mL) and brine, and the DCM extract was obtained and dried over anhydrous $MgSO_4$, followed by filtration. Concentration of the extract under reduced pressure afforded a white solid residue. Purification was carried out on a silica gel column (100% Hexanes/ 0% Ethyl Acetate – 100% Ethyl Acetate/ 0% Hexanes) followed by evaporation of the solvent to yield 58% of 4-(hydroxymethyl)phenyl pivalate, compound **1** as a white solid residue.

^{1}H NMR (500 MHz, $CDCl_3$) δ 7.37 (d, *J* = 8.5 Hz, 2H), 7.05 (d, *J* = 8.5 Hz, 2H), 4.69 (d, *J* = 6.0 Hz, 2H), 1.36 (s, 9H).

Compound **1** (6.00 g, 28.8 mmol, 2.15 eq) in 25 mL of THF was reacted with triethylamine (4.05 mL, 28.8 mmol, 2.15 eq) and allowed to stir under an Argon atmosphere until completely dissolved. The resulting mixture was added dropwise over 1 h into a solution of diisopropyl phosphoramidous dichloride (2.47 mL, 13.4 mmol, 1 eq) in THF (25 mL) under an Argon atmosphere over an ice bath. Upon completion, the reaction mixture was allowed to reach room temperature and was allowed to stir overnight. The reaction mixture was filtered three times under vacuum and was concentrated under reduced pressure to produce a clear oily residue. Purification was carried out on a silica gel column followed by evaporation of the solvent to yield 83% Bis(4-(hydroxymethyl)phenyl pivalate)-N,N-diisopropyl phosphoramidite, compound **2** as a white solid residue.

^{1}H NMR (500 MHz, $CDCl_3$) δ 7.34 (d, *J* = 6.3 Hz, 4H), 7.01 (d, *J* = 8.5 Hz, 4H), 4.76 – 4.65 (m, 4H), 3.72 – 3.65 (m, 2H), 1.35 (s, 18H), 1.20 (d, *J* = 6.8 Hz, 12H).

^{31}P NMR (202 MHz, $CDCl_3$) δ 147.99.

2.2.3 Synthesis of β-Bis(4-(hydroxymethyl)phenylpivalate)-3,4-epoxy-3-methyl-1-butyl pyrophosphate (Inhibitor 1)

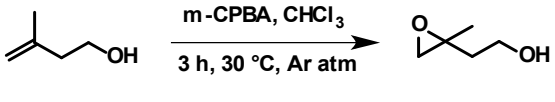

Scheme 2 Synthesis of 3,4-epoxy-3-methylbutan-1-ol.

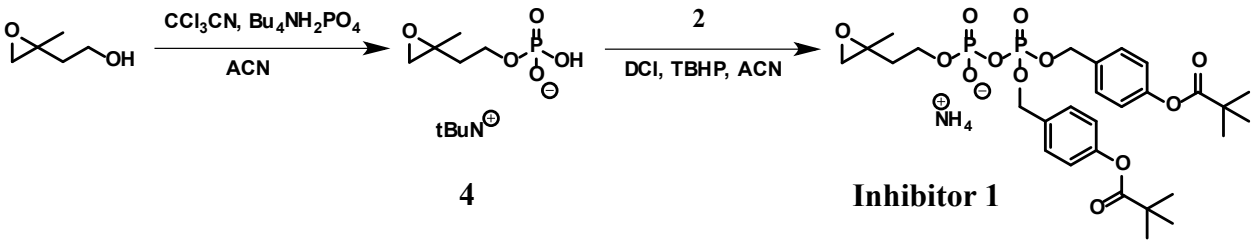

Scheme 3 Synthesis of β-Bis(4-(hydroxymethyl)phenylpivalate)-3,4-epoxy-3-methyl-1-butyl pyrophosphate.

The synthesis of inhibitor **1** proceeds with the use of 3,4-epoxy-3-methylbutan-1-ol, compound **3**, as the precursor material. 3-methylbut-3-en-1-ol (3.00 g, 34.8 mmol, 0.65 eq) in 20 mL of chloroform was reacted with 3-chloroperbenzoic acid (9.2 g, 53.3 mmol, 1 eq) dissolved in 60 mL of chloroform. The reaction mixture was stirred for 3 hours under an Argon atmosphere at 30 °C. The mixture was extracted with saturated K_2CO_3 (2 X 40 mL) and water. The chloroform fraction was extracted and dried over anhydrous $MgSO_4$ followed by filtration. Concentrating the filtrate under reduced pressure yielded 15% of compound **3** as a clear liquid.

^{1}H NMR (500 MHz, $CDCl_3$) δ 3.78 – 3.67 (m, 2H), 2.81 (d, *J* = 4.4 Hz, 1H), 2.64 (d, *J* = 4.5 Hz, 1H), 1.99 – 1.93 (m, 1H), 1.89 – 1.83 (m, 1H), 1.38 (s, 3H).

Compound **3** (200 mg, 1.96 mmol, 1.2 eq) and trichloro acetonitrile (196.5 µL, 1.96 mmol, 1.2 eq) was dissolved in dry ACN (2 mL) and was reacted with a solution of 0.4 M tetrabutyl ammonium phosphate in ACN (4.1 mL, 1.64 mmol, 1 eq) which was added dropwise over 30 minutes. Additional trichloro acetonitrile (20 µL) was added and the reaction mixture was stirred for 30 minutes under an Argon atmosphere. The solution was concentrated under reduced pressure and placed on the vacuum line overnight to form 3,4-epoxy-3-methyl-1-butyl monophosphate with the tetrabutyl ammonium counter ion, compound **4** as a viscous oil.
^{31}P NMR (202 MHz, $CDCl_3$) δ 0.97.

Compound **4** was reacted with compound **2** (480 mg, 0.98 mmol, 1.2 eq) and dissolved in dry ACN (1.5 mL). A solution of 0.25 M 4,5-dicyanoimidazole (96.8 mg, 0.82 mmol, 1 eq) in dry ACN (3.3 mL) was added in three fractions (1.1 mL each) at 5-minute intervals. The reaction mixture was stirred under an Argon atmosphere for 3-4 hours. Tertbutyl hydrogen peroxide (5.5 M in Decane, 178.2 µL, 0.98 mmol, 1.2 eq) was added and the reaction mixture was stirred for 45 minutes to 1 hour. The resulting solution was concentrated under reduced pressure. Purification was carried out on a C18 EcoFlex column followed by lyophilization. The lyophilized compound was subjected to ion exchange by gradient automated chromatography.

The compound was dissolved in approx. 0.5 mL solution of 25 mM ammonium bicarbonate and 2% isopropyl alcohol and passed through a column packed with 8g Dowex50WX8 and conditioned with DI water (30 minutes), 1M HCl (20 min), DI water (20 minutes), 25% ammonium hydroxide (20 minutes), and 25 mM ammonium bicarbonate with 2% isopropyl alcohol (20 minutes). The elution buffer used was 25 mM ammonium bicarbonate with

2% isopropyl alcohol. The ion exchanged compound was lyophilized and the resulting product was repurified on a C18 EcoFlex column. The product fractions were combined and subjected to lyophilization to yield 15% of β-Bis(4-(hydroxymethyl)phenyl pivalate)-3,4-epoxy-3-methyl-1-butyl pyrophosphate, **inhibitor 1**, as a low density white solid.

^{1}H NMR (500 MHz, CD$_3$OD_SPE) δ 7.40 (d, *J* = 8.7 Hz, 4H), 7.04 (d, *J* = 8.5 Hz, 4H), 5.12 (d, *J* = 8.4 Hz, 4H), 4.09 – 4.02 (m, 2H), 2.73 (d, *J* = 4.7 Hz, 1H), 2.56 (d, *J* = 4.6 Hz, 1H), 2.00 – 1.96 (m, 1H), 1.81 – 1.76 (m, 1H), 1.35 (s, 18H), 1.32 (s, 3H).

^{31}P NMR (202 MHz, CD$_3$OD_SPE) δ -11.50 (d, *J* = 21.3 Hz), -12.97 (d, *J* = 20.0 Hz).

2.2.4 Synthesis of β-Bis(4-(hydroxymethyl)phenyl pivalate)-3-butyn-1-yl pyrophosphate (Inhibitor 2)

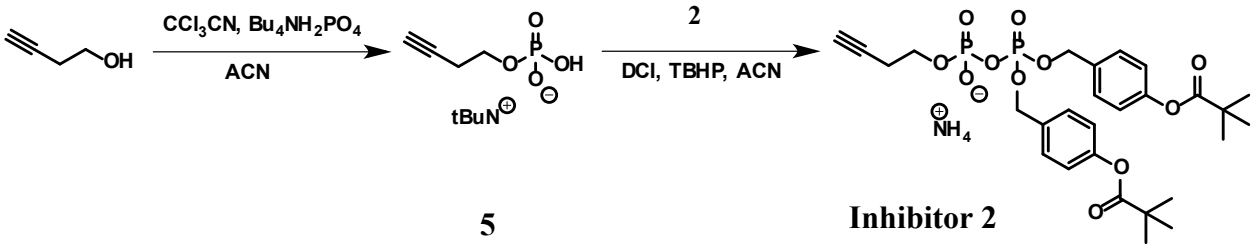

Scheme 4 Synthesis of β-Bis(4-(hydroxymethyl)phenyl pivalate)-3-butyn-1-yl pyrophosphate.

3-butyn-1-ol (300 mg, 4.28 mmol, 2 eq) and trichloro acetonitrile (370 mg, 2.56 mmol, 1.2 eq) was dissolved in dry ACN (3 mL) and was reacted with a solution of 0.4 M tetrabutyl ammonium phosphate in ACN (5.35 mL, 2.14 mmol, 1 eq) which was added dropwise over 30 minutes. Additional trichloro acetonitrile (20 μL) was added and the reaction mixture was stirred for 30 minutes under an Argon atmosphere. The solution was concentrated under reduced pressure and placed on the vacuum line overnight to form 3-butyn-1-yl monophosphate with the tetrabutyl ammonium counter ion, compound **5** as a viscous oil.

^{31}P NMR (202 MHz, CD_3CN) δ 0.31.

Compound **5** was reacted with compound **2** (1.25 g, 2.56 mmol, 1.2 eq) and dissolved in dry ACN (1.5 mL). A solution of 0.25 M 4,5-dicyanoimidazole (251 mg, 2.13 mmol, 1 eq) in dry ACN (8.52 mL) was added in three fractions (2.84 mL each) at 5-minute intervals. The reaction mixture was stirred for 3-4 hours under an Argon atmosphere. Tertbutyl hydrogen peroxide (5.5 M in Decane (465 μL, 2.56 mmol, 1.2 eq) was added and the reaction mixture was stirred for 45 minutes to 1 hour. The resulting solution was concentrated under reduced pressure. Purification was carried out on a C18 EcoFlex column followed by lyophilization. The lyophilized compound was subjected to ion exchange by gradient automated chromatography. The compound was dissolved in approx. 0.5 mL solution of 25 mM ammonium bicarbonate and 2% isopropyl alcohol and passed through a column packed with 8g Dowex50WX8 and conditioned with DI water (30 minutes), 1M HCl (20 min), DI water (20 minutes), 25% ammonium hydroxide (20 minutes), and 25 mM ammonium bicarbonate with 2% isopropyl alcohol (20 minutes). The elution buffer used was 25 mM ammonium bicarbonate with 2% isopropyl alcohol. The ion exchanged compound was lyophilized and the resulting product was repurified on a C18 EcoFlex column. The product fractions were combined and subjected to lyophilization to yield 29% of β-Bis(4-(hydroxymethyl) phenyl pivalate)-3-butyn-1-yl pyrophosphate **inhibitor 2**, as a low density white solid.

^{1}H NMR (500 MHz, MeOD) δ 7.40 (d, *J* = 8.7 Hz, 4H), 7.03 (d, *J* = 8.5 Hz, 4H), 5.13 (d, *J* = 8.5 Hz, 4H), 4.04 (d, *J* = 7.5 Hz, 2H), 2.53 – 2.51 (m, 2H), 2.24 (d, *J* = 2.7 Hz, 1H), 1.35 (s, 18H).

^{31}P NMR (202 MHz, MeOD) δ -11.81 (d, *J* = 21.3 Hz), -13.04 (d, *J* = 21.3 Hz).

2.2.5 Synthesis of β-Bis(4-(hydroxymethyl)phenyl pivalate)-2,3-butadien-1-yl pyrophosphate (Inhibitor 3)

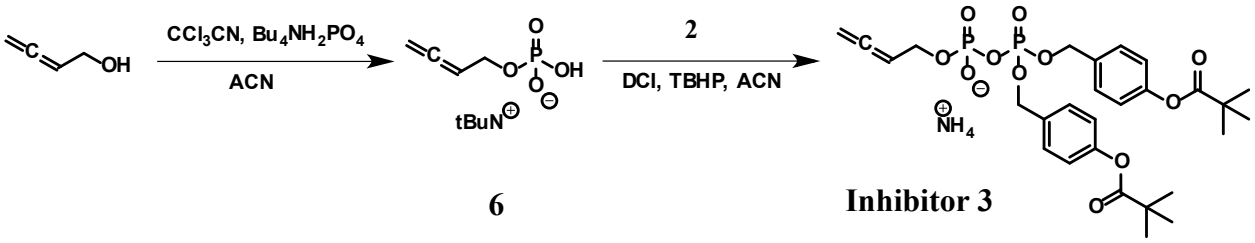

Scheme 5 Synthesis of β-Bis(4-(hydroxymethyl)phenyl pivalate)-2,3-butadien-1-yl pyrophosphate.

2,3-butadien-1-ol (250 mg, 3.57 mmol, 2 eq) and trichloro acetonitrile (214.6 µL, 2.14 mmol, 1.2 eq) was dissolved in dry ACN (2.5 mL) and was reacted with a solution of 0.4 M tetrabutyl ammonium phosphate in ACN (4.45 mL, 1.78 mmol, 1 eq) which was added dropwise over 30 minutes. Additional trichloro acetonitrile (0.2 eq) was added and the reaction mixture was stirred for 30 minutes under an Argon atmosphere. The solution was concentrated under reduced pressure and placed on the vacuum line overnight to form 2,3-butadien-1-yl monophosphate with the tetrabutyl ammonium counter ion, compound **6** as a viscous oil.

^{31}P NMR (202 MHz, CD_3CN) δ 0.39.

Compound **6** was reacted with compound **2** (1.05 g, 2.14 mmol, 1.2 eq) and dissolved in dry ACN (1.5 mL). A solution of 0.25 M 4,5-dicyanoimidazole (210.22 mg 1.78 mmol, 1 eq) in dry ACN (7.12 mL) was added in three fractions (2.4 mL each) at 5 minute intervals. The reaction mixture was stirred for 3-4 hours under an Argon atmosphere. Tertbutyl hydrogen peroxide (5.5 M in Decane, 389 µL, 2.14 mmol, 1.2 eq) was added and the reaction mixture was stirred for 45 minutes to 1 hour. The resulting solution was concentrated under reduced pressure. Purification was carried out on a C18 EcoFlex column followed by lyophilization. The lyophilized compound was subjected to ion exchange by gradient automated chromatography.

The compound was dissolved in approx. 0.5 mL solution of 25 mM ammonium bicarbonate and 2% isopropyl alcohol and passed through a column packed with 8g Dowex50WX8 and conditioned with DI water (30 minutes), 1M HCl (20 min), DI water (20 minutes), 25% ammonium hydroxide (20 minutes), and 25 mM ammonium bicarbonate with 2% isopropyl alcohol (20 minutes). The elution buffer used was 25 mM ammonium bicarbonate with 2% isopropyl alcohol. The ion exchanged compound was lyophilized and the resulting product was repurified on a C18 EcoFlex column. The product fractions were combined and subjected to lyophilization to yield 31% of β-Bis(4-(hydroxymethyl)phenyl pivalate)-2,3-butadien-1-yl pyrophosphate, **inhibitor 3**, as a low density white solid.

^{1}H NMR (500 MHz, $CDCl_3$) δ 7.29 (d, *J* = 8.5 Hz, 4H), 6.97 (d, *J* = 8.5 Hz, 4H), 5.28 (t, *J* = 6.8 Hz, 1H), 5.02 (d, *J* = 8.3 Hz, 4H), 4.74 – 4.70 (m, 2H), 4.42 – 4.37 (m, 2H), 1.33 (s, 18H).

^{31}P NMR (202 MHz, $CDCl_3$) δ -11.40 (d, *J* = 16.3 Hz), -11.82 (d, *J* = 15.0 Hz).

2.2.6 Synthesis of Bis(4-(hydroxymethyl)phenyl acetate)-N,N-diisopropyl phosphoramidite (Compound 8)

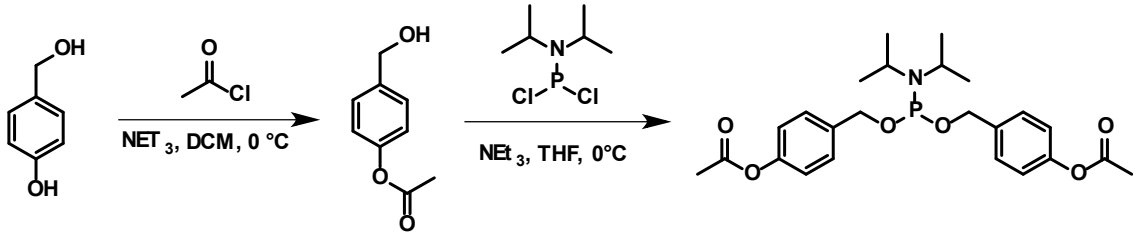

7 **8**

Scheme 6 Synthesis of Bis(4-(hydroxymethyl)phenyl acetate)-N,N-diisopropyl phosphoramidite.

4-hydroxybenzyl alcohol (7.45 g, 60 mmol, 1 eq) in 250 mL DCM was reacted with triethylamine (8.4 mL, 60 mmol, 1 eq) and the mixture was stirred under an Argon atmosphere

over an ice bath. Acetyl chloride (4.3 mL, 60 mmol, 1 eq) was added dropwise into the reaction mixture over 40 minutes, at a rate of 107.5 μL/min, and the reaction was allowed to stir for 24 hours. The resulting solution was extracted with water (2 x 100 mL) and brine, and the DCM extract was obtained and dried over anhydrous MgSO4, followed by filtration. Concentrating the extract under reduced pressure afforded a white solid residue. Purification was carried out on a silica gel column (100% Hexanes/ 0% Ethyl Acetate – 100% Ethyl Acetate/ 0% Hexanes) followed by evaporation of the solvent to yield 39% of 4-(hydroxymethyl)phenyl acetate compound **7** as a clear liquid.

^{1}H NMR (500 MHz, $CDCl_3$) δ 7.38 (d, *J* = 8.2 Hz, 2H), 7.08 (d, *J* = 8.5 Hz, 2H), 4.68 (d, *J* = 1.7 Hz, 2H), 2.30 (s, 3H).

Compound **7** (3.38 g, 20.32 mmol, 2.15 eq) in 25 mL of THF was reacted with triethylamine (2.85 mL, 20.32 mmol, 2.15 eq) and allowed to stir under an Argon atmosphere until completely dissolved. The resulting mixture was added dropwise over 1 h into a solution of diisopropyl phosphoramidous dichloride (1.81 mL, 9.45 mmol, 1 eq) in THF (25 ml) under an Argon atmosphere over an ice bath. Upon completion, the reaction mixture was allowed to reach room temperature and was allowed to stir overnight. The reaction mixture was filtered three times under vacuum and was concentrated under reduced pressure to produce a clear oily residue. Purification was carried out on a silica gel column followed by evaporation of the solvent to yield 30% of Bis(4-(hydroxymethyl)phenyl acetate)-N,N-diisopropyl phosphoramidite, compound **8** as a white solid residue.

^{1}H NMR (500 MHz, $CDCl_3$) δ 7.35 (d, *J* = 8.7 Hz, 4H), 7.04 (d, *J* = 8.5 Hz, 4H), 4.76 – 4.65 (m, 4H), 3.72 – 3.66 (m, 2H), 2.29 (s, 6H), 1.20 (d, *J* = 6.7 Hz, 12H).

^{31}P NMR (202 MHz, $CDCl_3$) δ 148.03.

2.2.7 Synthesis of β-Bis(4-(hydroxymethyl)phenyl acetate)-3,4-epoxy-3-methyl-1-butyl pyrophosphate (Inhibitor 4)

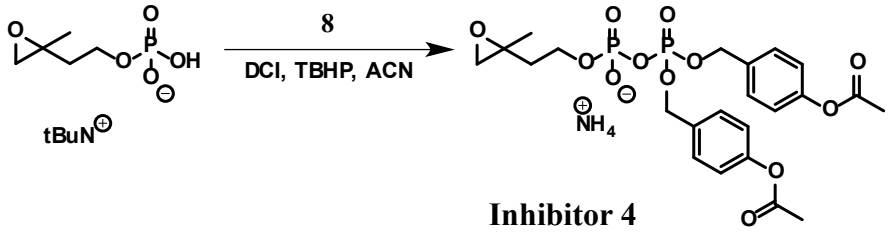

Inhibitor 4

Scheme 7 Synthesis of β-Bis(4-(hydroxymethyl)phenyl acetate)-3,4-epoxy-3-methyl-1-butyl pyrophosphate.

Compound **4** was reacted with compound **8** (500 mg, 1.08 mmol, 1.2 eq) and dissolved in dry ACN (1.6 mL). A solution of 0.25 M 4,5-dicyanoimidazole (106.29 mg, 0.90 mmol, 1 eq) in dry ACN (3.6 mL) was added in three fractions (1.2 mL each) at 5 minute intervals. The reaction mixture was stirred for 3-4 hours under an Argon atmosphere. Tertbutyl hydrogen peroxide (5.5 M in Decane, 196.4 µL, 1.08 mmol, 1.2 eq) was added and the reaction mixture was stirred for 45 minutes to 1 hour. The resulting solution was concentrated under reduced pressure. Purification was carried out on a C18 EcoFlex column followed by lyophilization. The lyophilized compound was subjected to ion exchange by gradient automated chromatography. The compound was dissolved in approx. 0.5 mL solution of 25 mM ammonium bicarbonate and 2% isopropyl alcohol and passed through a column packed with 8g Dowex50WX8 and conditioned with DI water (30 minutes), 1M HCl (20 min), DI water (20 minutes), 25% ammonium hydroxide (20 minutes), and 25 mM ammonium bicarbonate with 2% isopropyl alcohol (20 minutes). The elution buffer used was 25 mM ammonium bicarbonate with 2% isopropyl alcohol. The ion exchanged compound was lyophilized and the resulting product was

repurified on a C18 EcoFlex column. The product fractions were combined and subjected to lyophilization to yield 2% of β-Bis(4-(hydroxymethyl)phenyl acetate)-3,4-epoxy-3-methyl-1-butyl pyrophosphate, **inhibitor 4**, as a low density white solid.

^{1}H NMR (500 MHz, MeOD) δ 7.41 (d, *J* = 8.4 Hz, 4H), 7.08 (d, *J* = 8.5 Hz, 4H), 5.12 (d, *J* = 8.4 Hz, 4H), 4.07 – 4.03 (m, 2H), 2.72 (d, *J* = 4.7 Hz, 1H), 2.55 (d, *J* = 4.7 Hz, 1H), 2.27 (s, 6H), 1.96 (d, *J* = 7.0 Hz, 1H), 1.79 (d, *J* = 7.2 Hz, 1H), 1.31 (s, 3H).

^{31}P NMR (202 MHz, MeOD) δ -11.51 (d, *J* = 21.3 Hz), -13.00 (d, *J* = 21.3 Hz).

2.2.8 Synthesis of Bis(4-(hydroxymethyl)phenyl hexanoate) H-phosphonate (Compound 10)

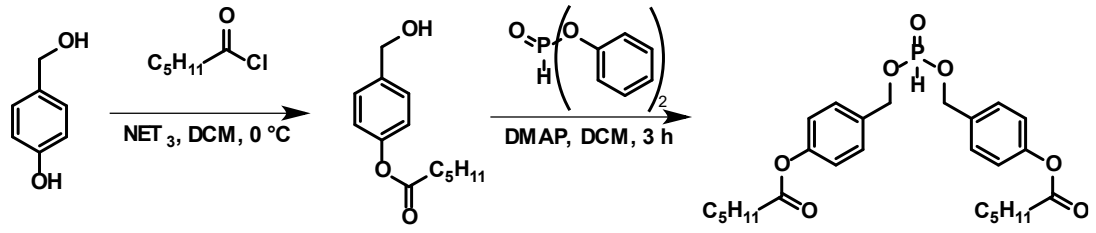

9 **10**

Scheme 8 Synthesis of Bis(4-(hydroxymethyl)phenyl hexanoate) H-phosphonate.

A masked H-phosphonate, compound **10**, was employed for the generation of the protected β-phosphate moiety of **inhibitor 5**, as an alternate route to the phosphoramidite pathway described in **2.1.2** and **2.1.6** (via compounds **2** and **8**). The synthesis proceeded via the oxidative chlorination of H-phosphonate by N-chlorosuccinimide, to generate a stronger leaving group to be replaced upon reaction with N-methylimidazole. Coupling with the monophosphate results in the formation of the phosphoanhydride bond (P-O-P) of the pyrophosphate, eliminating the requirement for oxidation for phosphorous by tertbutyl hydrogen peroxide. **Inhibitor 5** was purified by gradient

automated reverse phase chromatography, followed by ion exchange chromatography to exchange the cytotoxic tetrabutyl ammonium ion for ammonium ions.

The synthesis of masked H-phosphonates proceeds via the synthesis of the masked benzyl alcohol compounds. 4-hydroxybenzyl alcohol (3.10 g, 25 mmol, 1 eq) in 150 mL DCM was reacted with triethylamine (3.51 mL, 25 mmol, 1 eq) and the mixture was stirred under an Argon atmosphere over an ice bath. Hexanoyl chloride (3.5 mL, 25 mmol, 1 eq) was added dropwise into the reaction mixture over 40 minutes, at a rate of 87.35 µL/min, and the reaction was stirred for 24 hours. The resulting solution was extracted with water (2 x 150 mL) and brine, and the DCM extract was obtained and dried over anhydrous $MgSO_4$, followed by filtration. Concentration of the extract under reduced pressure afforded a white solid residue. Purification was carried out on a silica gel column (100% Hexanes/ 0% Ethyl Acetate – 100% Ethyl Acetate/ 0% Hexanes) followed by evaporation of the solvent to yield 56% of 4-(hydroxymethyl)phenyl hexanoate, compound **9**.

^{1}H NMR (500 MHz, $CDCl_3$) δ 7.37 (d, *J* = 8.7 Hz, 2H), 7.07 (d, *J* = 8.5 Hz, 2H), 4.68 (s, 2H), 2.55 (t, *J* = 7.5 Hz, 2H), 1.76 (p, *J* = 7.4 Hz, 2H), 1.43 – 1.36 (m, 4H), 0.96 – 0.91 (m, 3H).

Compound **9** (2.18 g, 9.8 mmol, 2 eq) and diphenyl phosphite (940 µL, 4.9 mmol, 1 eq) in 60 mL of DCM was reacted with 4-dimethyl aminopyridine (119.7 mg, 0.98 mmol, 0.2 eq). The reaction mixture was stirred for 24 hours under an Argon atmosphere. Purification was carried out on a silica gel column followed by evaporation of the solvent to yield 61% of Bis(4-(hydroxymethyl)phenyl hexanoate) H-phosphonate, compound **10** as a clear oily residue.

^{1}H NMR (500 MHz, $CDCl_3$) δ 7.64 (s, 0.5H), 7.36 (d, *J* = 8.5 Hz, 4H), 7.08 (d, *J* = 8.5 Hz, 4H), 6.23 (s, 0.5H), 5.08 – 5.00 (m, 4H), 2.55 (t, *J* = 7.6 Hz, 4H), 1.76 (t, *J* = 7.5 Hz, 4H), 1.39 (q, *J* =

3.6 Hz, 8H), 0.93 (t, *J* = 7.2 Hz, 6H).

^{31}P NMR (202 MHz, $CDCl_3$) δ 7.68.

2.2.9 Synthesis of β-Bis(4-(hydroxymethyl)phenyl hexanoate)-3-butyn-1-yl pyrophosphate (**Inhibitor 5)**

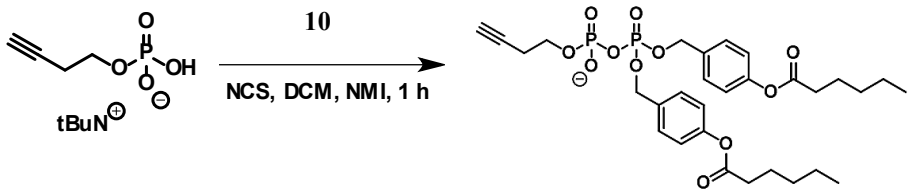

Inhibitor 5

Scheme 9 Synthesis of β-Bis(4-(hydroxymethyl)phenyl hexanoate)-3-butyn-1-yl pyrophosphate.

The crude monophosphate, compound **5**, was reacted with H-phosphonate (compound **10**) (346.2 mg, 0.85 mmol, 1 eq) and dissolved in DCM (8.5 mL). N-chlorosuccinimide (136.2 mg, 1.02 mmol, 1 eq), and N-methylimidazole (203.3 µL, 2.55 mmol, 3 eq) was added into the reaction mixture and stirred for 1 hour under an Argon atmosphere. The resulting solution was concentrated under reduced pressure.

Purification was carried out on a C18 EcoFlex column followed by lyophilization. The lyophilized compound was subjected to ion exchange by manual chromatography. The compound was dissolved in approx. 0.5 mL solution of 25 mM ammonium bicarbonate and 2% isopropyl alcohol and passed through a column packed with 8g Dowex50WX8 and conditioned with DI water (200 mL), 1M HCl (150 mL), DI water (200 mL), 25% ammonium hydroxide (150 mL), and 25 mM ammonium bicarbonate with 2% isopropyl alcohol (400 mL). The elution buffer used was 25 mM ammonium bicarbonate with 2% isopropyl alcohol. The ion exchanged compound was lyophilized and the resulting product was repurified on a C18 EcoFlex column.

The product fractions were combined and subjected to lyophilization to yield 54% of β-Bis(4 (hydroxymethyl)phenyl hexanoate)-3-butyn-1-yl pyrophosphate **inhibitor 5**, as a low density white solid.

^{1}H NMR (500 MHz, MeOD) δ 7.40 (d, *J* = 8.7 Hz, 4H), 7.06 (d, *J* = 8.5 Hz, 4H), 5.12 (d, *J* = 8.5 Hz, 4H), 4.07 – 4.01 (m, 2H), 2.57 (t, *J* = 7.4 Hz, 4H), 2.52 (td, *J* = 7.1, 2.7 Hz, 2H), 2.24 (t, *J* = 2.7 Hz, 1H), 1.77 – 1.71 (m, 4H), 1.43 – 1.38 (m, 8H), 0.97 – 0.93 (m, 6H).

^{31}P NMR (202 MHz, MeOD) δ -11.82 (d, *J* = 20.0 Hz), -13.04 (d, *J* = 21.3 Hz).

2.3 Evaluation of inhibitory potential

2.3.1 Materials

Type 1 Human Isopentenyl Diphosphate Isomerase Recombinant Protein was purchased from Boster Biological Technology. AlamarBlue^{TM} HS cell viability reagent was purchased from Invitrogen. All plated cells were subjected to imaging and analysis using the Cytation 1 cell imaging multiplate reader and Gen5 software from BioTek Instruments (Winooski, VT).

2.3.2 In vitro evaluation of inhibitory potential

The inhibitory potential of **inhibitors 1-3**, against hIDI-1 enzyme was measured at concentrations of 100 µM, 10 µM, 1 µM, and 0.1 µM. A 50 µL volume of sample mixtures were prepared by the addition of Brevianamide F (2 µL, 25 mM), NOTF (1.15 µL, 218 µM in pH 7.9 buffer containing Tris HCl, NaCl and glycerol), IPP (1.5 µL, 50 mM), inhibitor (1 µL, 5 mM/ 0.5 mM/ 0.05 mM/ 0.005 mM prepared by sequential dilution in DMSO), PLE (5 µL) and hIDI-1 (20 µL, 1 µM in pH 8.0 buffer containing Tris HCl, DTT, NaCl and glycerol) into a solution of $MgCl_2.6H_2O$ (1 µL, 250 mM) and pH 7.9 buffer solution (18.35 µL). The positive control for the

quantification of Deoxy brevianamide E was prepared by the Brevianamide F (2 µL, 25 mM), NOTF (1.15 µL, 218 µM in pH 7.9 buffer), IPP (1.5 µL, 50 mM) and hIDI-1 (20 µL, 1 µM in pH 8.0 buffer) into a solution of $MgCl_2.6H_2O$ (1 µL, 250 mM) and pH 7.9 buffer solution (24.35 µL).

The samples were prepared in triplicate and were incubated at 30 °C for 24 hours. A 20 µL volume of each sample was extracted into a conical vial and quenched with 20 µL of HPLC grade Methanol. The mixture was vortexed for 10 seconds and centrifuged for 10 minutes at 16000 xg. A 5 µL volume of the resulting supernatant was extracted and diluted with 750 µL of DI water in an autosampler vial. The inhibitory potential of each inhibitor was evaluated by analyzing the variation in peak area observed for Brevianamide F and Deoxy brevianamide E via liquid-chromatography high-resolution mass spectrometry analysis (LC-HRMS).

LC-HRMS spectra were recorded on a Agilent 6530 mass spectrometer coupled to an Agilent 1290 Infinity UHPLC with an Agilent HPH Poroshell C18 column (2.7 µm) for chromatography under the following conditions,

Mobile Phase A: 0.05% Ammonium Hydroxide in water

Mobile Phase B: 1:1 Methanol: Acetonitrile

Injection Volume: 3 µL

Quadrupole Time-of-flight (QTOF) Mass Spectrometry conditions,

Polarity: Negative ion mode

Gas Temperature: 300 °C

Vaporizer/Sheath Gas Temperature: 350 °C

Nebulizer pressure: 25 psig

Acquisition Mode: Mass Spectrometry (MS), High Resolution

Data analysis was conducted using Agilent MassHunter Quantitative analysis software.

2.3.3 In vivo evaluation of inhibitory potential

The cellular evaluation of inhibitory potential was conducted by Dillon McBee, a fifth-year graduate student at the Baccile lab, using the procedure described herein.

MDA-MB-231 cell line was prepared by growing the cells approximately 5 mL of DMEM supplemented with 1% penicillin/streptomycin and 10% Fetal Bovine serum (FBS) in a humidified incubator at 37 °C and 5% CO_2. The cells were plated at approximately 80% confluency 24 well plates at 50,000 cells/mL per well, were incubated for 24 hours and imaged using the Cytation 1 imager before feeding of the sample compounds.

Preparation of well plates with sample compounds

All compounds were premixed with the surfactant pluronics and plated in triplicate (**Table 2-6**) in two 24 well plates and incubated for 48 hours at 37 °C, 5% CO_2, before conducting the cell viability assay.

Monitoring cell viability of inhibitor-treated cells

Cell viability was monitored by adding 100 µL of prewarmed alamarBlue HS into each well and subjecting the well plates to incubation for a time period of 4 hours. Fluorescence measurements were then obtained at 590 nm and normalized as a percentage using the following equation,

$$Percentage\ Fluorescence = \left[\frac{Sample_{\ 590\ nm}}{Vehicle_{\ 590\ nm}}\right] \times 100$$

Table 2 Plating layout for monitoring the rescue of Pitavastatin (PITA) treated – MDA cells with GGOH, Piv-GPP.

	1	2	3	4	5	6
A	Vehicle (1µL DMSO)	Vehicle (1µL DMSO)	Vehicle (1µL DMSO)	PITA (100 nM, 1 µL)	PITA (100 nM, 1 µL)	PITA (100 nM, 1 µL)
B	PITA (500 nM, 0.5 µL)	PITA (500 nM, 0.5 µL)	PITA (500 nM, 0.5 µL)	PITA (1 µM, 1 µL)	PITA (1 µM, 1 µL)	PITA (1 µM, 1 µL)
C	PITA (10 µM)+ Piv-GPP (100 µM, 2µL)+ 15% PLUR in DMSO	PITA (10 µM)+ Piv-GPP (100 µM, 2µL)+ 15% PLUR in DMSO	PITA (10 µM)+ Piv-GPP (100 µM, 2µL)+ 15% PLUR in DMSO	PITA (10 µM) + GGOH (20 µM, 1µL)	PITA (10 µM) + GGOH (20 µM, 1µL)	PITA (10 µM) + GGOH (20 µM, 1µL)
D	PITA (5 µM, 0.5 µL)	PITA (5 µM, 0.5 µL)	PITA (5 µM, 0.5 µL)	PITA (10 µM, 1 µL)	PITA (10 µM, 1 µL)	PITA (10 µM, 1 µL)

Table 3 Plating layout for monitoring the dose dependent inhibition of Inhibitor 1 (eIPP-Piv) treated – MDA cells.

	1	2	3	4	5	6
A	Vehicle (2.5 µL DMSO, 2.5 µL 15% Plur)	Vehicle (2.5 µL DMSO, 2.5 µL 15% Plur)	Vehicle (2.5 µL DMSO, 2.5 µL 15% Plur)	eIPP (1 µM, 1 µL [from 1:1000 dilution in DMSO], + Plur (15%, 1µL)	eIPP (1 µM, 1 µL [from 1:1000 dilution in DMSO], + Plur (15%, 1µL)	eIPP (1 µM, 1 µL [from 1:1000 dilution in DMSO], + Plur (15%, 1µL)
B	eIPP (10 µM, 1 µL[From 1:100 dilution in DMSO), + Plur (15%, 1µL)	eIPP (10 µM, 1 µL[From 1:100 dilution in DMSO), + Plur (15%, 1µL)	eIPP (10 µM, 1 µL[From 1:100 dilution in DMSO), + Plur (15%, 1µL)	eIPP (25 µM, 0.25 µL),+DMSO (0.75 µL) + Plur (15%, 1µL)	eIPP (25 µM, 0.25 µL),+DMSO (0.75 µL) + Plur (15%, 1µL)	eIPP (25 µM, 0.25 µL),+DMSO (0.75 µL) + Plur (15%, 1µL)
C	eIPP (50 µM, 0.5 µL),+ DMSO (0.5 µL) + Plur (15%, 1µL)	eIPP (50 µM, 0.5 µL),+ DMSO (0.5 µL) + Plur (15%, 1µL)	eIPP (50 µM, 0.5 µL),+ DMSO (0.5 µL) + Plur (15%, 1µL)	eIPP (100 µM, 1 µL), + Plur (15%, 1µL)	eIPP (100 µM, 1 µL), + Plur (15%, 1µL)	eIPP (100 µM, 1 µL), + Plur (15%, 1µL)
D	eIPP (175 µM, 1.75 µL), + Plur (15%, 1.75 µL)	eIPP (175 µM, 1.75 µL), + Plur (15%, 1.75 µL)	eIPP (175 µM, 1.75 µL), + Plur (15%, 1.75 µL)	eIPP (250 µM, 2.5 µL), + Plur (15%, 2.5 µL)	eIPP (250 µM, 2.5 µL), + Plur (15%, 2.5 µL)	eIPP (250 µM, 2.5 µL), + Plur (15%, 2.5 µL)

Table 4 Plating layout for monitoring the rescue of Inhibitor 1 (eIPP-Piv) treated – MDA cells with GGOH, Piv-DMAPP and Piv-GPP.

	1	2	3	4	5	6
A	Vehicle (2 µL DMSO, 2 µL 15% Plur)	Vehicle (2 µL DMSO, 2 µL 15% Plur)	Vehicle (2 µL DMSO, 2 µL 15% Plur)	eIPP (100 µM, 1 µL), + Plur (15%, 1µL)	eIPP (100 µM, 1 µL), + Plur (15%, 1µL)	eIPP (100 µM, 1 µL), + Plur (15%, 1µL)
B	eIPP (100 µM, 1 µL), Piv-DMAPP (100 µM, 1 µL),+ Plur (15%, 2µL)	eIPP (100 µM, 1 µL), Piv-DMAPP (100 µM, 1 µL),+ Plur (15%, 2µL)	eIPP (100 µM, 1 µL), Piv-DMAPP (100 µM, 1 µL),+ Plur (15%, 2µL)	eIPP (100 µM, 1 µL), GGOH (20 µM, 1 uL),+ Plur (15%, 1µL)	eIPP (100 µM, 1 µL), GGOH (20 µM, 1 uL),+ Plur (15%, 1µL)	eIPP (100 µM, 1 µL), GGOH (20 µM, 1 uL),+ Plur (15%, 1µL)
C	eIPP (100 µM, 1 µL), Piv-GPP (100 µM, 1 uL),+ Plur (15%, 2µL)	eIPP (100 µM, 1 µL), Piv-GPP (100 µM, 1 uL),+ Plur (15%, 2µL)	eIPP (100 µM, 1 µL), Piv-GPP (100 µM, 1 uL),+ Plur (15%, 2µL)	Piv-GPP (100 µM, 1 µL),+ Plur (15%, 2 µL)	Piv-GPP (100 µM, 1 µL),+ Plur (15%, 2 µL)	Piv-GPP (100 µM, 1 µL),+ Plur (15%, 2 µL)
D	GGOH (20 µM, 1 µL)	GGOH (20 µM, 1 µL)	GGOH (20 µM, 1 µL)	Piv-DMAPP (100 µM, 1 µL),+ Plur (15%, 1µL)	Piv-DMAPP (100 µM, 1 µL),+ Plur (15%, 1µL)	Piv-DMAPP (100 µM, 1 µL),+ Plur (15%, 1µL)

Table 5 Plating layout for monitoring the rescue of Inhibitor 1 (eIPP-Piv) and Pitavastatin treated – MDA cells with GGOH.

	1	2	3	4	5	6
A	Vehicle (2µL DMSO, 2 µL 15% Plur)	Vehicle (2µL DMSO, 2 µL 15% Plur)	Vehicle (2µL DMSO, 2 µL 15% Plur)	PITA (10µM, 1µL)	PITA (10µM, 1µL)	PITA (10µM, 1µL)
B	eIPP (100 µL 1:1 Plur 2µL Tot), PITA (500 nM, 0.5µL)	eIPP (100 µL 1:1 Plur 2µL Tot), PITA (500 nM, 0.5µL)	eIPP (100 µL 1:1 Plur 2µL Tot), PITA (500 nM, 0.5µL)	eIPP (100 µL 1:1 Plur 2µL Tot), PITA (500 nM, 0.5µL), GGOH (20 µM, 1 µL)	eIPP (100 µL 1:1 Plur 2µL Tot), PITA (500 nM, 0.5µL), GGOH (20 µM, 1 µL)	eIPP (100 µL 1:1 Plur 2µL Tot), PITA (500 nM, 0.5µL), GGOH (20 µM, 1 µL)
C	eIPP (100 µL 1:1 Plur 2µL Tot), PITA (1 µM, 1 µL)	eIPP (100 µL 1:1 Plur 2µL Tot), PITA (1 µM, 1 µL)	eIPP (100 µL 1:1 Plur 2µL Tot), PITA (1 µM, 1 µL)	eIPP (100 µL 1:1 Plur 2µL Tot), PITA (1 µM, 1 µL), GGOH (20 µM, 1 µL)	eIPP (100 µL 1:1 Plur 2µL Tot), PITA (1 µM, 1 µL), GGOH (20 µM, 1 µL)	eIPP (100 µL 1:1 Plur 2µL Tot), PITA (1 µM, 1 µL), GGOH (20 µM, 1 µL)
D	eIPP (100 µL 1:1 Plur 2µL Tot), PITA (10 µM, 1 µL)	eIPP (100 µL 1:1 Plur 2µL Tot), PITA (10 µM, 1 µL)	eIPP (100 µL 1:1 Plur 2µL Tot), PITA (10 µM, 1 µL)	eIPP (100 µL 1:1 Plur 2µL Tot), PITA (10 µM, 1 µL), GGOH (20 µM, 1 µL)	eIPP (100 µL 1:1 Plur 2µL Tot), PITA (10 µM, 1 µL), GGOH (20 µM, 1 µL)	eIPP (100 µL 1:1 Plur 2µL Tot), PITA (10 µM, 1 µL), GGOH (20 µM, 1 µL)

Table 6 Plating layout for monitoring the rescue of Inhibitor 2 (1-OPP-Piv) treated – MDA cells with GGOH, Piv-DMAPP and Piv-GPP.

	1	2	3	4	5	6
A	Veh (4.5 µL DMSO)	Veh (4.5 µL DMSO)	Veh (4.5 µL DMSO)	Pita (10 µM, 1 µL)	Pita (10 µM, 1 µL)	Pita (10 µM, 1 µL)
B	1-OPP-Piv (100 µM, 1:1 plur)	1-OPP-Piv (100 µM, 1:1 plur)	1-OPP-Piv (100 µM, 1:1 plur)	1-OPP-Piv (10 µM, 1:1 plur [10x from stock])	1-OPP-Piv (10 µM, 1:1 plur [10x from stock])	1-OPP-Piv (10 µM, 1:1 plur [10x from stock])
C	1-OPP-Piv (100 µM, 1:1 plur) + Pita (10 µM)	1-OPP-Piv (100 µM, 1:1 plur) + Pita (10 µM)	1-OPP-Piv (100 µM, 1:1 plur) + Pita (10 µM)	1-OPP-Piv (100 µM, 1:1 plur) + GGOH (20 µM)	1-OPP-Piv (100 µM, 1:1 plur) + GGOH (20 µM)	1-OPP-Piv (100 µM, 1:1 plur) + GGOH (20 µM)
D	1-OPP-Piv (100 µM, 1:1 plur) + Pita (10 µM) + GGOH (20 µL)	1-OPP-Piv (100 µM, 1:1 plur) + Pita (10 µM) + GGOH (20 µL)	1-OPP-Piv (100 µM, 1:1 plur) + Pita (10 µM) + GGOH (20 µL)	1-OPP-Piv (100 µM) + DMAPP-Piv (100 µM) 1:1:1 Plur	1-OPP-Piv (100 µM) + DMAPP-Piv (100 µM) 1:1:1 Plur	1-OPP-Piv (100 µM) + DMAPP-Piv (100 µM) 1:1:1 Plur

Monitoring variations in cell count and nuclear size of inhibitor-treated cells

After conducting the cell viability assay, the media was removed, and the wells were washed twice with Phosphate Buffer Saline (PBS). The cells were then fixed by the addition of 300 µL of paraformaldehyde into each well and was incubated for 15 minutes. A stock solution of DAPI prolong stain was prepared by mixing 2 drops of DAPI with every 1 mL of PBS following the guidelines provided by Fisher Scientific. A 250 µL volume of the prepared DAPI staining solution was added to each well. Cells imaging and counting was performed on the Cytation 1 imager.

2.4 Purification of 4-(hydroxymethyl)phenyl pivalate *o*-nitrobenzyl isopentenyl pyrophosphate (Compound 11)

Synthesis and initial purification of compound **11** was conducted by the Rossi lab at the Department of Chemistry, State University of New York at Cortland. The compound was

subjected to ion exchange by manual chromatography. The compound was dissolved in approx. 0.5 mL solution of 25 mM ammonium bicarbonate and 2% isopropyl alcohol and passed through a column packed with 8g Dowex50WX8 and conditioned with DI water (200 mL), 1M HCl (150 mL), DI water (200 mL), 25% ammonium hydroxide (150 mL), and 25 mM ammonium bicarbonate with 2% isopropyl alcohol (400 mL). The elution buffer used was 25 mM ammonium bicarbonate with 2% isopropyl alcohol. The ion exchanged compound was lyophilized and the resulting product was repurified on a C18 EcoFlex column. The product fractions were combined and subjected to lyophilization to yield compound **11**, as a viscous oil.

^{1}H NMR (500 MHz, $CDCl_3$) δ 8.05 (d, *J* = 8.2 Hz, 1H), 7.68 (d, *J* = 7.2 Hz, 1H), 7.61 (t, *J* = 7.6 Hz, 1H), 7.41 (t, *J* = 8.5 Hz, 1H), 7.36 (d, *J* = 8.5 Hz, 2H), 6.98 (d, *J* = 8.5 Hz, 2H), 5.49 – 5.43 (m, 2H), 5.12 (d, *J* = 9.2 Hz, 2H), 4.72 (s, 1H), 4.67 (s, 1H), 3.98 (q, *J* = 6.9 Hz, 2H), 2.28 (t, *J* = 7.3 Hz, 2H), 1.66 (s, 3H), 1.33 (s, 9H).

^{31}P NMR (202 MHz, $CDCl_3$) δ -11.21 (d, *J* = 15.0 Hz), -11.97 (d, *J* = 15.0 Hz).

2.4.1 Evaluation of photocleavage efficiency

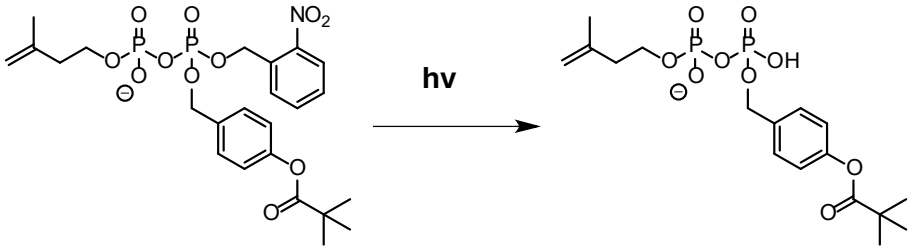

Compound 11 **Compound 12**
Monoester protected intermediate

Figure 9 Photocleavage of compound 11 to generate the monoester protected intermediate.

The cleavage efficiency of compound **11** upon exposure to UV light over a known time period was evaluated by monitoring the amount of intermediate compound **12** produced via LC-HRMS analysis.

Two identical 24 well plates were obtained and four sets of samples (two sets of reaction samples and two sets of control samples) were each plated in triplicate. Reaction sample 1 was prepared by mixing compound **11** (9.9 µL, 5 mM in DMSO) in PBS (290.1 µL), and control sample 1 was prepared by mixing DMSO (9.9 µL) in PBS (290.1 µL). Compound **11** (9.9 µL, 5 mM in DMSO) and PLE (3.3 µL) was added to PBS (286.8 µL) to prepare reaction sample 2. The control sample 2 was prepared by mixing DMSO (9.9 µL) and PLE (3.3 µL) in PBS (286.8 µL). Both well plates were placed in a dark cupboard to eliminate exposure to natural light. One of the well plates were exposed to 365 nm UV light, and the other was left in the dark. Aliquots of 10 µL were extracted into a conical vial and quenched with HPLC grade methanol (30 µL) at time intervals of 30 s, 2 min, 4 min, 16 min, 32 min, 2 h and 4 h, and was flash freezed in liquid nitrogen for storage at -80 °C. Samples were thawed, subjected to sonication for 5 minutes and centrifuged for 18 minutes at 18000 xg. The supernatant was transferred into an autosampler vial to evaluate the photocleavage efficiency by monitoring the peak area of the intermediate compound **12** by utilizing LC-HRMS analysis (Agilent MassHunter Quantitative analysis software) following the conditions in section **2.2**.

CHAPTER THREE

RESULTS AND DISCUSSION

3.1 Evaluation of inhibitory potential

The in vitro bioassay for the evaluation of inhibitory potential of the synthesized inhibitors, was designed on the basis of the prenylation of indole alkaloids (**Figure 10**). Prenyl transferases catalyze the normal and reverse prenylation of metabolites by the C1 and C3 of the prenylating moiety, respectively.[91-93] It has been reported that Notoamide F (NotF) isolated from the marine derived Aspergillus protuberus has been characterized as the reverse prenyl transferase of the indole alkaloid, Brevianamide F (BrevF), exhibiting optimal activity at 30 °C.[91,94-97] NotF displays high specificity for BrevF, incontrast to its homolog BrepT, isolated from Aspergillus versicolor, which displays a broader substrate scope despite their highly conserved active site residues.[91,98]

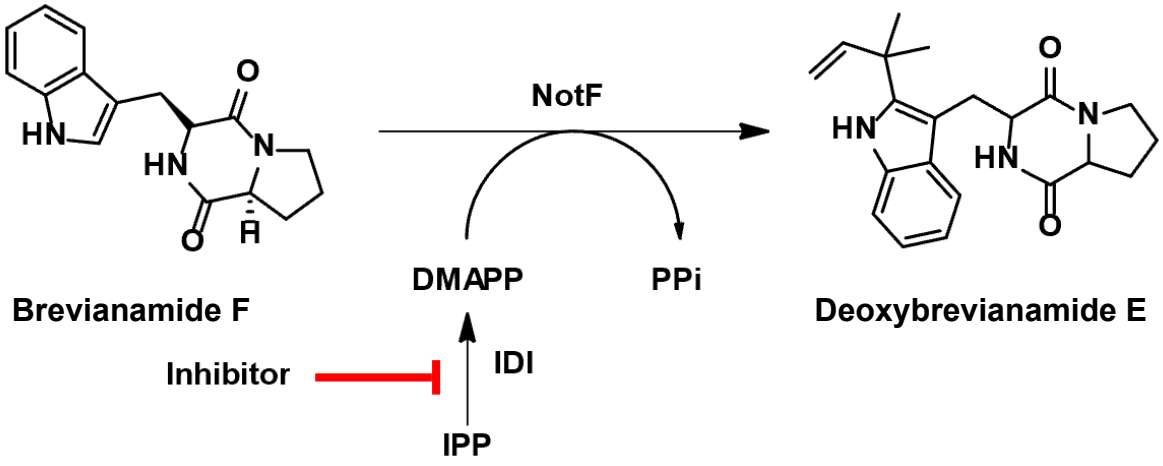

Figure 10 Experimental design for the in vitro analysis of inhibitory potential. NotF (Notoamide F), DMAPP (Dimethylallyl pyrophosphate), IPP (Isopentenyl pyrophosphate), PPi (Inorganic phosphate).

The isomerization of IPP to DMAPP is catalyzed by hIDI-1, which is subjected to inhibition by the developed inhibitors. The efficiency of the inhibitors determine the extent of DMAPP available for mediating the regioselective reverse prenylation of BrevF at C2 of the indole ring, catalyzed by NotF, for the synthesis of Deoxybrevianamide E (DBE).

The invitro inhibitory potential was primarily evaluated for **inhibitors 1-3**, by monitoring the disappearance of BrevF (**Figure 11**) and formation of DBE (**Figure 12**) via liquid chromatography-high resolution mass spectrometry (LC-HRMS), where the observed peak areas are proportional to the concentration. The chromatographic peaks corresponding to BrevF and DBE were observed at retention times of 5.60 minutes and 7.70 minutes respectively. eIPP-Piv (**1**) demonstrated a gradual increase in peak area for BrevF and a decrease for DBE, with an increase in inhibitor concentration (0.1, 1, 10 and 100 μM). These results were in contrast to 1-OPP-Piv (**2**) and 2-OPP-Piv (**3**) which exhibited an indefinite variation in peak area of BrevF. A nearly constant variation was observed for the formation of DBE with increase in inhibitor concentration, maintaining overall higher peak areas than eIPP-Piv. Therefore, it can be deduced that eIPP-Piv is a highly potent inhibitor of hIDI-1, followed by 1-OPP-Piv and 2-OPP-Piv.

After establishing a fundamental understanding of the inhibitory activity of inhibitors **1-3**, against the isolated human IDI-1 enzyme, we sought to determine the inhibitory potential of eIPP (inhibitor **1**) and 1-OPP (inhibitor **2**) against cellular IDI-1 enzyme in a human cancer cell line. The MDA-MB-231 cell line is a triple negative breast cancer cell line consisting of cells with an elongated spindle shaped morphology and only type 1 hIDI as an isopentenyl diphosphate isomerase. The presence of only hIDI-1 allows us to streamline our investigations by avoiding potential interferences by type 2 hIDI and monitor the specificity of the synthesized inhibitors.

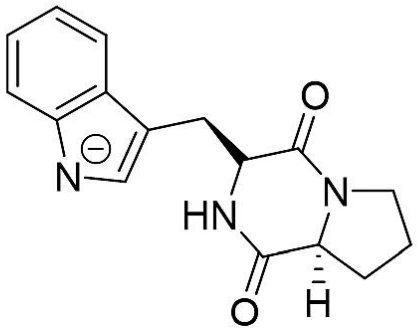

Brevianamide F – negative ion
(Exact mass = 282.1248, Retention time = 7.70 min)

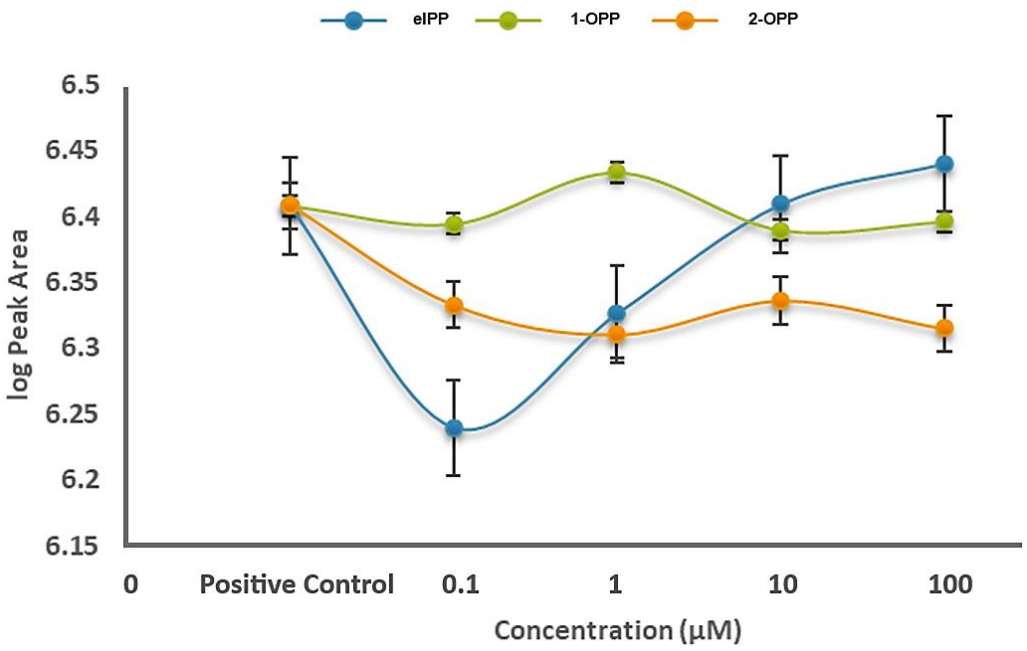

Figure 11 LC-HRMS analysis of the variation in brevianamide F in the presence of inhibitor 1 (eIPP-Piv), inhibitor 2 (1-OPP-Piv) and inhibitor 3 (2-OPP-Piv) at 0.1 µM, 1 µM, 10 µM and 100 µM concentrations.

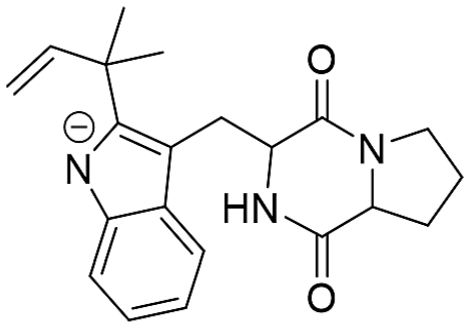

Deoxybrevianamide E – negative ion
(Exact mass = 350.1874, Retention time = 5.60 min)

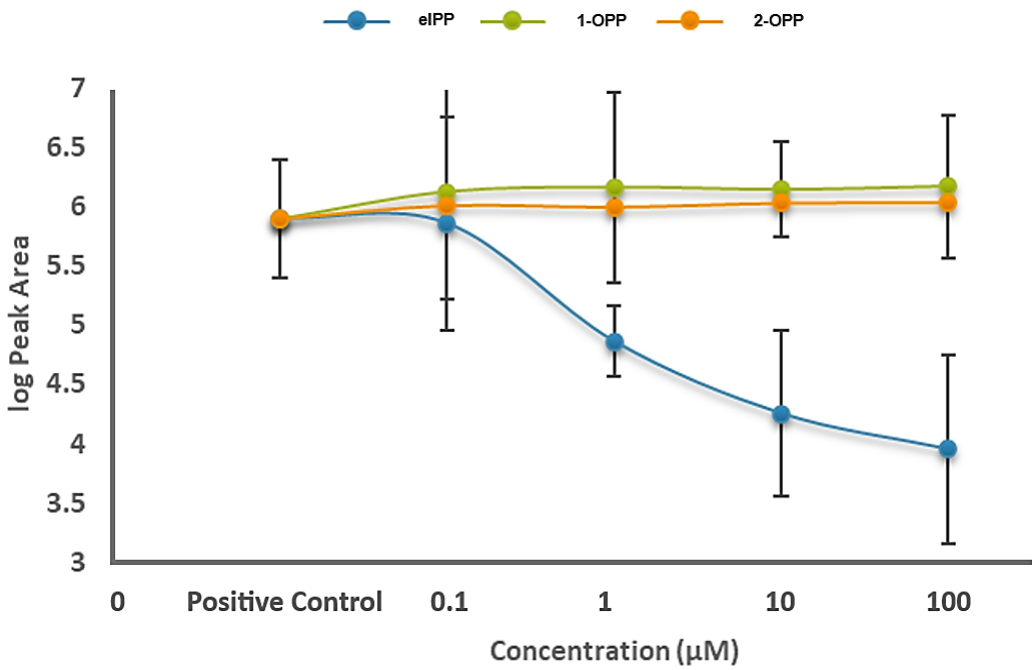

Figure 12 LC-HRMS analysis of the variation in deoxybrevianamide E in the presence of inhibitor 1 (eIPP-Piv), inhibitor 2 (1-OPP-Piv) and inhibitor 3 (2-OPP-Piv) at 0.1 µM, 1 µM, 10 µM and 100 µM concentrations.

The present study demonstrated that treatment of MDA-MB-231 cells with the statin pita, results in a loss of cell viability and cell count, and an increase in nuclear size indicative of cell cycle arrest (**Figure 13**). These observations could be attributed to the abrogation of protein prenylation resulting from the inhibition of HMG CoA reductase and inactivation of the mevalonate pathway. These effects are reversed and cell rescue can occur by the addition of geranylgeraniol (GGOH) which is a free polyprenol involved in the polyprenol salvage pathway undergoing phosphorylation to generate GGPP. We reasoned that the application of hIDI-1 inhibitors synthesized by employing the prodrug approach, would allow for cell permeation of inhibitors enabling the inhibition of hIDI-1 active site, with a similar comparative trend in activity as determined by the invitro analysis. Therefore, similarly to pita, cell viability studies were conducted on both eIPP-Piv (**1**) and 1-OPP- Piv (**2**) whereas the effect on cell count and nuclear size were also evaluated for inhibitor **1** (**Figure 14**). The cell count analysis of eIPP-Piv reveals a significant decrease in cell proliferation with an increase in the concentration of eIPP. A nearly 95% decrease was exhibited at 250 μM of eIPP, relative to the vehicle. An approximate doubling in nuclear size with 250 μM and nearly 50% increase with 100 μM was observed relative to the vehicle, which is indicative of ell cycle arrest. However, despite enhanced cell size and apparent cell cycle arrest, the cell viability appeared to be unaffected by treatment with 100 μM inhibitor **1**. Similarly, 100 μM inhibitor **2** demonstrated an insignificant change in cell viability. Ideally, a loss of cell viability would be expected if the compounds were effectively inhibiting hIDI-1, due to the resulting loss of DMAPP production and ultimate decrease in levels of FPP and GGPP leading to diminished protein prenylation. The results could be attributed to the accumulation of the monoester protected intermediate, compound **12**, resulting from the low rate of release of the second SIE, leading to their potential efflux from the cytosol and into the

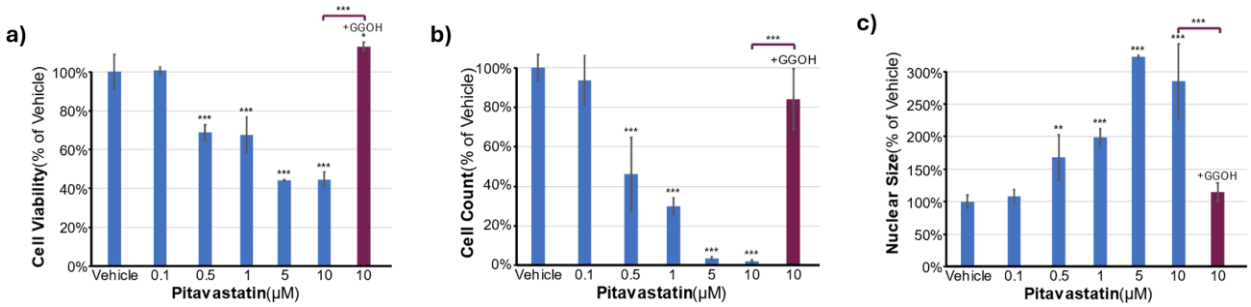

Figure 13 Inhibitory analysis on MDA-MB-231 cells treated with Pitavastatin. a) cell viability, b) cell count and c) nuclear size.

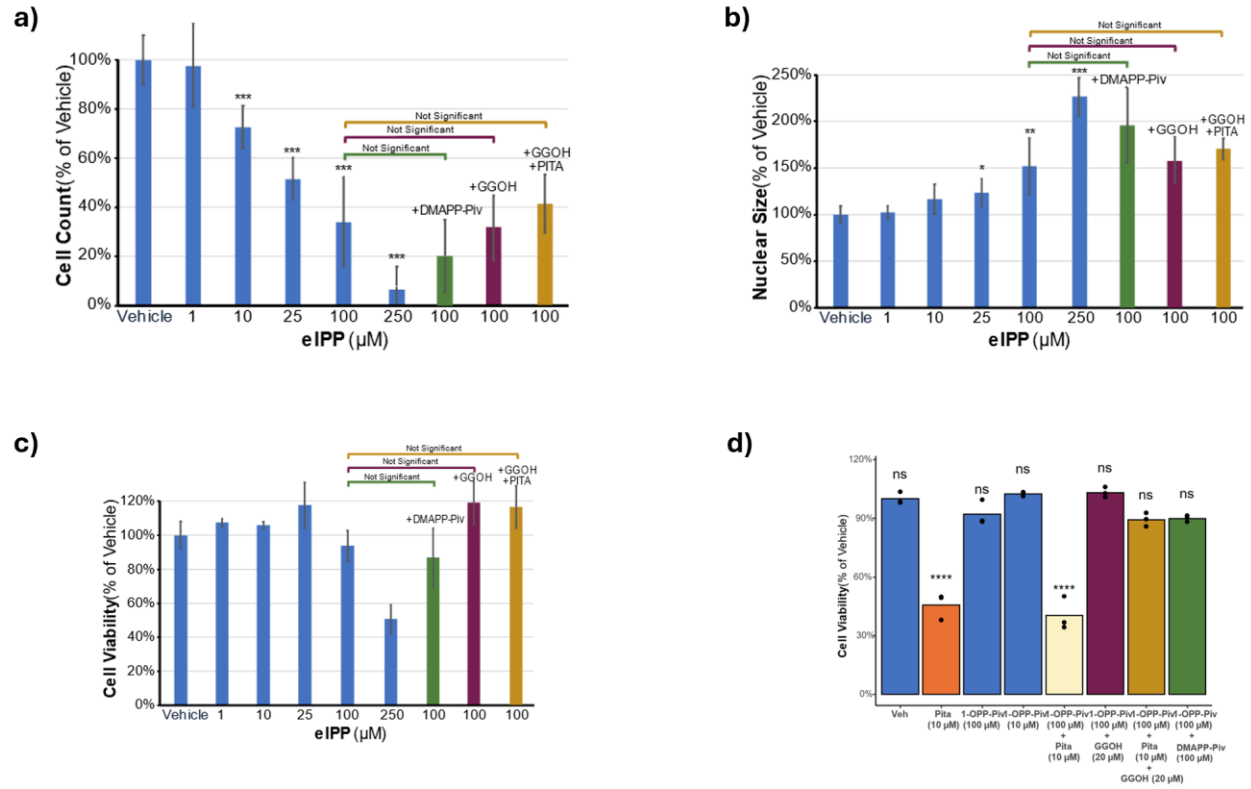

Figure 14 Inhibitory analysis on MDA-MB-231 cells treated with inhibitor 1 - a) cell viability, b) cell count and c) nuclear size. d) Inhibitor 2.

extracellular matrix and altering the intracellular inhibitor concentration. Therefore, the accuracy of results could be improved by monitoring the concentration of inhibitor in the cytosol at a given time. Furthermore, despite a majority of active site residues amongst IDI-1 isolated from different species are conserved, and the inhibitory mechanisms studied, the inhibitory mechanism of the inhibitors against hIDI-1 has not been investigated. The enzyme-inhibitor binding mechanisms plays a vital role in the efficiency of the inhibitor. A plausible explanation for the low inhibitory activity exhibitied by 1-OPP and 2-OPP would be that they behave as alternative substrates at the active site of hIDI-1 interacting via weak non-covalent interactions. The isomerization to 1-OPP to 2-OPP at the active site may result in the equilibration of the two isomers resulting in an averaged activity resulting in an overall repressed inhibition. eIPP is reportedly an irreversible covalent inhibitor of IDI-1 with a mechanism of inhibition involving protonation of the epoxide. Furthermore, the observed variations in cell viability, cell count and nuclear size indicates possible off target effects demonstrated by eIPP. Although eIPP exhibited significant inhibitory potential in an vitro setting, the observed results for cell viability in in vivo analysis, despite the indication of cell cycle arrest, suggests that the function of hIDI-1 is not limited to the isomerization of IPP for the supply of DMAPP and instead may engage in additional essential functions that require further interrogation.

3.2 Evaluation of photocleavage efficiency

The evaluation of photoinduced cleavage efficiency of the mixed photocage IPP, compound **11**, was analyzed by sample exposure to UV light of 365 nm for a predetermined time interval. The disappearance of compound **11** and formation of the monoester protected intermediate, compound **12**, was monitored by LC-HRMS. The chromatographic bands for compounds **11** and **12** were observed at the retention times of 7.1 minutes and 3.7 minutes

respectively, with a shift of 3.4 minutes due to the increased polarity of compound **12**, relative to **11**. The formation of the fully deprotected compound, i.e IPP was not monitored due to the short retention time of < 0.5 minutes, as a result of its high polarity. **Figure 15a** reveals the rapid cleavage of the oNB group by irradiation with UV light, while the acyloxy benzyl SIE was stable under these conditions. However, the simultaneous decay and decrease in cleavage rate observed for the starting material and intermediate, after the 8 minute time interval, can be attributed to the absorption of the irradiated photons by the nitroso benzaldehyde by product released during photocleavage of oNB, reducing the quantum yield of the desired photoreaction. This theory can be confirmed by conducting UV/Vis analysis to measure the intensity of byproduct absorption at 365 nm, and repeating the photocleavage analysis of **11** by altering the wavelength of irradiation to prevent photon absorption by the by product.

The experiment can be refined by conducting the aforementioned UV/Vis analysis as a preliminary step to identify the ideal wavelength to initiate photocleavage and avoid excitation of the by-product. Furthermore, conducting LC-HRMS analysis for all prepared samples exposed to UV light for the time intervals 0 s, 30 s, 2 min, 4 min, 8 min, 16 min, 32 min, 2 h and 4 h, would provide sufficient data points to accurately determine the cleavage efficiency. The cellular application of the mixed photocage probe would ideally proceed via the initial cleavage of the SIE due to hydrolysis by native esterases, followed by photo release of the substrate, IPP. Therefore, the stability of the resulting mono-photocaged intermediate should be monitored in simulated esterase-containing conditions by conducting LC-HRMS analysis on reaction sample 2 prepared with the promiscuous porcine liver esterase (PLE) as described in **2.4.2**.

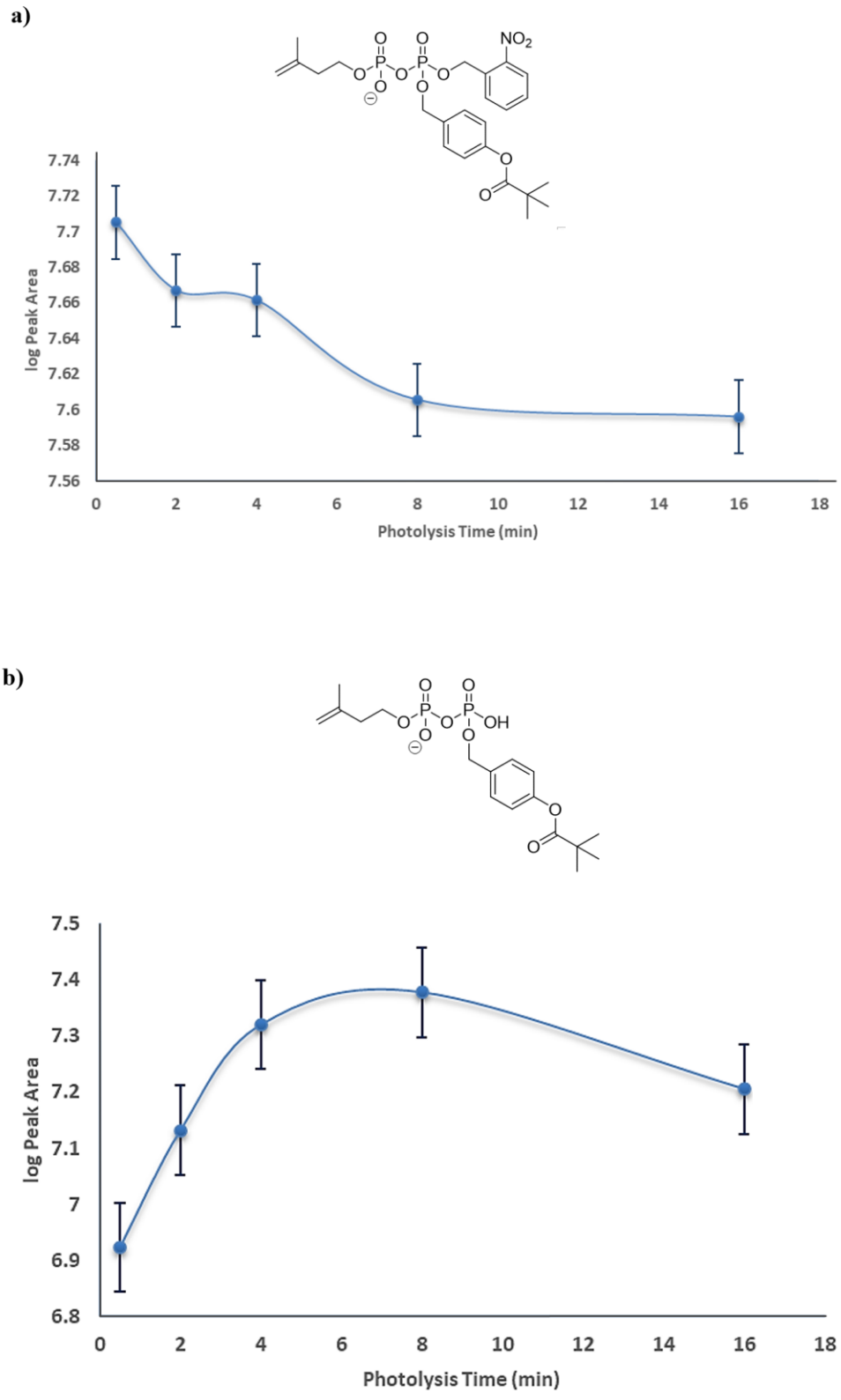

Figure 15 LC-HRMS analysis of the variation in a) mixed photocaged IPP, compound 11 and b) monoester protected intermediate, compound 12 after irradiation with 365 nm light.

CHAPTER FOUR

CONCLUSIONS

The present work reveals that the prodrug approach which utilizes self immolative esters for the selective masking of the negative charges on the β-phosphate of pyrophosphate molecules can be effectively applied to induce lipophilicity and attain cell permeability enabling the successful synthesis a series of next generation cell permeant inhibitors of hIDI-1. However, further analysis into the inhibitory potential of selected inhibitors, eIPP, 1-OPP and 2-OPP, revealed the inability to leverage them as efficient inhibitors of hIDI-1. Significant inefficiencies in inhibition were demonstrated by the variations in cell viability, cell count and nuclear size of MDA-MB-231 breast cancer cells, despite their in vitro activities exhibited for the prenylation of the indole alkaloid, brevianamide F. Overall, the findings suggest that the function of hIDI-1 in the regulation of cellular activities and metabolism may not be limited to the isomerization of IPP and DMAPP, and instead may display a broader substrate scope and engage in other biosynthetic pathways. Therefore, it is recommended to utilize alternate approaches for the targeted degradation of hIDI-1, such as Proteolysis targeting chimeras (PROTACS) or genetic knockout studies, to isolate IPP and DMAPP for the interrogation of their independent metabolic activities. The mixed photocaged IPP demonstrated promising results, which indicate their potential application in exogenous delivery followed by employing UV light for the non-invasive dose and time-controlled release of metabolites within the cells and preventing cellular efflux. However, further investigations with samples analyzed at additional time intervals must be conducted to obtain a conclusive result for the photouncaging efficiency of oNB. Furthermore, it is recommended to consider the use of substituted oNB derivatives to allow for a bathochromic

shift of the light source to reduce potential cytotoxic effects which may result from cell exposure to low wavelength light.

REFERENCES

1. Holstein, S. A.; Hohl, R. J. Isoprenoids: Remarkable Diversity of Form and Function. Lipids **2004**, 39 (4), 293–309.
2. Tetali, S. D. Terpenes and Isoprenoids: A Wealth of Compounds for Global Use. *Planta* **2018**, *249* (1), 1–8.
3. Berthelot, K.; Estevez, Y.; Deffieux, A.; Peruch, F. Isopentenyl Diphosphate Isomerase: A Checkpoint to Isoprenoid Biosynthesis. *Biochimie* **2012**, *94* (8), 1621–1634.
4. Miziorko, H. M. Enzymes of the Mevalonate Pathway of Isoprenoid Biosynthesis. *Archives of Biochemistry and Biophysics* **2011**, *505* (2), 131–143.
5. Kuzuyama, T.; Seto, H. Two Distinct Pathways for Essential Metabolic Precursors for Isoprenoid Biosynthesis. *Proceedings of the Japan Academy, Series B* **2012**, *88* (3), 41–52.
6. Rohmer, M.; Seemann, M.; Horbach, S.; Bringer-Meyer, S.; Sahm, H. Glyceraldehyde 3-Phosphate and Pyruvate as Precursors of Isoprenic Units in an Alternative Non-Mevalonate Pathway for Terpenoid Biosynthesis. **1996**, *118* (11), 2564–2566.
7. Vranová, E.; Coman, D.; Gruissem, W. Network Analysis of the MVA and MEP Pathways for Isoprenoid Synthesis. *Annual Review of Plant Biology* **2013**, *64* (1), 665–700.
8. Frank, A.; Groll, M. The Methylerythritol Phosphate Pathway to Isoprenoids. *Chemical Reviews* **2016**, *117* (8), 5675–5703.
9. Dickschat, J. S. Bacterial Terpene Cyclases. *Natural Product Reports* **2016**, *33* (1), 87–110.

10. Quin, M. B.; Flynn, C. M.; Schmidt-Dannert, C. Traversing the Fungal Terpenome. *Natural product reports* **2014**, *31* (10), 1449–1473.

11. Ajikumar, P. K.; Tyo, K.; Carlsen, S.; Mucha, O.; Phon, T. H.; Stephanopoulos, G. Terpenoids: Opportunities for Biosynthesis of Natural Product Drugs Using Engineered Microorganisms. *Molecular Pharmaceutics* **2008**, *5* (2), 167–190.

12. Breitmaier, E. Terpenes: Importance, General Structure, andBiosynthesis; Wiley-VCH Verlag GmbH & Co. KGaA: Weinheim,Germany, 2006; pp1−9

13. Bohlmann, J.; Keeling, C. I. Terpenoid Biomaterials. *The Plant Journal* **2008**, *54* (4), 656–669.

14. Moses, T.; Pollier, J.; Thevelein, J. M.; Goossens, A. Bioengineering of Plant (Tri)Terpenoids: From Metabolic Engineering of Plants to Synthetic Biologyin Vivoandin Vitro. *New Phytologist* **2013**, *200* (1), 27–43.

15. Buhaescu, I.; Izzedine, H. Mevalonate Pathway: A Review of Clinical and Therapeutical Implications. *Clinical Biochemistry* **2007**, *40* (9-10), 575–584.

16. Tippmann, S.; Chen, Y.; Siewers, V.; Nielsen, J. From Flavors and Pharmaceuticals to Advanced Biofuels: Production of Isoprenoids in*Saccharomyces Cerevisiae*. *Biotechnology Journal* **2013**, *8* (12), 1435–1444.

17. Goldstein, J. L.; Brown, M. S. Regulation of the Mevalonate Pathway. *Nature* **1990**, *343* (6257), 425–430.

18. Hinson, D. D.; Chambliss, K. L.; Toth, M. J.; Tanaka, R. D.; Gibson, K. M. Post-Translational Regulation of Mevalonate Kinase by Intermediates of the Cholesterol and Nonsterol Isoprene Biosynthetic Pathways. *Journal of Lipid Research* **1997**, *38* (11), 2216–2223.

19. Feodor Lynen; Wessely, L.; Wieland, O.; Rueff, L. β-Oxidation of Fatty Acids. *Angewandte Chemie* **1952**, *64* (24), 687–687.

20. Gehring, U.; Feodor Lynen. 13 Thiolase. *The Enzymes* **1972**, 391–405.

21. Rohmer, M.; Knani, M.; Simonin, P.; Sutter, B.; Sahm, H. Isoprenoid Biosynthesis in Bacteria: A Novel Pathway for the Early Steps Leading to Isopentenyl Diphosphate. *Biochemical Journal* **1993**, *295* (2), 517–524.

22. Roitelman, J.; Simoni, R. D. Distinct Sterol and Nonsterol Signals for the Regulated Degradation of 3-Hydroxy-3-Methylglutaryl-CoA Reductase. *Journal of Biological Chemistry* **1992**, *267* (35), 25264–25273.

23. Tchen, T. T. Mevalonic Kinase: Purification and Properties. *Journal of Biological Chemistry* **1958**, *233* (5), 1100–1103.

24. Huang, M.; Wei, K.; Li, X.; McClory, J.; Hu, G.; Zou, J.-W.; Timson, D. Phosphorylation Mechanism of Phosphomevalonate Kinase: Implications for Rational Engineering of Isoprenoid Biosynthetic Pathway Enzymes. *The Journal of Physical Chemistry B* **2016**, *120* (41), 10714–10722.

25. Dorsey, J. K.; Porter, J. W. The Inhibition of Mevalonic Kinase by Geranyl and Farnesyl Pyrophosphates. *Journal of Biological Chemistry* **1968**, *243* (18), 4667–4670.

26. Voynova, N. E.; Rios, S. E.; Miziorko, H. M. *Staphylococcus Aureus* Mevalonate Kinase: Isolation and Characterization of an Enzyme of the Isoprenoid Biosynthetic Pathway. *Journal of Bacteriology* **2004**, *186* (1), 61–67.

27. Bloch, K.; Chaykin, S.; Phillips, A. H.; de Waard, A. Mevalonic Acid Pyrophosphate and Isopentenylpyrophosphate. *Journal of Biological Chemistry* **1959**, *234* (10), 2595–2604.

28. Sprenger, G. A.; Ulrich Schörken; Wiegert, T.; Grolle, S.; de, A.; Taylor, S.; Begley, T. P.; Bringer-Meyer, S.; Sahm, H. Identification of a Thiamin-Dependent Synthase in *Escherichia Coli* Required for the Formation of the 1-Deoxy- D -Xylulose 5-Phosphate Precursor to Isoprenoids, Thiamin, and Pyridoxol. **1997**, *94* (24), 12857–12862.

29. Lange, B. M.; Wildung, M. R.; McCaskill, D.; Croteau, R. A Family of Transketolases That Directs Isoprenoid Biosynthesis via a Mevalonate-Independent Pathway. *Proceedings of the National Academy of Sciences* **1998**, *95* (5), 2100–2104.

30. Eisenreich, W.; Schwarz, M.; Cartayrade, A.; Arigoni, D.; Zenk, M. H.; Bacher, A. The Deoxyxylulose Phosphate Pathway of Terpenoid Biosynthesis in Plants and Microorganisms. *Chemistry & Biology* **1998**, *5* (9), R221–R233.

31. Flesch, G.; Rohmer, M. Prokaryotic Hopanoids: The Biosynthesis of the Bacteriohopane Skeleton. Formation of Isoprenic Units from Two Distinct Acetate Pools and a Novel Type of Carbon/Carbon Linkage between a Triterpene and D-Ribose. *European journal of biochemistry* **1988**, *175* (2), 405–411.

32. Lange, B. M.; Croteau, R. Isopentenyl Diphosphate Biosynthesis via a Mevalonate-Independent Pathway: Isopentenyl Monophosphate Kinase Catalyzes the Terminal Enzymatic Step. *Proceedings of the National Academy of Sciences* **1999**, *96* (24), 13714–13719.

33. Tritsch, D.; Hemmerlin, A.; Bach, T. J.; Rohmer, M. Plant Isoprenoid Biosynthesis via the MEP Pathway: In Vivo IPP/DMAPP Ratio Produced by (E)-4-Hydroxy-3-Methylbut-2-Enyl Diphosphate Reductase in Tobacco BY-2 Cell Cultures. *FEBS Letters* **2009**, *584* (1), 129–134.

34. A.A. Kandutsch; Paulus, H.; Levin, E.; Bloch, K. Purification of Geranylgeranyl Pyrophosphate Synthetase from Micrococcus Lysodeikticus. *Journal of Biological Chemistry* **1964**, *239* (8), 2507–2515.

35. Beytia, E.; Qureshi, A. A.; Porter, J. W. Squalene Synthetase. *Journal of Biological Chemistry* **1973**, *248* (5), 1856–1867.

36. Topol, E. J. Intensive Statin Therapy — a Sea Change in Cardiovascular Prevention. *New England journal of medicine/˜The œNew England journal of medicine* **2004**, *350* (15), 1562–1564.

37. Dunford, J. E.; Thompson, K.; Coxon, F. P.; Luckman, S. P.; Hahn, F. M.; Poulter, C. D.; Ebetino, F. H.; Rogers, M. J. Structure-Activity Relationships for Inhibition of Farnesyl Diphosphate Synthase in Vitro and Inhibition of Bone Resorption in Vivo by Nitrogen-Containing Bisphosphonates. *Journal of Pharmacology and Experimental Therapeutics* **2001**, *296* (2), 235–242.

38. Luckman, S. P.; Hughes, D. E.; Coxon, F. P.; Russell, R. G. G.; Rogers, M. J. Nitrogen-Containing Bisphosphonates Inhibit the Mevalonate Pathway and Prevent Post-Translational Prenylation of GTP-Binding Proteins, Including Ras. *Journal of Bone and Mineral Research* **1998**, *13* (4), 581–589.

39. Reszka, A. A.; Halasy-Nagy, J. M.; Masarachia, P. J.; Rodan, G. A. Bisphosphonates Act Directly on the Osteoclast to Induce Caspase Cleavage of Mst1 Kinase during Apoptosis. *Journal of Biological Chemistry* **1999**, *274* (49), 34967–34973.

40. Benford, H. L.; Frith, J. C.; Seppo Auriola; Jukka Mönkkönen; Rogers, M. J. Farnesol and Geranylgeraniol Prevent Activation of Caspases by Aminobisphosphonates:

Biochemical Evidence for Two Distinct Pharmacological Classes of Bisphosphonate Drugs. *Molecular Pharmacology* **1999**, *56* (1), 131–140.

41. Taya, Y.; Tanaka, Y.; Nishimura, S. 5′-AMP Is a Direct Precursor of Cytokinin in Dictyostelium Discoideum. *Nature* **1978**, *271* (5645), 545–547.
42. Milstone, D. S.; Vold, B. S.; Glitz, D. G.; Shutt, N. Antibodies to N^6-(Δ^2-Isopentenyl) Adenosine and Its Nucleotide: Interaction with Purified TRNAs and with Bases, Nucleosides and Nucleotides of the Isopentenyladenosine Family. *Nucleic Acids Research* **1978**, *5* (9), 3439–3455.
43. Mönkkönen, H.; Lehenkari, P.P.; Kellinsalmi, M. A new mechanism of action for bisphosphonates: Apppi dedicated cytotoxicity of N-BPs. *Bone* **2004**;34,S66–7.
44. Morello, G.; Guarnaccia, M.; Spampinato, A. G.; La Cognata, V.; D'Agata, V.; Cavallaro, S. Copy Number Variations in Amyotrophic Lateral Sclerosis: Piecing the Mosaic Tiles Together through a Systems Biology Approach. *Molecular Neurobiology* **2017**, *55* (2), 1299–1322
45. Aronica, E.; Baas, F.; Anand; Ten, L. M. A.; Morello, G.; Cavallaro, S. Molecular Classification of Amyotrophic Lateral Sclerosis by Unsupervised Clustering of Gene Expression in Motor Cortex. *Neurobiology of Disease* **2015**, *74*, 359–376.
46. Kato, T.; Mitsuru Emi; Sato, H.; Shigeki Arawaka; Wada, M.; Toru Kawanami; Katagiri, T.; Kenji Tsuburaya; Toyoshima, I.; Tanaka, F.; Gen Sobue; Matsubara, K. Segmental Copy-Number Gain within the Region of Isopentenyl Diphosphate Isomerase Genes in Sporadic Amyotrophic Lateral Sclerosis. *Biochemical and biophysical research communications* **2010**, *402* (2), 438–442.

47. S.K. Krisans; Ericsson, J.; Edwards, P. A.; Keller, G. A. Farnesyl-Diphosphate Synthase Is Localized in Peroxisomes. Journal of biological chemistry/*The Journal of biological chemistry* **1994**, *269* (19), 14165–14169.

48. Jeong, A.; Auger, S. A.; Sanjay Maity; Fredriksen, K.; Zhong, R.; Li, L.; Distefano, M. D. In Vivo Prenylomic Profiling in the Brain of a Transgenic Mouse Model of Alzheimer's Disease Reveals Increased Prenylation of a Key Set of Proteins. *ACS chemical biology* **2022**, *17* (10), 2863–2876.

49. Babu, N.; Advani, J.; Solanki, H. S.; Patel, K.; Jain, A.; Khan, A. A.; Radhakrishnan, A.; Sahasrabuddhe, N. A.; Mathur, P. P.; Nair, B.; Keshava Prasad, T. S.; Chang, X.; Sidransky, D.; Gowda, H.; Chatterjee, A. MiRNA and Proteomic Dysregulation in Non-Small Cell Lung Cancer in Response to Cigarette Smoke. *MicroRNA* **2018**, *7* (1), 38–53.

50. Ohmori, K.; Kamei, A.; Watanabe, Y.; Abe, K. Gene Expression over Time during Cell Transformation due to Non-Genotoxic Carcinogen Treatment of Bhas 42 Cells. *International Journal of Molecular Sciences* **2022**, *23* (6), 3216.

51. Davies, B. S. J.; Fong, L. G.; Yang, S. H.; Coffinier, C.; Young, S. G. The Posttranslational Processing of Prelamin a and Disease. *Annual review of genomics and human genetics* **2009**, *10*, 153–174.

52. Zheng, W.; Sun, F.; Bartlam, M.; Li, X.; Li, R.; Rao, Z. The Crystal Structure of Human Isopentenyl Diphosphate Isomerase at 1.7 Å Resolution Reveals Its Catalytic Mechanism in Isoprenoid Biosynthesis. *Journal of Molecular Biology* **2007**, *366* (5), 1447–1458.

53. Wouters, J.; Yamina Oudjama; Barkley, S. W.; Tricot, C.; Stalon, V.; Droogmans, L.; C. Dale Poulter. Catalytic Mechanism of Escherichia Coli Isopentenyl Diphosphate Isomerase Involves Cys-67, Glu-116, and Tyr-104 as Suggested by Crystal Structures of

Complexes with Transition State Analogues and Irreversible Inhibitors. **2003**, *278* (14), 11903–11908.

54. Wouters, J.; Oudjama, Y.; Ghosh, S.; Stalon, V.; Droogmans, L.; Oldfield, E. Structure and Mechanism of Action of Isopentenylpyrophosphate-Dimethylallylpyrophosphate Isomerase. *Journal of the American Chemical Society* **2003**, *125* (11), 3198–3199.
55. Wouters, J.; Yin, F.; Song, Y.; Zhang, Y.; Yamina Oudjama; Stalon, V.; Droogmans, L.; Morita, C. T.; Oldfield, E. A Crystallographic Investigation of Phosphoantigen Binding to Isopentenyl Pyrophosphate/Dimethylallyl Pyrophosphate Isomerase. *Journal of the American Chemical Society* **2004**, *127* (2), 536–537.
56. Lu, X. J.; Christensen, D. J.; Poulter, C. D. Isopentenyl-Diphosphate Isomerase: Irreversible Inhibition by 3-Methyl-3,4-Epoxybutyl Diphosphate. *Biochemistry* **1992**, *31* (41), 9955–9960.
57. Nagai, T.; Unno, H.; Janczak, M. W.; Yoshimura, T.; Poulter, C. D.; Hemmi, H. Covalent Modification of Reduced Flavin Mononucleotide in Type-2 Isopentenyl Diphosphate Isomerase by Active-Site-Directed Inhibitors. *Proceedings of the National Academy of Sciences* **2011**, *108* (51), 20461–20466.
58. Sharma, N. K.; Pan, J. J.; Poulter, C. D. Type II isopentenyl diphosphate isomerase: probing the mechanism with alkyne/allene diphosphate substrate analogues. *Biochemistry* **2010**, *49* (29), 6228-6233.
59. Muehlbacher, M.; Poulter, C. D. Isopentenyl Diphosphate:dimethylallyl Diphosphate Isomerase. Irreversible Inhibition of the Enzyme by Active-Site-Directed Covalent Attachment. *Journal of the American Chemical Society* **1985**, *107* (26), 8307–8308.

60. Matsson, P.; Doak, B. C.; Over, B.; Kihlberg, J. Cell Permeability beyond the Rule of 5. *Advanced Drug Delivery Reviews* **2016**, *101*, 42–61.

61. Kratz, F.; Müller, Ivonne A.; Ryppa, C.; Warnecke, A. Prodrug Strategies in Anticancer Chemotherapy. *ChemMedChem* **2008**, *3* (1), 20–53.

62. Bundgaard, H. The Double Prodrug Concept and Its Applications. *Advanced Drug Delivery Reviews* **1989**, *3* (1), 39–65.

63. Papot, S.; Tranoy, I.; Tillequin, F.; Florent, J.; Gesson, J. Design of Selectively Activated Anticancer Prodrugs: Elimination and Cyclization Strategies. *Current Medicinal Chemistry-Anti-Cancer Agents* **2002**, *2* (2), 155–185.

64. Wakselman M. 1,4- and 1,6-Eliminations from Hydroxy- and Amino-Substituted Benzyl Systems: Chemical and Biochemical Applications. *New Journal of Chemistry* **1983**, *7* (7), 439–447.

65. Carl, P. L.; Chakravarty, P. K.; Katzenellenbogen, J. A. A Novel Connector Linkage Applicable in Prodrug Design. *Journal of Medicinal Chemistry* **1981**, *24* (5), 479–480.

66. Rossi, F.; McBee, D.; Trybala, T.; Hulsey, Z.; Camila Gonzalez Curbelo; Mazur, W.; Baccile, J. Membrane Permeant Analogs for Independent Cellular Introduction of the Terpene Precursors Isopentenyl- and Dimethylallyl-Pyrophosphate. *ChemBioChem* **2022**, *24* (1).

67. Hansen, M. J. Controlling Biological Function with Light. *the University of Groningen research portal* **2018**.

68. Gautier, A.; Gauron, C.; Volovitch, M.; Bensimon, D.; Ludovic Jullien; Vriz, S. How to Control Proteins with Light in Living Systems. *Nature Chemical Biology* **2014**, *10* (7), 533–541.

69. Szymański, W.; Beierle, J. M.; Kistemaker, H. A. V.; Velema, W. A.; Feringa, B. L. Reversible Photocontrol of Biological Systems by the Incorporation of Molecular Photoswitches. *Chemical Reviews* **2013**, *113* (8), 6114–6178.

70. Brieke, C.; Rohrbach, F.; Gottschalk, A.; Mayer, G.; Heckel, A. Light-Controlled Tools. *Angewandte Chemie International Edition* **2012**, *51* (34), 8446–8476.

71. Jeschik, N.; Schneider, T.; Meier, C. Photocaged and Mixed Photocaged Bioreversible-Protected ATP Derivatives as Tools for the Controlled Release of ATP. *European Journal of Organic Chemistry* **2020**, *2020* (43), 6776–6789.

72. Smith, A. M., Mancini, M. C. & Nie, S. Second window for in vivo imaging. *Nat. Nanotechnol.* **2009**, *4*, 710–711.

73. Josa-Culleré, L.; Llebaria, A. In the Search for Photocages Cleavable with Visible Light: An Overview of Recent Advances and Chemical Strategies. *ChemPhotoChem* **2020**, *5* (4), 296–314.

74. Rubinstein, N., Liu, P., Miller, E. W. & Weinstain, R. meso-Methylhydroxy BODIPY: a scaffold for photo-labile protecting groups. *ChemComm* **2015**, *51*, 6369–6372.

75. Jun, J. V., Chenoweth, D. M. & Petersson, E. J. Rational design of small molecule fluorescent probes for biological applications. *Org. Biomol. Chem*. **2020**,*18*, 5747–5763 (2020).

76. Klán, P. et al. Photoremovable Protecting Groups in Chemistry and Biology: Reaction Mechanisms and Efficacy. *Chem. Rev*. **2013**, *113*, 119–191.

77. Hansen, M. J., Velema, W. A., Lerch, M. M., Szymanski, W. & Feringa, B. L. Wavelength-selective cleavage of photoprotecting groups: strategies and applications in dynamic systems. *Chem. Soc. Rev*. **2015**, *44*, 3358–3377.

78. Singh, P. K.; Majumdar, P.; Singh, S. P. Advances in BODIPY Photocleavable Protecting Groups. *Coordination Chemistry Reviews* **2021**, *449*, 214193.

79. Weinstain, R.; Slanina, T.; Dnyaneshwar Kand; Petr Klán. Visible-To-NIR-Light Activated Release: From Small Molecules to Nanomaterials. *Chemical Reviews* **2020**, *120* (24), 13135–13272.

80. Truong, V. X., Li, F. & Forsythe, J. S. Visible Light Activation of Nucleophilic Thiol-X Addition via Thioether Bimane Photocleavage for Polymer Cross-Linking. *Biomacromolecules* **2018**, *19*, 4277–4285.

81. Chaudhuri, A., Venkatesh, Y., Behara, K. K. & Singh, N. D. P. Bimane: A Visible Light Induced Fluorescent Photoremovable Protecting Group for the Single and Dual Release of Carboxylic and Amino Acids. *Org*. **2017**, *19*, 1598–1601.

82. Givens, R. S., Rubina, M. & Wirz, J. Applications of p-hydroxyphenacyl (pHP) and (coumarin-4-yl) methyl photoremovable protecting groups. *Photochem. Photobiol.* **2012**, *11*, 472.

83. Weinstain, R.; Slanina, T.; Dnyaneshwar Kand; Petr Klán. Visible-To-NIR-Light Activated Release: From Small Molecules to Nanomaterials. *Chemical Reviews* **2020**, *120* (24), 13135–13272.

84. Klán, P.; Šolomek, T.; Bochet, C. G.; Blanc, A.; Givens, R.; Rubina, M.; Popik, V.; Kostikov, A.; Wirz, J. Photoremovable Protecting Groups in Chemistry and Biology: Reaction Mechanisms and Efficacy. *Chemical Reviews* **2012**, *113* (1), 119–191.

85. Miroslav Zabadal; Anna Paola Pelliccioli; Petr Klán; Wirz, J. 2,5-Dimethylphenacyl Esters: A Photoremovable Protecting Group for Carboxylic Acids. *Journal of Physical Chemistry A* **2001**, *105* (45), 10329–10333.

86. Patchornik, A.; Amit, B.; Woodward, R. B. Photosensitive Protecting Groups. *Journal of the American Chemical Society* **1970**, *92* (21), 6333–6335.

87. Bayley, H.; Chang, C. Y.; Miller, W. T.; Niblack, B.; Pan, P. [7] Caged Peptides and Proteins by Targeted Chemical Modification. *Methods in enzymology on CD-ROM/Methods in enzymology* **1998**, 117–135.

88. Givens, R. S.; L. William Kueper. Photochemistry of Phosphate Esters. **1993**, *93* (1), 55–66.

89. Literák, J.; Wirz, J.; Klán, P. 2,5-Dimethylphenacyl Carbonates: A Photoremovable Protecting Group for Alcohols and Phenols. *Photochem. Photobiol. Sci.* **2005**, *4* (1), 43–46.

90. Barton, D. H. R.; Chow, Y. L.; Cox, A.; Kirby, G. W. 654. Photochemical Transformations. Part XIX. Some Photosensitive Protecting Groups. *Journal of the Chemical Society (Resumed)* **1965**, 3571.

91. Fraley, A. E.; Sherman, D. H. Enzyme Evolution in Fungal Indole Alkaloid Biosynthesis. *The FEBS journal* **2020**, *287* (7), 1381–1402.

92. Maiya, S.; Grundmann, A.; Li, S.; Turner, G. The Fumitremorgin Gene Cluster of *Aspergillus Fumigatus* : Identification of a Gene Encoding Brevianamide F Synthetase. *ChemBioChem* **2006**, *7* (7), 1062–1069.

93. Jingfang Qian-Cutrone; Huang, S.; Shu, Y.-Z.; Vyas, D. M.; Fairchild, C. R.; Menendez, A. T.; Krampitz, K.; Dalterio, R. A.; Klohr, S. E.; Gao, Q. Stephacidin a and B: Two Structurally Novel, Selective Inhibitors of the Testosterone-Dependent Prostate LNCaP Cells. **2002**, *124* (49), 14556–14557.

94. Martínez-Luis, S.; Rodríguez, R.; Acevedo, L.; González, M. C.; Lira-Rocha, A.; Mata, R. Malbrancheamide, a New Calmodulin Inhibitor from the Fungus Malbranchea Aurantiaca. *Tetrahedron* **2006**, *62* (8), 1817–1822.

95. Ding, Y.; Jeffrey; Cavalcoli, J. D.; Li, S.; Greshock, T. J.; Miller, K. G.; Finefield, J. M.; Sunderhaus, J. D.; McAfoos, T.; Tsukamoto, S.; Williams, R. W.; Sherman, D. H. Genome-Based Characterization of Two Prenylation Steps in the Assembly of the Stephacidin and Notoamide Anticancer Agents in a Marine-Derived *Aspergillus* Sp.. *Journal of the American Chemical Society* **2010**, *132* (36), 12733–12740.

96. Tsukamoto, S.; Kawabata, T.; Kato, H.; Greshock, T. J.; Hirota, H.; Ohta, T.; Williams, R. M. Isolation of Antipodal (−)-Versicolamide B and Notoamides L−N from a Marine-Derived *Aspergillus* Sp.. *Organic Letters* **2009**, *11* (6), 1297–1300.

97. Tsukamoto, S.; Kato, H.; Greshock, T. J.; Hirota, H.; Ohta, T.; Williams, R. M. Isolation of Notoamide E, a Key Precursor in the Biosynthesis of Prenylated Indole Alkaloids in a Marine-Derived Fungus, Aspergillus Sp. *Journal of the American Chemical Society* **2009**, *131* (11), 3834–3835.

98. Yin, S.; Yu, X.; Wang, Q.; Liu, X.-Q.; Li, S.-M. Identification of a Brevianamide F Reverse Prenyltransferase BrePT from Aspergillus Versicolor with a Broad Substrate Specificity towards Tryptophan-Containing Cyclic Dipeptides. *Applied Microbiology and Biotechnology* **2012**, *97* (4), 1649–1660.

APPENDIX

^{1}H NMR of 4-(hydroxymethyl)phenyl pivalate

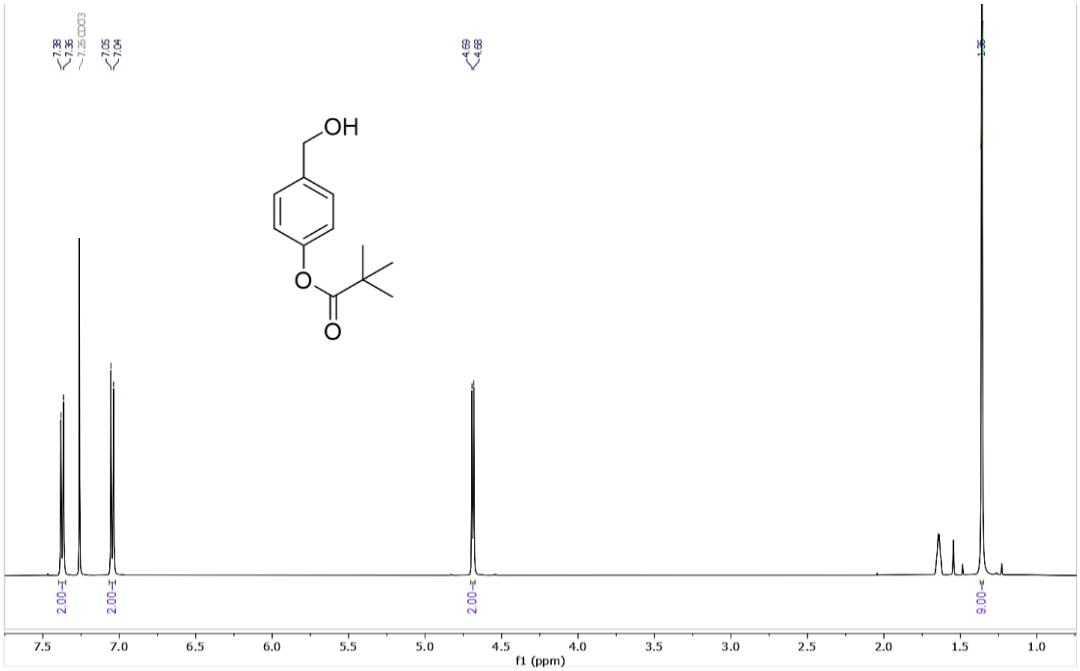

^{1}H NMR of Bis(4-(hydroxymethyl)phenyl pivalate)-N,N-diisopropyl phosphoramidite

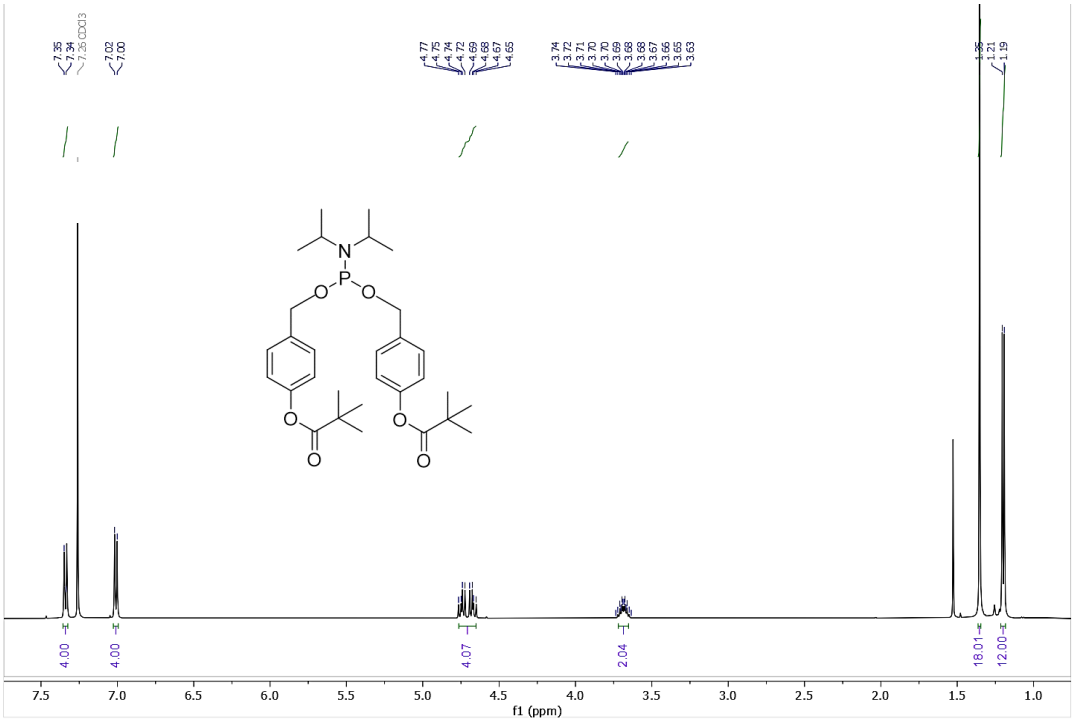

^{31}P NMR of Bis(4-(hydroxymethyl)phenyl pivalate)-N,N-diisopropyl phosphoramidite

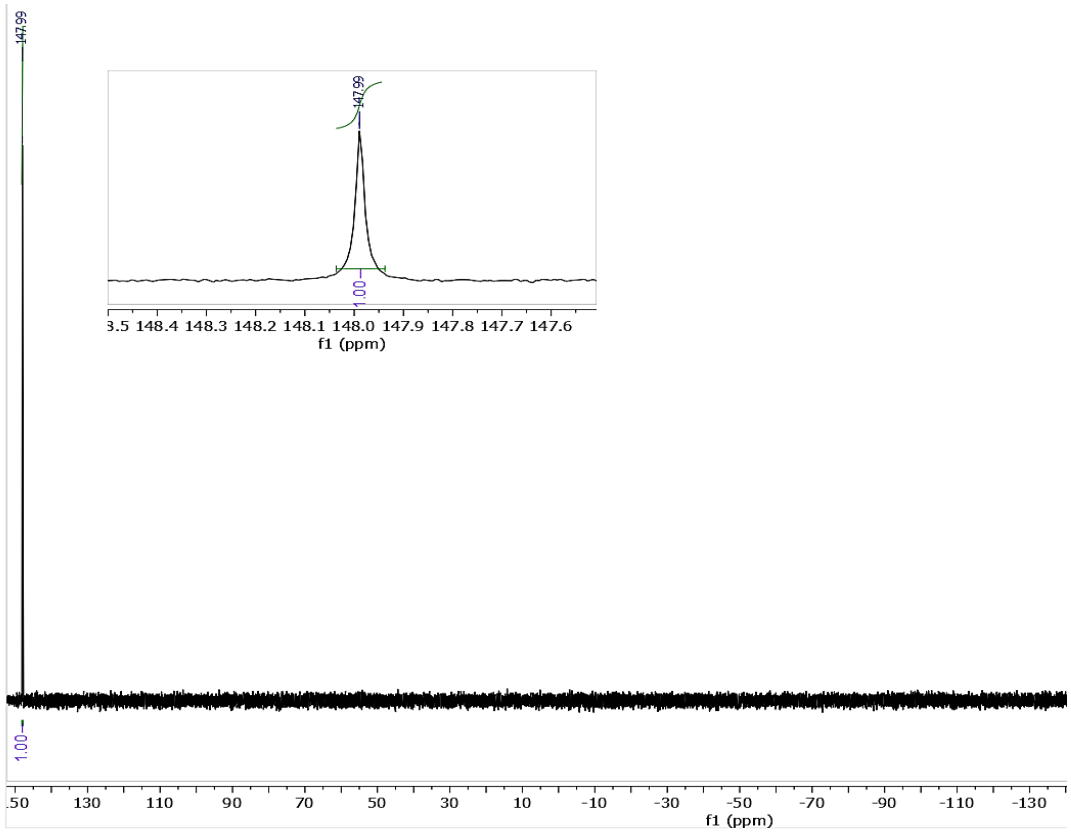

^{1}H NMR of 3,4-epoxy-3-methylbutan-1-ol

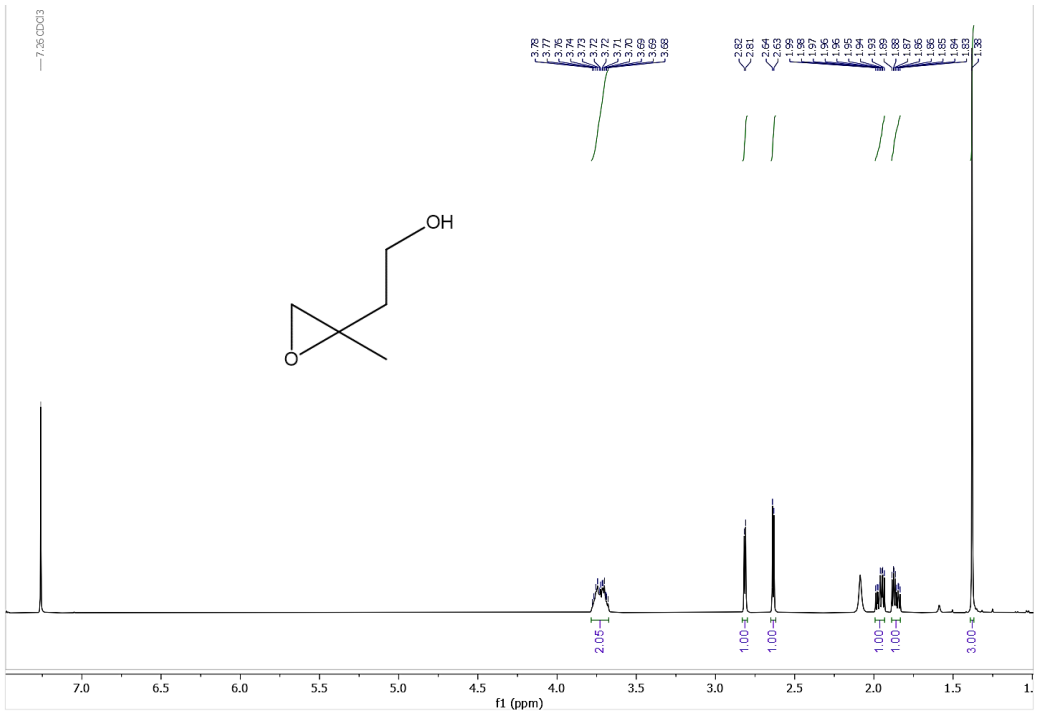

^{31}P NMR of 3,4-epoxy-3-methyl-1-butyl monophosphate (crude)

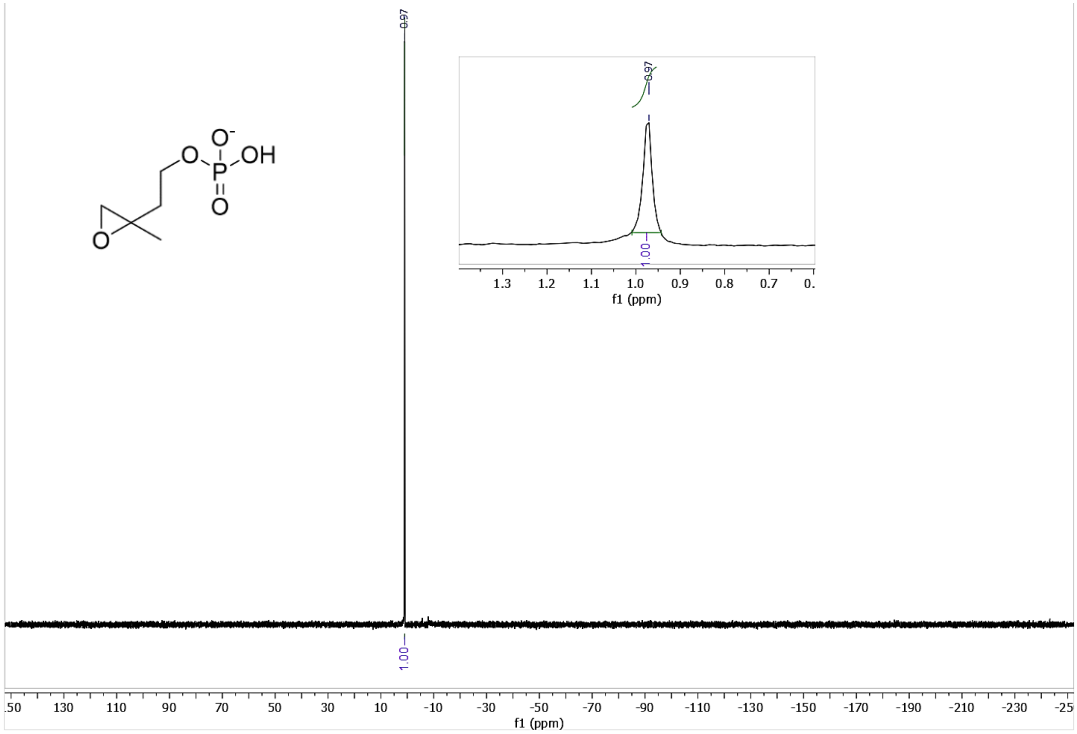

^{1}H NMR of β-Bis(4-(hydroxymethyl)phenyl pivalate)-3,4-epoxy-3-methyl-1-butyl pyrophosphate

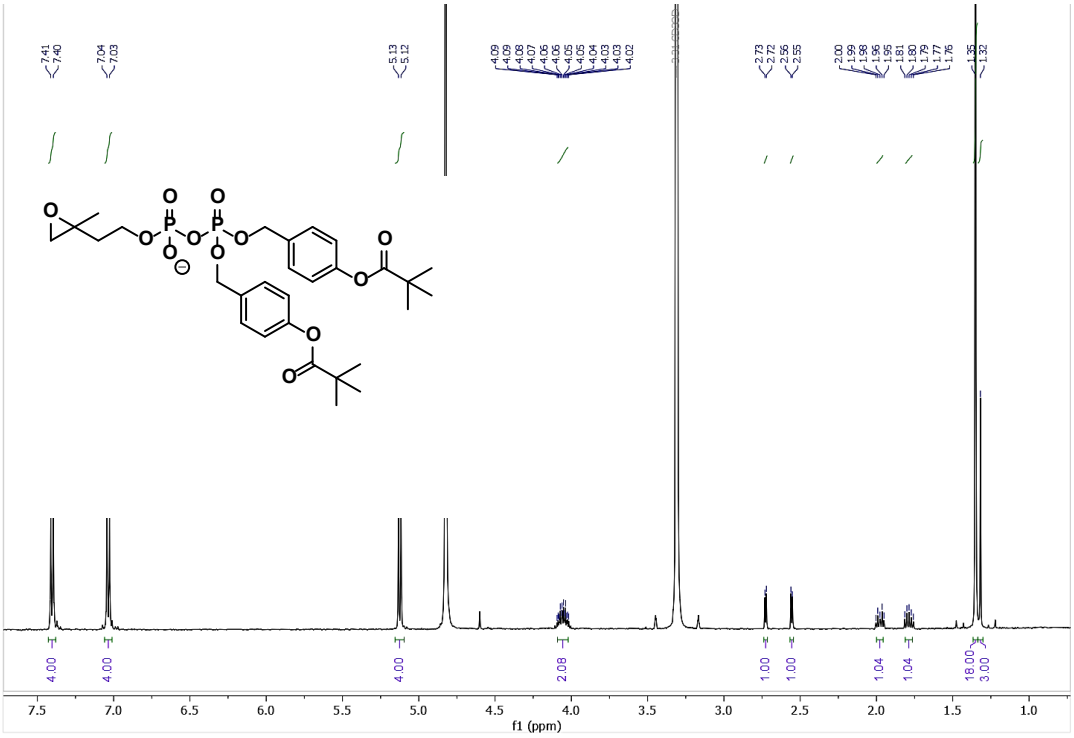

^{31}P NMR of β-Bis(4-(hydroxymethyl)phenyl pivalate)-3,4-epoxy-3-methyl-1-butyl pyrophosphate

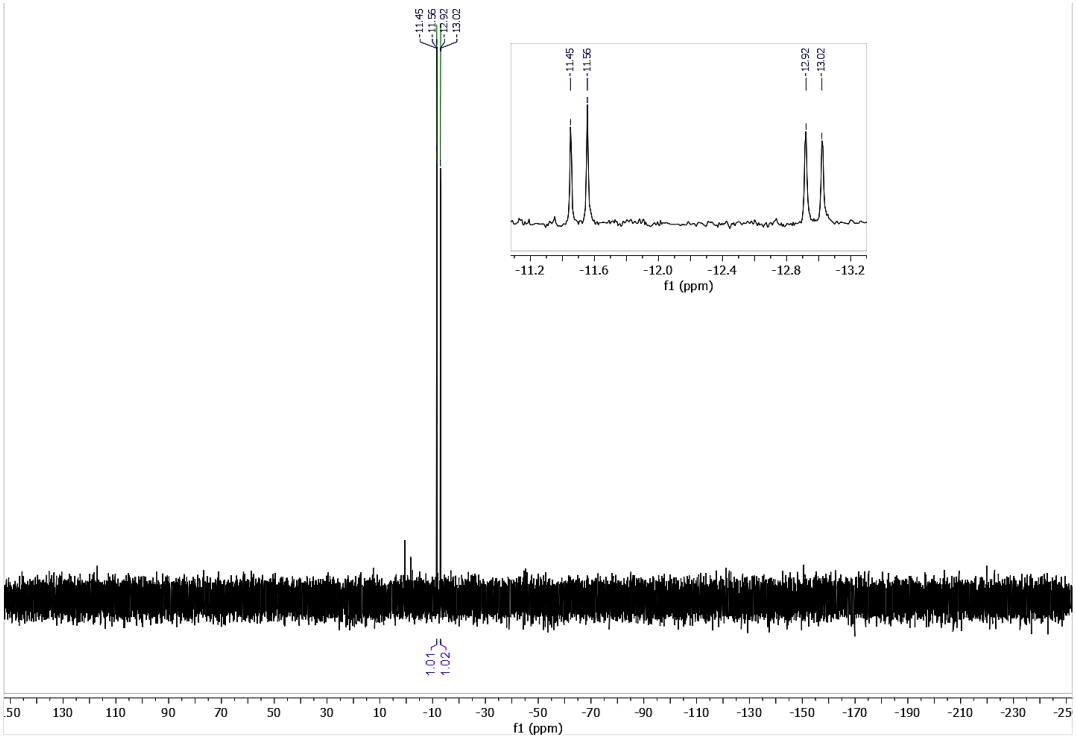

^{31}P NMR of 3-butyn-1-yl monophosphate (crude)

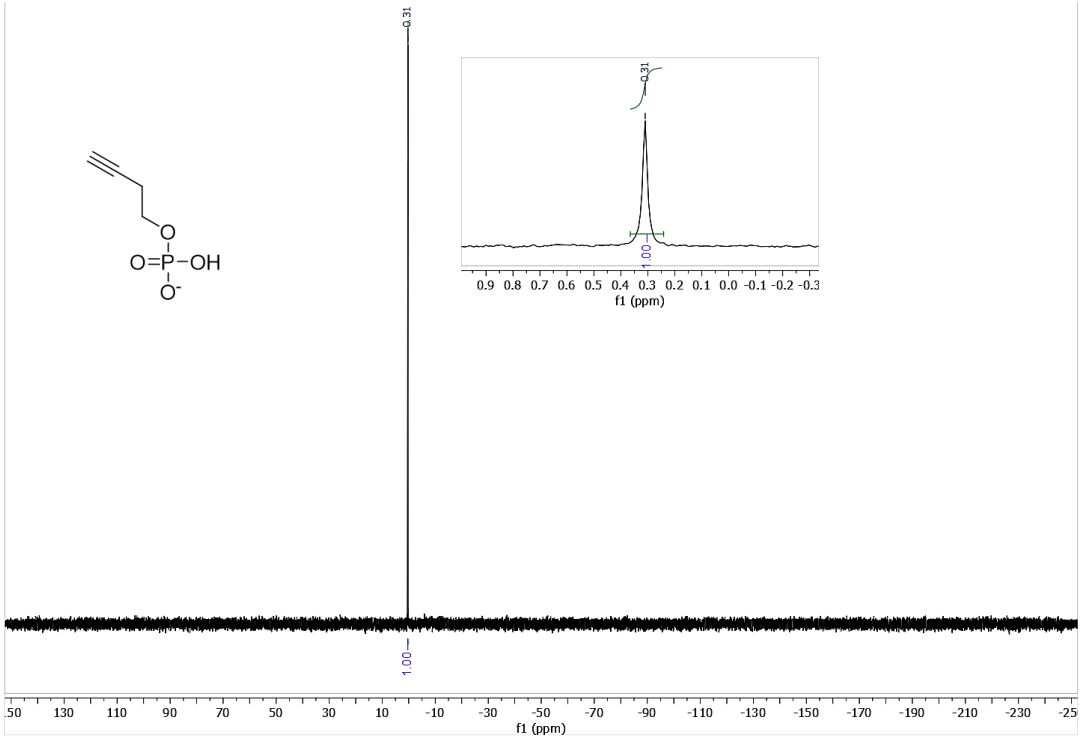

^{1}H NMR of β-Bis(4-(hydroxymethyl)phenyl pivalate)-3-butyn-1-yl pyrophosphate

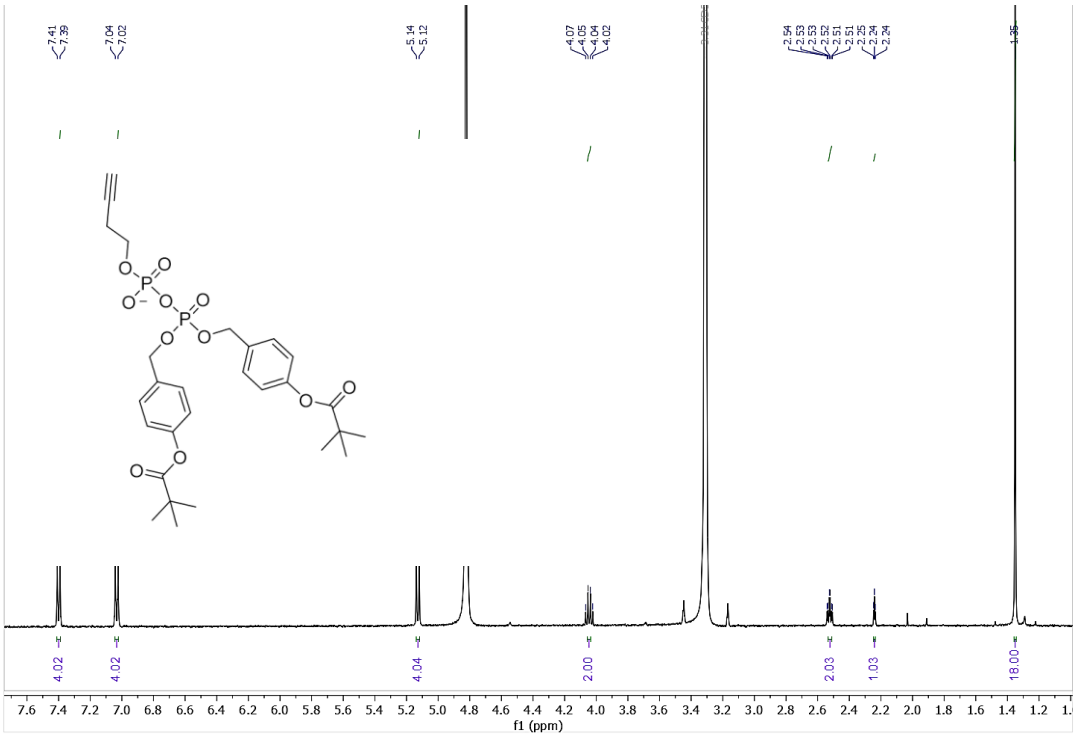

^{31}P NMR of β-Bis(4-(hydroxymethyl)phenyl pivalate)-3-butyn-1-yl pyrophosphate

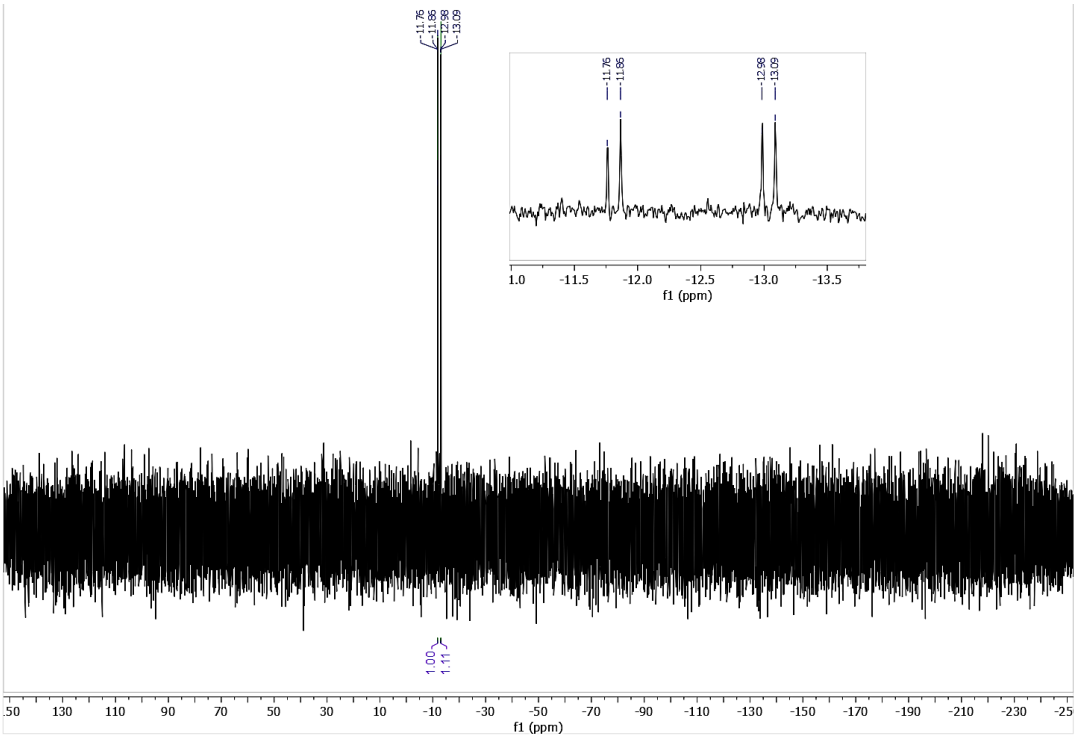

^{31}P NMR of 2,3-butadien-1-yl monophosphate (crude)

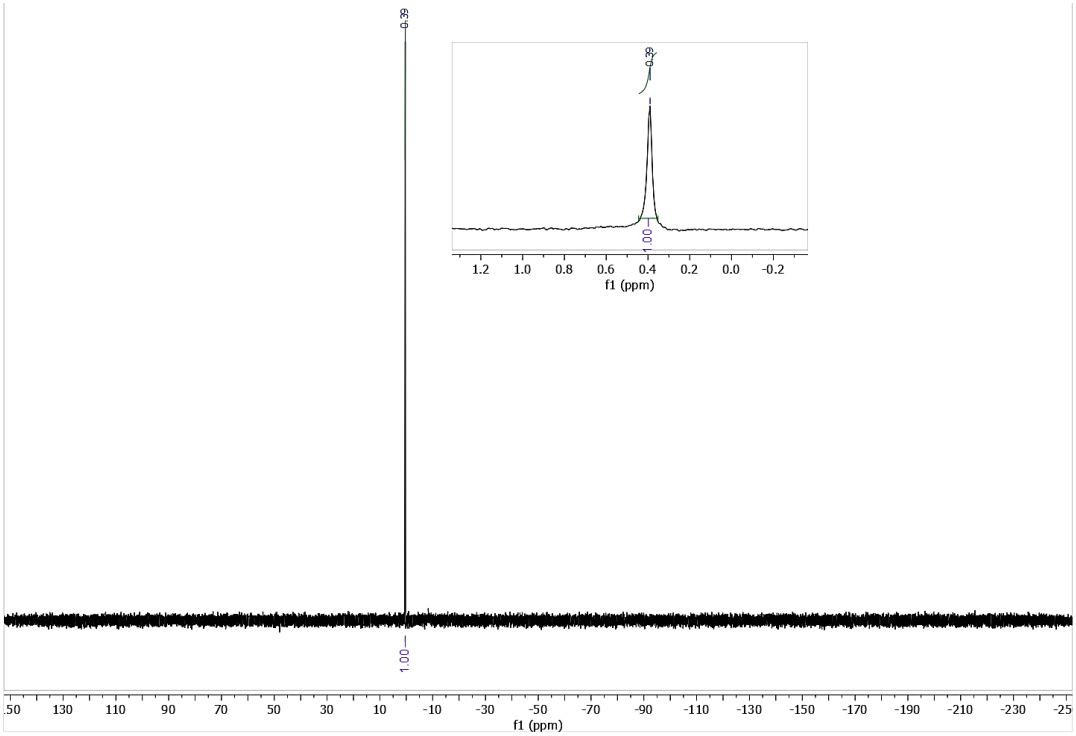

^{1}H NMR of β-Bis(4-(hydroxymethyl)phenyl pivalate)-2,3-butadien-1-yl pyrophosphate

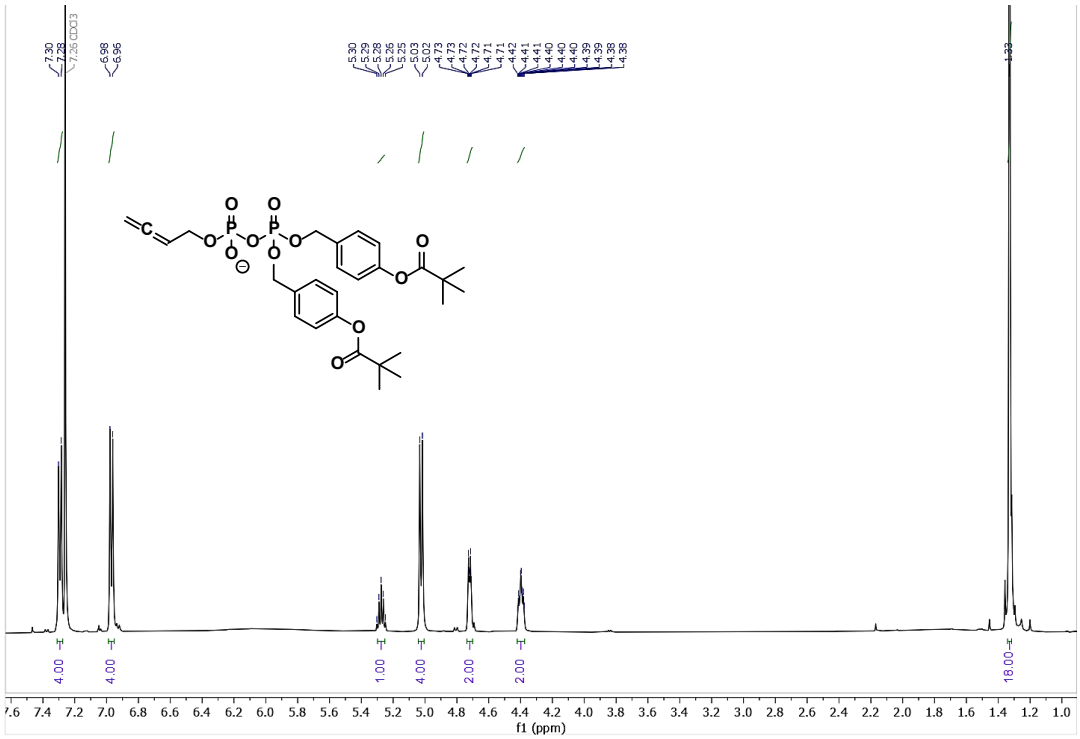

^{31}P NMR of β-Bis(4-(hydroxymethyl)phenyl pivalate)-2,3-butadien-1-yl pyrophosphate

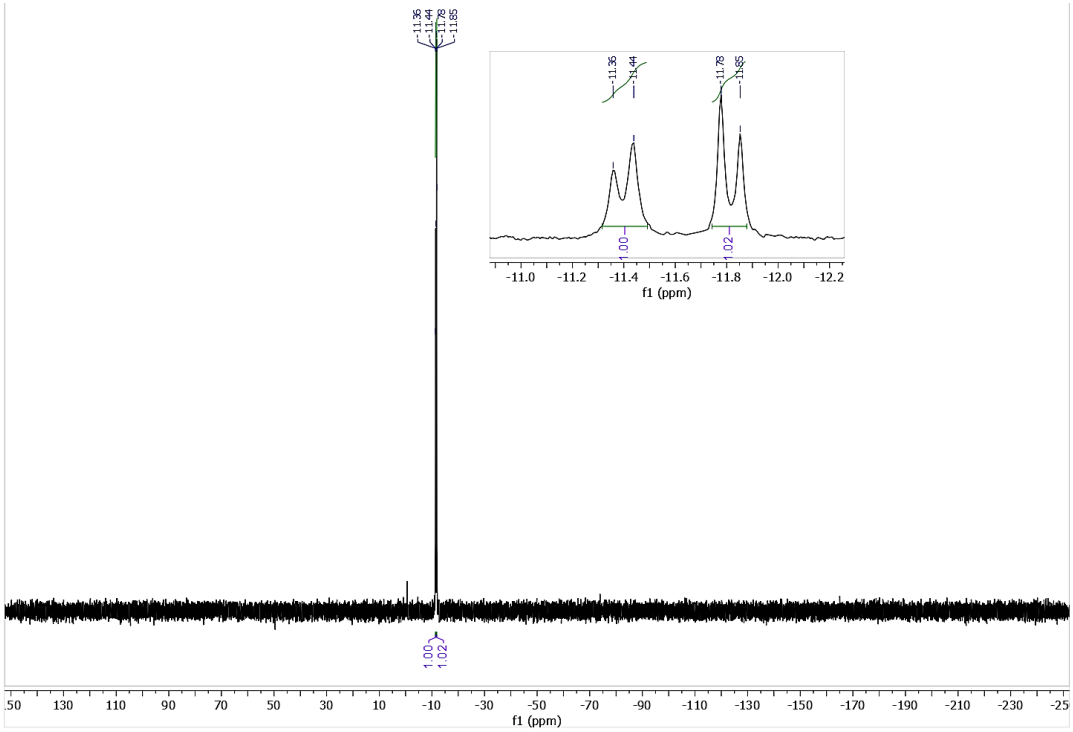

^{1}H NMR of 4-(hydroxymethyl)phenyl acetate

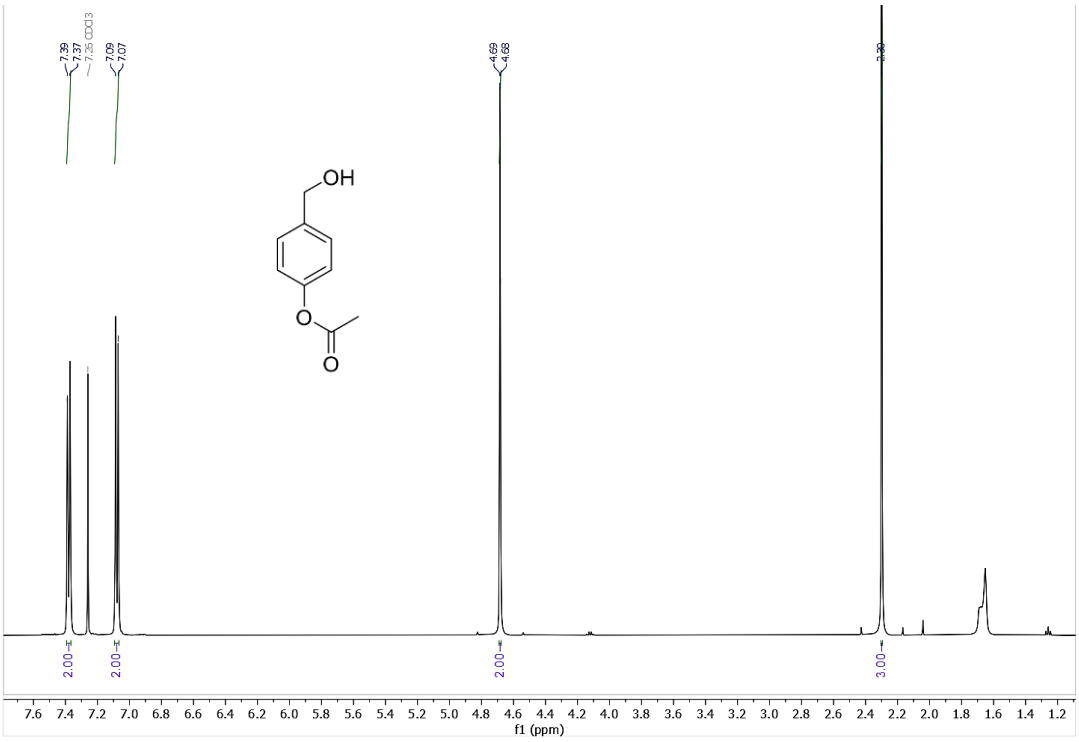

^{1}H NMR of Bis(4-(hydroxymethyl)phenyl acetate)-N,N-diisopropyl phosphoramidite

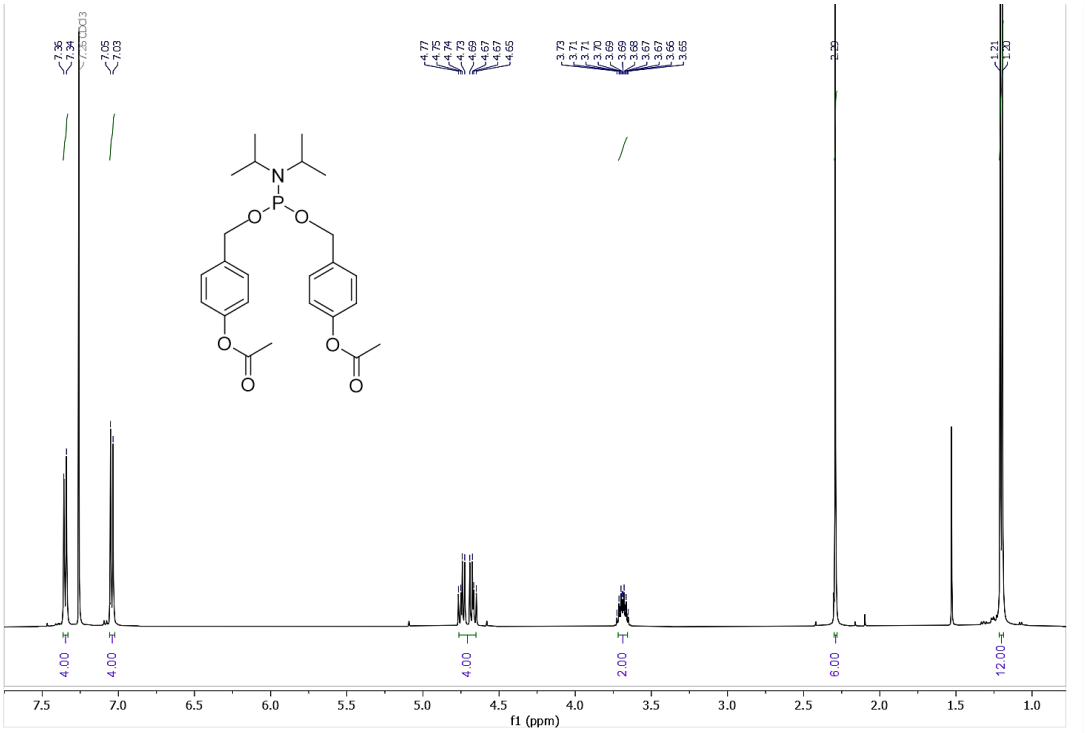

^{31}P NMR of Bis(4-(hydroxymethyl)phenyl acetate)-N,N-diisopropyl phosphoramidite

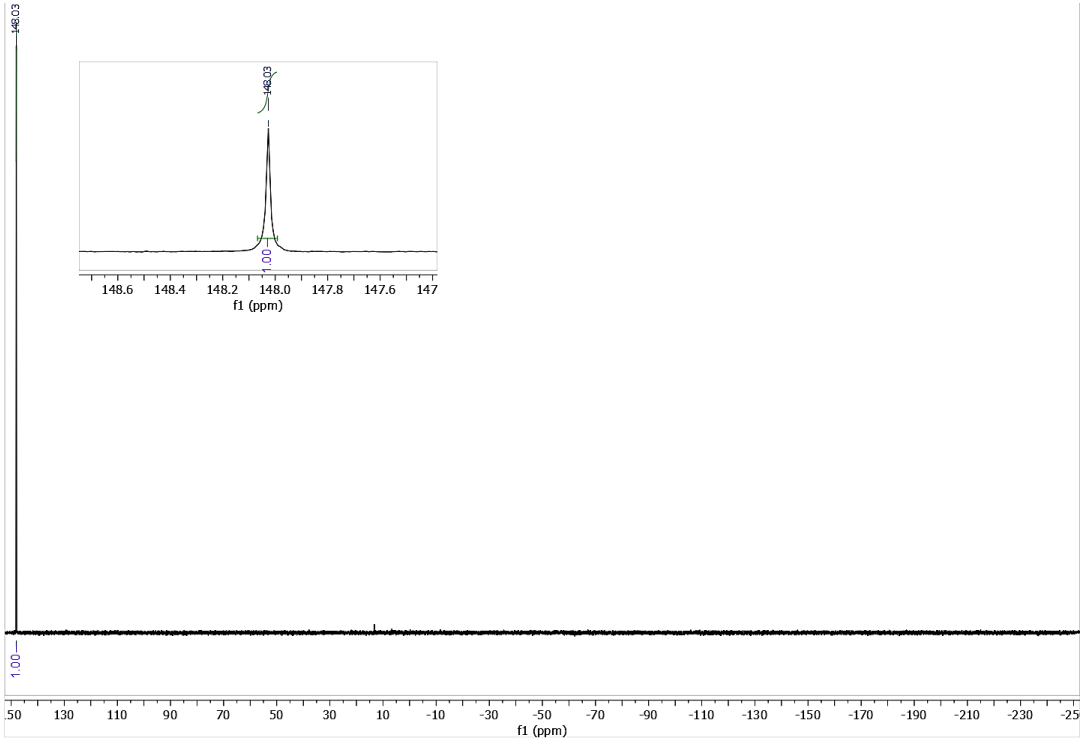

^{1}H NMR of β-Bis(4-(hydroxymethyl)phenyl acetate)-3,4-epoxy-3-methyl-1-butyl pyrophosphate

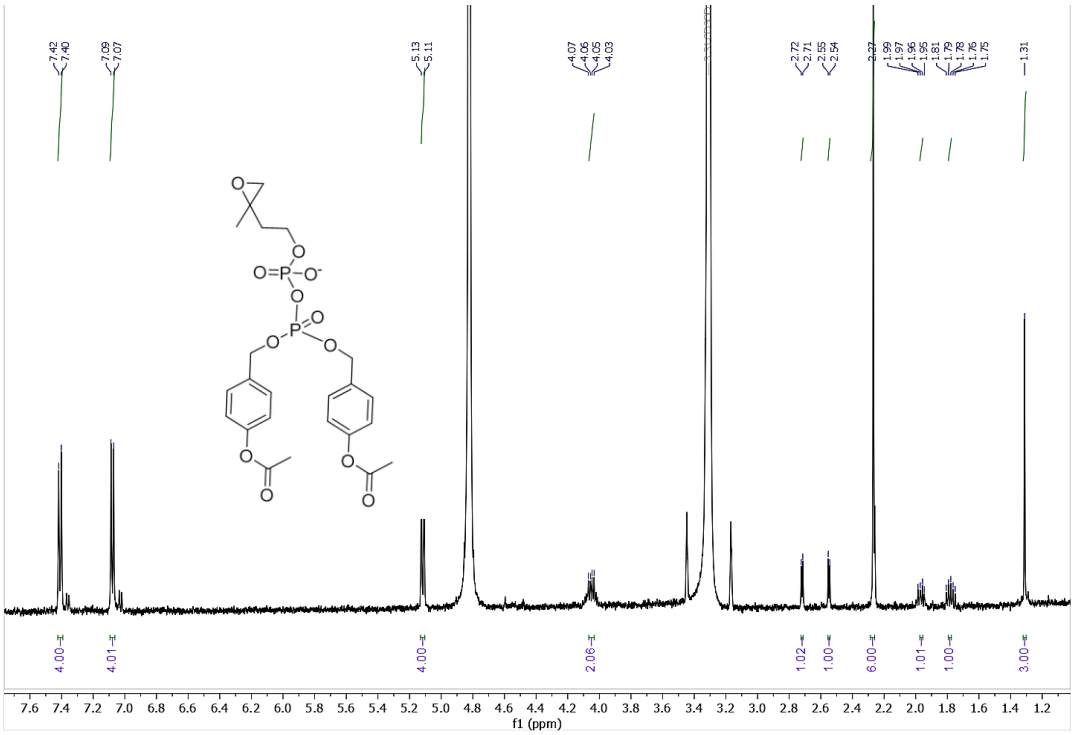

^{31}P NMR of β-Bis(4-(hydroxymethyl)phenyl acetate)-3,4-epoxy-3-methyl-1-butyl pyrophosphate

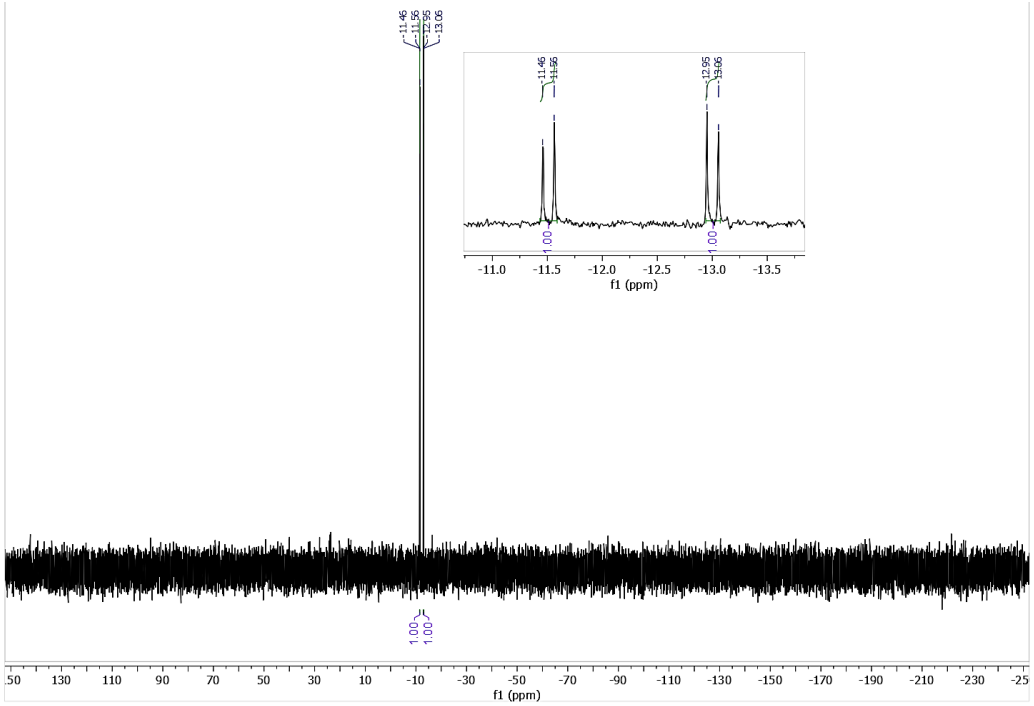

^{1}H NMR of 4-(hydroxymethyl)phenyl hexanoate

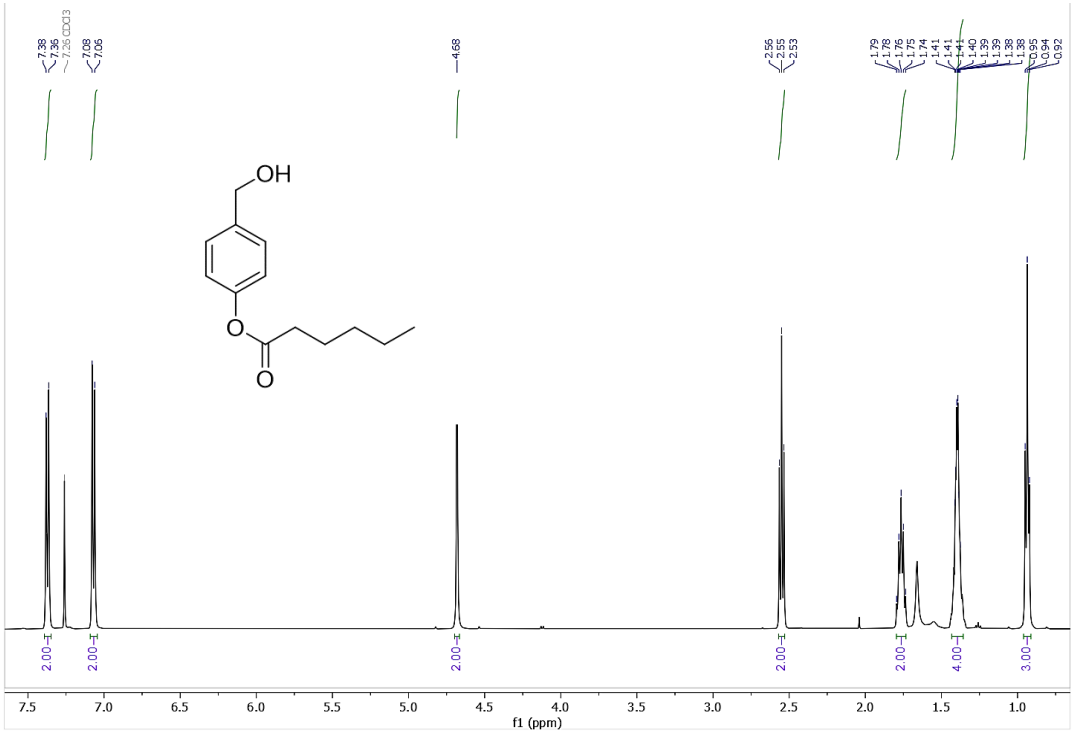

^{1}H NMR of Bis(4-(hydroxymethyl)phenyl hexanoate) H-phosphonate

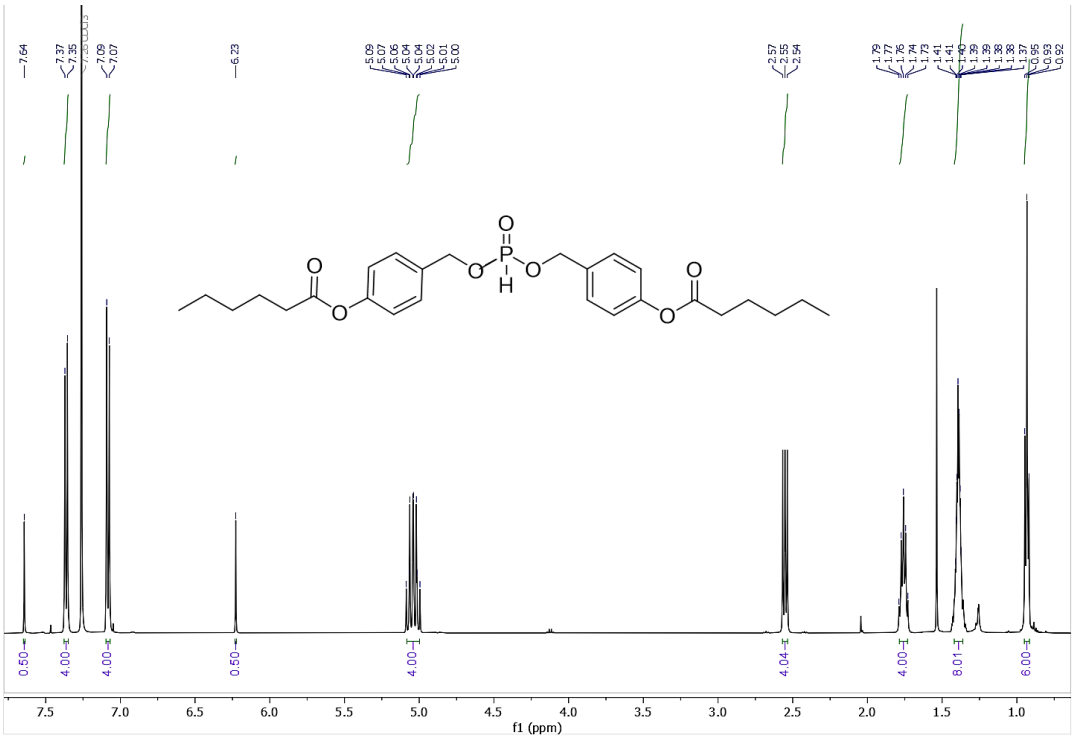

^{31}P NMR of Bis(4-(hydroxymethyl)phenyl hexanoate) H-phosphonate

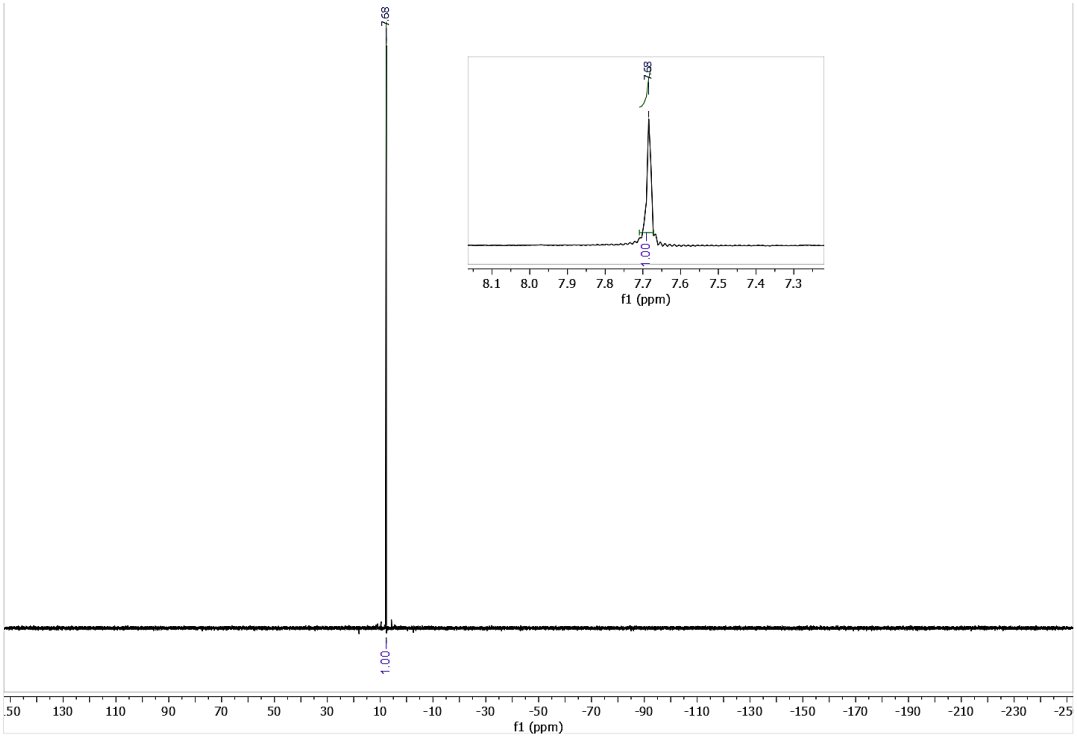

^{1}H NMR of β-Bis(4-(hydroxymethyl)phenyl hexanoate)-3-butyn-1-yl pyrophosphate

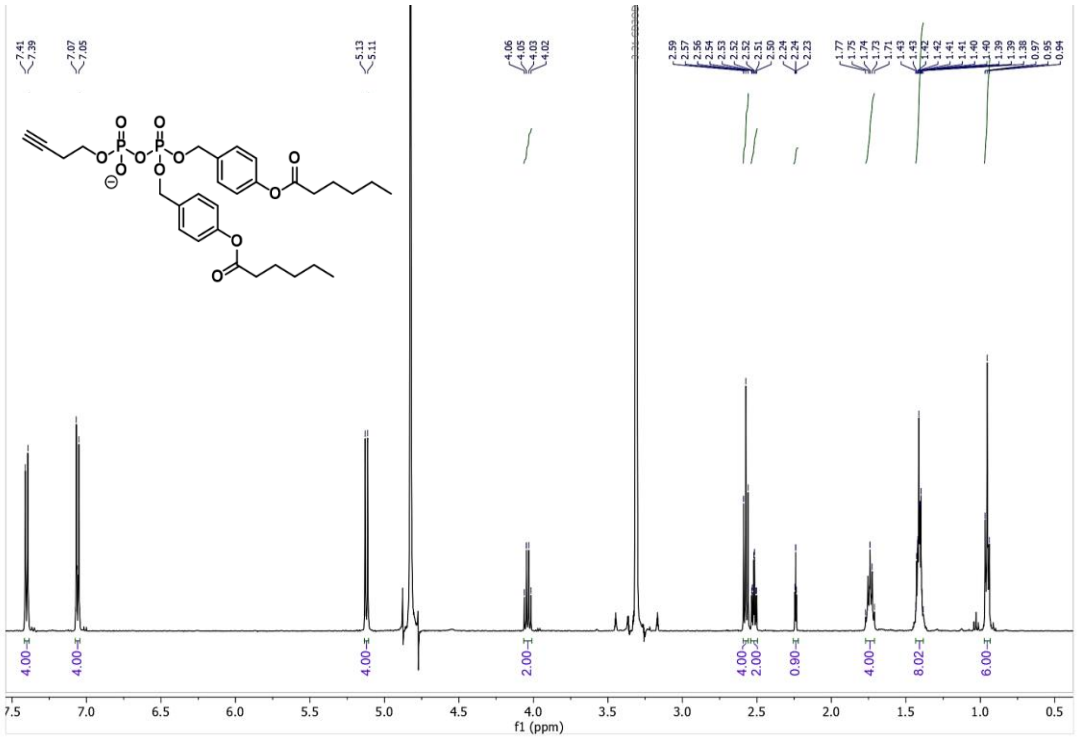

^{31}P NMR of β-Bis(4-(hydroxymethyl)phenyl hexanoate)-3-butyn-1-yl pyrophosphate

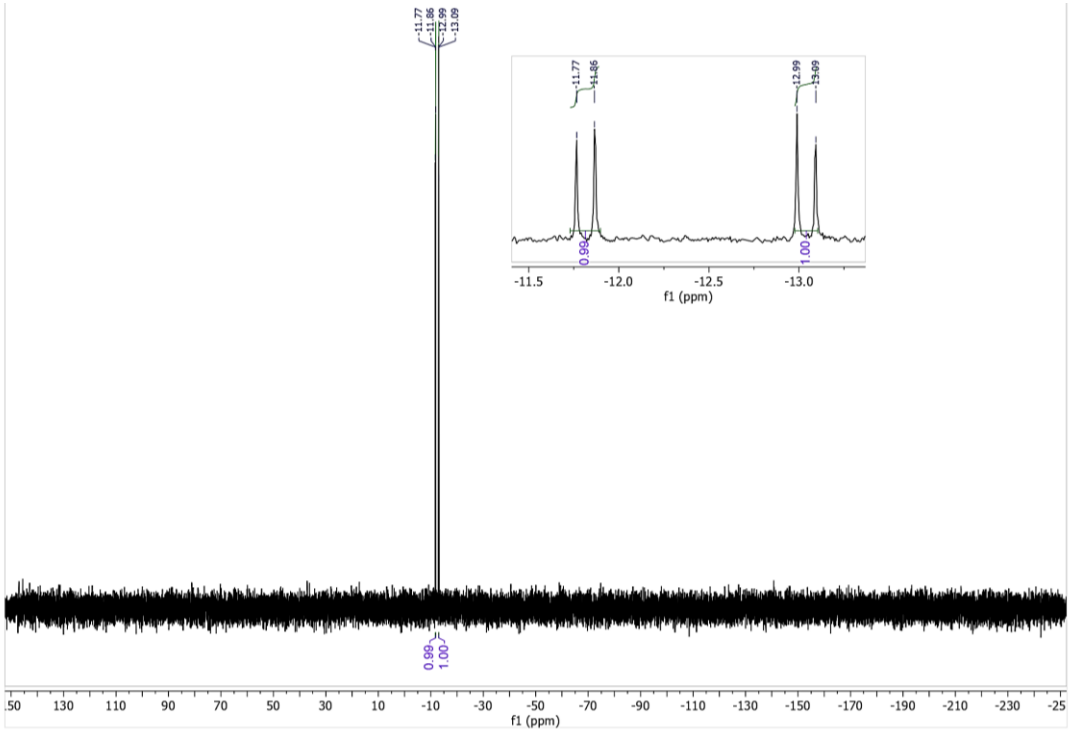

^{1}H NMR of Compound 11

^{31}P NMR of Compound 11

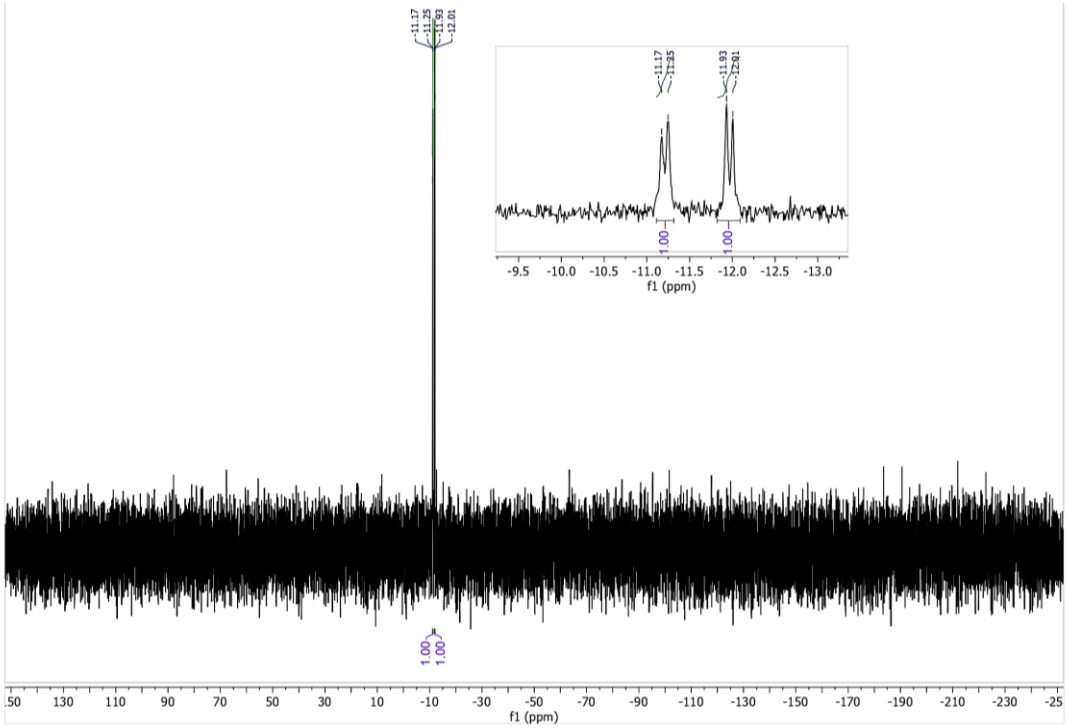

VITA

Vijani Wijayasekera is originally from Sri Lanka, where she completed her early education and undergraduate studies. She earned a Graduateship in Chemistry, equivalent to a Bachelor of Science, from the College of Chemical Sciences at the Institute of Chemistry, Ceylon. During this time, she conducted research under the mentorship of Dr. Dinusha Udukala, whose guidance was instrumental in shaping her research foundation. In 2022, Vijani furthered her passion for chemistry by enrolling in the Master of Science program in Chemistry at the University of Tennessee, Knoxville, where she conducted graduate research under the supervision of Professor Baccile, focusing on the synthesis of cell-permeant inhibitors through prodrug approaches for application on human cells. Upon graduation, Vijani intends to continue her academic journey by pursuing doctoral studies that explore the applications of nanocarriers in drug delivery, aiming to make significant contributions to the field of drug delivery through her research.